TUM School of Engineering and Design
Technische Universität München

Sustainable Design of Electric Vertical Take-Off and Landing Aircraft for Urban Air Mobility

Nicolas André

Vollständiger Abdruck der von der TUM School of Engineering and Design der Technischen Universität München zur Erlangung des akademischen Grades eines

Doktor der Ingenieurwissenschaften

genehmigten Dissertation.

Vorsitzender:
    Prof. Dr. mont. habil. Dr. rer. nat. h.c. Dr. h.c. Ewald A. Werner

Prüfende der Dissertation:
    1. Prof. Dr.-Ing. Manfred Hajek
    2. Prof. Dr. Sophie Armanini

Die Dissertation wurde am 30.08.2021 bei der Technischen Universität München eingereicht und durch die TUM School of Engineering and Design am 08.02.2022 angenommen.

Abstract

How should electric Vertical Take-Off and Landing aircraft (eVTOL) be designed to facilitate a sustainable Urban Air Mobility? Many different concepts in development promise to provide an emission-free alternative to ground-based transportation in urban and regional areas. To investigate the promise, this thesis assesses the environmental life cycle impact of eVTOLs in terms of carbon emissions.

The thesis develops and implements a methodology for the integrated conceptual design and life cycle assessment of eVTOL. The computational framework allows an evaluation of arbitrary configurations using alternative electrochemical energy carriers in diverse scenarios. It facilitates a discussion of existing eVTOL configurations and provides a baseline for a regression-based conceptual design of environmentally optimized configurations. The framework further supports depicting the effects of uncertainties present in the involved domains through a sensitivity analysis module.

The application of the methodology shows that eVTOLs can, given a set of coinciding, advantageous circumstances, be designed and operated so that their associated carbon emissions are comparable to or below those of electrically powered cars. The environmental competitiveness is facilitated by the following factors: First, a high cruise efficiency of aircraft, as in fixed-wing concepts, given the expected short hover shares of transport missions. Second, the availability of energy carriers that exceed the specific energy of today's Lithium-Ion Batteries, like Lithium-Air Batteries and hydrogen, especially on longer ranges. Third, the operation of eVTOLs on routes close to their specified design range, excluding short urban commutes below 25km due to their relatively high hover share. Fourth, a high seat utilization and high circuity factor compared to ground-based routes. And fifth, low carbon emissions in the primary energy production and the sourcing of often-replaced components like batteries and fuel cells. In essence, the carbon impact of eVTOL is dominated by the consumed specific energy per transported passenger, the system's energy conversion efficiency, and the primary energy production impact. As the latter can be even more decisive than the choice of configuration, it illustrates the importance of the manufacturers', operators', and regulator's policies regarding sustainable sourcing and supply. The author concludes that eVTOL may provide a sustainable transport mode if applied complementarily to ground-based modes, but suggests further, individual analyses.

The thesis demonstrates that the applied modeling fidelity using system-level metrics is sufficient to assess an eVTOL's sustainability. To handle the apparent uncertainties it suggests scenario-based assessments, complementing sensitivity analyses, and data improvements. Future research may consequently improve data and modeling fidelity, implement additional environmental and techno-economic metrics, and focus on the methodologies evolution toward eVTOL design optimization.

Zusammenfassung

Wie sollten elektrische Senkrechtstarter (engl. electric Vertical Take-Off and Landing aircraft, kurz eVTOL) konzipiert sein, um eine nachhaltige urbane Luftmobilität zu ermöglichen? Die vielen in Entwicklung befindlichen Konzepte versprechen, eine emissionsfreie Alternative zum bodengebundenen Transport in städtischen und regionalen Gebieten zu schaffen. Diese Arbeit beleuchtet das Versprechen, in dem sie die Umweltauswirkungen von eVTOL in Bezug auf die Kohlenstoffemissionen untersucht.

Dazu wird eine integrierte Methodik für Konzeptentwurf und Ökobilanzierung von eVTOL entwickelt. Diese erlaubt die Bewertung beliebiger Konfigurationen, alternativer elektrochemischer Energieträger und verschiedener Szenarien. Damit wird die Diskussion bestehender eVTOL-Konfigurationen ermöglicht und die Grundlage für einen regressionsbasierten Konzeptentwurf umweltoptimierter Konfigurationen geschaffen. Sensitivitätsanalysen verdeutlichen die Auswirkungen vorhandener Unsicherheiten.

Die Anwendung der Methodik zeigt, dass eVTOL vergleichbare oder geringere spezifische Kohlenstoffemissionen als Elektrofahrzeuge aufweisen können, falls entsprechende Rahmenbedingungen erfüllt sind. Diese umfassen: Erstens eine größtmögliche Vorwärtsflugeffizienz der eVTOL, wie sie Starrflüglerkonzepte aufweisen. Zweitens, und insbesondere auf längeren Strecken, die Verfügbarkeit von Energieträgern, deren spezifische Energiekapazität jene heutiger Lithium-Ionen-Batterien übertrifft, wie Lithium-Luft-Batterien oder Wasserstoff. Drittens einen Einsatz auf Routen, die nur geringfügig von der spezifizierten Maximalreichweite abweichen. Routen unter 25km sind aufgrund des hohen Schwebeanteils nicht ökoeffizient. Viertens eine hohe Sitzplatzauslastung und große Reichweitenersparnis im Vergleich zu bodengebundenen Strecken. Und fünftens niedrige Emissionen in der Primärenergieerzeugung und der Beschaffung von häufig zu ersetzenden Komponenten des Antriebsstrangs. Die Arbeit zeigt, dass die Lebenszyklusemissionen von eVTOL von der verbrauchten spezifischen Energie, der Systemeffizienz und der Emissionsintensität der Primärenergieerzeugung bestimmt werden. Dies verdeutlicht die Bedeutung nachhaltiger Entscheidungen von Herstellern und Betreibern in der Auswahl von Zulieferern und Energieversorgern. Der Autor schließt daraus, dass eVTOL im komplementären Einsatz zu bodengebundener Mobilität ein nachhaltige Transportmode darstellen können, schlägt aber weitere, individuelle Analysen vor.

Die Arbeit zeigt, dass die hier angewandte Modellierungsgüte des Konzeptentwurfs zur Bewertung der Nachhaltigkeit von eVTOL ausreichend ist. Die Auswirkungen von Unsicherheiten können durch szenariobasierte Bewertungen, ergänzende Sensitivitätsanalysen und eine verbesserte Datenlage reduziert werden. Für zukünftige Forschungsarbeiten werden eine Verbesserung der Daten- und Modellierungsgüte, die Implementierung zusätzlicher ökologischer und techno-ökonomischer Metriken und eine Weiterentwicklung der Methodik zur regressionsbasierten Optimierung von eVTOL vorgeschlagen.

Contents

List of Figures

List of Tables

Acronyms

GH2   Gaseous Hydrogen Storage.

AFC   Alkaline Fuel Cell.

BEV   Battery Electric Vehicle.
BMS   Battery Management System.

CSE   Consumed Specific Energy.

DEP   Distributed Electric Propulsion.
DGM   Design Gross Mass.
DLR   German Aerospace Center.
DOE   US Department of Energy.
DoH   Degree of Hybridization.

EASA   European Union Aviation Safety Agency.
EV   Electric Vehicle.
eVTOL   Electric Vertical Take-Off and Landing.

FCV   Fuel Cell Vehicle.

GHG   Greenhouse Gas.

HES   High Energy System.
HPS   High Power System.

IATA   International Air Transport Association.
IEA   International Energy Agency.
IOA   Input-Output Analysis.
IPD   Integrated Product Development.

LAB   Lithium-Air Battery.
LCA   Life Cycle Assessment.
LCC   Life Cycle Costs.
LCI   Life Cycle Inventory Analysis.
LCIA   Life Cycle Impact Assessment.

Acronyms

LIB	Lithium-Ion Battery.
LMB	Lithium-Metal Battery.
LPO	Lithium-Polymer Battery.
MCFC	Molten Carbonate Fuel Cell.
NASA	National Aeronautics and Space Administration.
NDARC	NASA Design and Analysis of Rotorcraft.
PAFC	Phosphoric Acid Fuel Cell.
PEMFC	Proton-Exchange Membrane Fuel Cell.
PKT	Passenger-Kilometer Traveled.
RCOTOOLS	RotorCraft Optimization Tools.
SA	Sensitivity Analysis.
SCI	Specific Carbon Impact.
SE	Systems Engineering.
SOFC	Solid Oxide Fuel Cell.
SPAC	Special Purpose Acquisition Company.
STOL	Short Take-Off and Landing.
UAM	Urban Air Mobility.
UQ	Uncertainty Quantification.
VFS	Vertical Flight Society.
WEF	World Economic Forum.

1 Introduction

1.1 The Dream and the Impact of Flying

The dream of flying is as old as humankind. The past century has made this dream a reality, as commercial aviation evolved into a commodity for many. Past decades unveiled a significant downside of this reality. Commercial aviation accounts for $2.5\,\%$ of annual global CO_2 emissions, but through radiative forcing contributes to $3.5\,\%$ of anthropogenic climate change [1]. Climate change increases land and ocean temperatures, the frequency and duration of heatwaves, and heavy precipitation events, among other effects [2]. Besides the economic cost, the human impact is vast. Over the past two decades, a total count of 1.3 million deaths is related to geophysical disasters, of which over 90% are associated with the effects of global warming [3]. In efforts such as the Paris Agreement, many nations commit themselves to limit global warming to well below 2 degrees, preferably 1.5 degrees Celsius, compared to pre-industrial levels [4]. In this context, commercial aviation pledges to reduce its impact as well. For instance, the International Air Transport Association (IATA) aims to reduce net aviation carbon emissions by 50% by 2050, relative to 2005 levels [5].

Meanwhile, the recent decade brought forward a potential novel form of aviation, known as Urban Air Mobility (UAM). Electric Vertical Take-Off and Landing (eVTOL) aircraft are envisioned to provide a new transportation mode and promise to make flying more individual, economic, and cleaner than ever before. UAM has evolved from the idea of a few innovators into a billion-dollar sector within a matter of years. In light of the apparent hype around UAM and the array of unresolved issues, critics question the sector's promises. Technological viability, affordability, and public acceptance due to potentially high noise emissions have yet to be proven.

The advent of UAM reflects global megatrends like urbanization, individualization, and electrification of the transportation sector. The latter is seen as an essential enabler to decarbonizing the economy [6], and UAM companies accordingly claim to provide a zero-emission mode of transport. However, a thorough environmental impact assessment requires to account for upstream and downstream emissions, i. e. including the production of electricity. Using conventional, carbon-intense electricity, battery-powered eVTOL would fall short of that promise [7]. A brief calculus example illustrates that the footprint of UAM could become significant: With the bold end of predictions of around $400k$ vehicles in service by 2040 [8] and given the current average European energy mix the global UAM sector would account for a total 250 megatons of Greenhouse Gas (GHG) emissions, roughly the equivalent of Spain's total GHG emissions in 2018 [9]. Although grid carbon intensities are anticipated to decrease, the potential amount of GHG emissions emphasizes the importance of an early assessment of the sector.

1.2 Aim and Scope of the Thesis

This thesis assesses the sustainability, i. e. the environmental impact in light of global warming, of eVTOLs and UAM. The question can be regarded from different perspectives, including assessments limited to the operation of single eVTOL aircraft, comparative analyses of alternative transport modes, and macroscopic studies on future UAM and transportation systems. Systematically addressing the different perspectives, this thesis pursues the following aims:

1. In light of the remarkable variety of eVTOL configuration approaches, it focuses on how design choices regarding alternative configurations and propulsion types affect the environmental impact of eVTOLs.

2. Yielding a tangible result on the sustainability of eVTOLs, it compares the carbon impact of various eVTOL configurations with that of electric cars as an alternative transport mode.

3. Addressing the predictive nature of environmental assessments of future systems, it intends to facilitate a discussion of the result's confidence and sensitivity toward uncertainties.

The aims pose a range of challenges: Thoroughly quantifying a system's carbon impact requires to include all effects occurring upstream and downstream of its use. Therefore, the thesis applies the Life Cycle Assessment (LCA) methodology. LCA typically takes a posterior perspective, building on extensive knowledge of the system's characteristics and its interactions with the underlying ecosystem. However, such insight is missing in the case of UAM, as the operation of eVTOL aircraft in such a sector has yet to become a reality. Therefore, at its core, the analysis requires a model of eVTOL aircraft. Such a model can be established through conceptual design. While the conceptual design of conventional vertical lift aircraft, i. e. helicopters, is facilitated by clearly defined mission requirements and knowledge from previous designs, eVTOL design is performed on a blank slate. To complicate matters, assessing an eVTOL's carbon impact requires to include further domains such as energy storage technology and future power infrastructure. Modeling and assessing an eVTOL aircraft based on a specific mission profile, using a particular configuration type, set in a certain future energy scenario is well possible. However, it cannot be validated and thus lacks significance. Consequently, the task is subject to vast unknowns and uncertainties and poses the challenge of not only producing results, but producing meaningful results.

The thesis develops an integrated methodology to conceptually design and environmentally assess eVTOL aircraft through a three-pillar approach: At its core, a conceptual design framework describes arbitrary eVTOL configurations (see Section 4.1). Subsequently, environmental assessment is provided by an LCA module that accounts for all relevant life cycle phases of the eVTOL (see Section 4.1). Stochastic evaluations support both steps to account for uncertainties. Ultimately, an integrated approach allows assessing design choices in a generalized fashion and provides the baseline for future studies (see Section 4.3).

1.3 Outline

The thesis is organized as follows: Chapter 2 reviews and introduces the state-of-the-art. Section 2.1 delves into Urban Air Mobility as a potential novel transportation mode, introduces representative eVTOL designs, and reviews the literature on technological and operational considerations to point out and discuss the main challenges. Section 2.2 discusses challenges in conceptual design of eVTOL aircraft based on the existing aircraft and rotorcraft design literature. It then reviews current approaches to conceptual design, including Wirth's hierarchical model-based design methodology, which serves as a baseline for this thesis [10]. Section 2.2 then provides an overview of the most prominent design environments and tools used by eVTOL researchers. Subsequently, Section 2.3 presents a brief introduction to the topic and terminology of sustainability and outlines the utilized LCA methodology. Chapter 2 concludes by reviewing the state of technology of electrochemical energy carriers that are likely to be used to power eVTOL aircraft.

Chapter 3 presents the methodology developed in this thesis. Based on the aforementioned shortcomings of state-of-the-art approaches, Section 3.1 introduces the idea of architectural domains and the procedural framework. Next, Section 3.2 outlines the design method, used models, and mathematical representations. Section 3.3 then applies the LCA scheme to the subject and scope of the study, thus modeling the respective system and presenting the impact assessment framework.

Chapter 4 covers the results and discussion thereof and is subdivided into three parts. First, Section 4.1 provides the conceptual design and performance analysis results concerning a set of representative eVTOL configurations. Descriptive data, including system-level metrics, model parameters, and mission requirements are comprehensively presented, and characteristics of available powertrain and energy carrier technology are introduced. Conceptual sizing and analysis of the identified eVTOL configurations is performed, deterministically and stochastically, and concluded by a sensitivity analysis. Second, Section 4.2 presents the environmental LCA of the reference configurations, determining GHG emissions associated with the eVTOL system and its operation. Therefore, the section includes raw material impact data, sourcing impacts of electrochemical energy carriers, and scenarios on the availability of clean energy, together with the impact assessment itself and a discussion of the findings in the context of a tangible case study. Lastly, Section 4.3 generalizes the methodology through randomization of eVTOL configurations. An introduction of identified empirical relations between system-level metrics in eVTOL aircraft is followed by comprehensive applications of the conceptual design, performance analysis, and carbon impact assessment modules to identify and understand crucial design drivers and considerations.

Chapter 5 concludes the thesis by summarizing the essential findings and pointing out future areas of research.

2 State-of-the-Art

2.1 Urban Air Mobility

Urban Air Mobility (UAM) is a novel mobility sector that aims to provide on-demand or scheduled air transportation services within metropolitan areas [11]. At prices comparable to today's means of transport, small, lightweight, and electrically powered aircraft are envisioned to serve customers, for instance, by providing intracity commutes or airport shuttles [12]. Common to the vast majority of concepts that have been announced to partake in the challenge is the ability to vertically take-off and land, like a helicopter, leading to the agreed-upon name for the emerging class of aircraft: electric VTOL, or eVTOL. The emergence of UAM and eVTOL has initiated a frenzy in public interest and private investment. Today, at least four of the sector's startups[1] are labeled *unicorns*, implying they are worth more than one billion dollars. The four have recently announced a public offering of their companies, allowing them to grow their funds further. Despite impressive funding, it is uncertain whether any of the proposed air transportation services will eventually come to life, and if so, when this is about to happen. Besides the technological challenges that naturally emerge with the introduction of novel technology, the sector has promised to deliver a formidable list of characteristics and has yet to live up to that promise. Moore, who is arguably one of the sector's visionaries, identifies crucial characteristics of UAM to be its ease of use through autonomous operation or minimum pilot training requirements, as well as safety, reliability, affordability, community-friendliness, and sustainability [13]. Uber Elevate, a subsidy to the ride-hailing company until acquired by UAM company *Joby* in December 2020, and a public promoter of the UAM sector, early on provided a review and assessment of the sector's requirements [14]. The multitude of challenges regarding UAM has since then been assessed by many institutions and researchers. Comprehensive works have been provided by Vascik et al., Thipphavong et al., and Straubinger et al. [11], [15], [16]. This section introduces a variety of eVTOL configurations and subsequently delves into the challenges and limitations of UAM within and beyond the technological domain.

2.1.1 Introduction and representative designs

Several technological factors have enabled the advent of UAM and eVTOL in recent years. Most decisive regarding novel vertical lift configurations are distributed electric propulsion (DEP) systems. Individually controllable electric motors, powered by electrochemical power sources like batteries, fuel cells, or electrochemical capacitors, allow for greater flexibility in vehicle configuration and simplified propulsion system design,

---

[1] Joby Aviation, Archer, Lilium, Vertical Aerospace

compared to traditional rotorcraft. Electric motors are available in various sizes and can provide a range of torque and rotational speed (rpm), other than large piston or turboshaft engines, which provide power at high rpm and require transmission systems. Smaller propellers powered by electric motors, often rpm controlled, may render large rotor systems, controlled through collective and cyclic blade pitch, unnecessary. However, vast challenges and technological boundaries are apparent, and a substitution of traditional rotorcraft by eVTOLs is in many applications considered unlikely in the coming years. For one, rotorcraft systems like helicopters have matured over decades and are known for their versatility, robustness, and capabilities. Additionally, vertical DEP aircraft suffer significantly from the limited specific energy of currently available electrochemical power sources. Many authors have pointed out how today's best-in-class battery capabilities fail to enable significant use cases of eVTOLs.
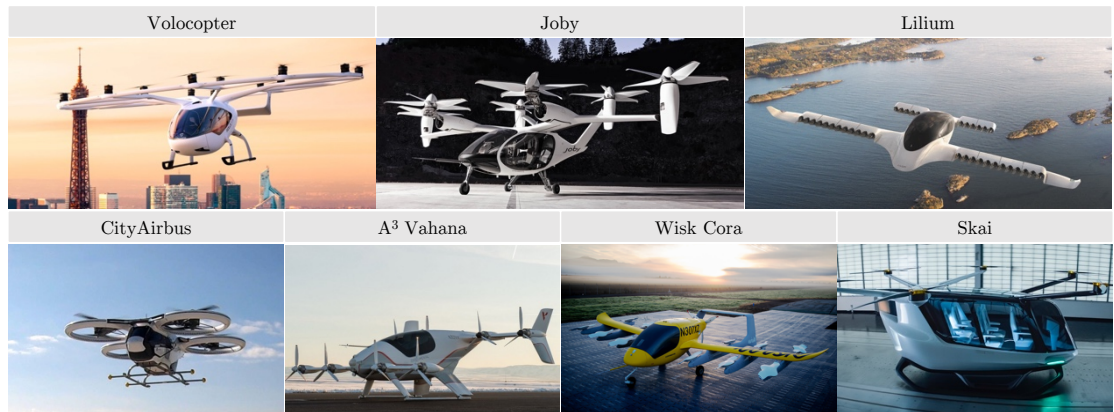
Figure 2.1: Representative configurations of eVTOL aircraft.

Over 200[2] eVTOL aircraft, as counted by the Vertical Flight Society (VFS)[3], an international technical society, are being developed worldwide [17]. VFS categorizes eVTOL aircraft by the type and configuration of the vehicle's thrusters into Wingless (i. e. Multi-Rotor), Lift & Cruise, and Vectored Thrust configurations [17]. Of the 200, this section identifies seven configurations representative for the sector. Depicted in Figure 2.1, the seven projects are the *VoloCity* by Volocopter, *"Cora"* by Wisk[4], *"CityAirbus"* by Airbus, *"Vahana"* by A[3] (A *cubed*), an Airbus subsidy, *Joby Aviation*, *Lilium*, and the hydrogen-powered *Skai* eVTOL by Alakai. This selection features aircraft of all basic configuration types, i. e. Wingless, Lift & Cruise, and Vectored Thrust. It covers the full scope of proposed eVTOL mission ranges and contains battery-powered as well as hydrogen-powered aircraft. However note, that the selection of those seven aircraft concepts is not exhaustive. For instance, although among the top-funded eVTOL companies, the aforementioned startup Archer is left out of this selection due to its relative

---

[2]Excluding hover bikes and electric helicopters
[3]formerly: American Helicopter Society
[4]formerly known as Kitty Hawk

novelty. The following paragraphs briefly present each of the selected aircraft and their configuration. The data representation of the configurations is presented collectively at the beginning of Section 4.1, as it requires knowledge of the methodology.

VoloCity. Founded as early as 2007 in Bruchsal, Germany, the company Volocopter has developed and tested an array of full-scale prototypes. Volocopter's prototypes have logged more than $1,000$ test flights, manned and unmanned, and have been showcased in multiple cities, including Singapore and Stuttgart. Their VoloCity eVTOL represents their fourth generation vehicle and is currently in the process of receiving a type certificate from the European Union Aviation Safety Agency (EASA), intending to start operations around 2022 to 2023. The company had raised a total $132\,\text{M\$}$ as of January 2021 [18]. Volocopters aircraft have all been developed in a wingless, Multi-Rotor configuration. While earlier prototypes were significantly lighter, the VoloCity is said to have a maximum take-off mass of $900\,\text{kg}$, and will transport one passenger and one pilot (or two passengers if it may be operated autonomously) over a range of $35\,\text{km}$ with a maximum flight speed of $110\,\text{km/h}$. It is powered by 18 propellers of a $2.3\,\text{m}$ diameter. The nine battery packs are planned to be swapped in around five minutes.

Skai. Located in the greater Boston area, the US startup Skai was the first among UAM companies to announce a liquid hydrogen powertrain eVTOL in early 2019 [19]. Apart from the powertrain development, Skai's configuration is simple compared to many competitors. Six low-rpm propellers provide lift in vertical and horizontal flight, without any tilting mechanisms or attached wings. The vehicle is supposed to carry a payload of around $450\,\text{kg}$, cruise at around $185\,\text{km/h}$ to cover a distance of up to $644\,\text{km}$ [17]. However, the vehicle's operational *everyday sweet spot* range will be between 15 and $240\,\text{km}$, as suggested by Alakai. According to a report published in June 2020 by News Atlas, a news web page, Skai has already tested its airframe structure in tethered flight, while reportedly integrating and testing the liquid hydrogen powertrain [20]. While the company does not provide any specifics on its powertrain, Val Miftakhov, founder and CEO of ZeroAvia, a startup developing a sub-regional aircraft powered by hydrogen, estimates the liquid tank's potential mass fraction at around $30\,\%$. Compared to the 10 to $11\,\%$ hydrogen tank mass fractions assumed by ZeroAvia for their gaseous hydrogen storage, the higher fraction would result in a comparably low tank mass [21].

City Airbus. As a major aviation company, Airbus took an interest in UAM early on and has developed two battery-powered eVTOL demonstrator aircraft, one of which is the *"CityAirbus"*. Being engineered by Airbus' helicopter division, the concept is arguably building heavily on helicopter design principles like a low disk loading for high efficiency in hover flight. The quasi-quad configuration has eight fixed-pitch propellers arranged in four coaxial and slightly ducted propulsors with a rotor radius of $1.4\,\text{m}$ and is designed to carry four passengers at around $120\,\text{km/h}$ over a range of $60\,\text{km}$. Airbus initiated a test campaign in early 2019 and has since completed a range of test cases, such as a fully automated flight as well as transitions to cruise flight [22].

Vahana. Besides City Airbus, the company developed and tested the concept Vahana through its Palo Alto-based subsidy A^3 (*A-cubed*). Two versions of Vahana were built,

both in a Tilt-Wing configuration with eight rotors. The *Alpha* prototype was designed to carry one passenger over a range of 50 km at a cruise speed of 190 km/h [23]. The *Beta* prototype was designed for two passengers in tandem, for a total cruise range of 100 km. As one of the earliest companies in the sector A[3] published footage of a full aerodynamic transition from vertical to horizontal flight. In total, the Vahana program completed 138 test flights, and over 13 hours and 903 km of flight time and range [24]. The program was suspended in 2020.

Cora. Initially being developed by Kitty Hawk, a startup backed by Google's co-founder Larry Page, the concept Cora is now pursued by Wisk, a joint venture between Kitty Hawk and aircraft company Boeing [25]. The battery-electric aircraft is designed as a Lift & Cruise configuration for two passengers, with a 160 km/h cruise speed, and is envisioned to cover ranges up to 100 km. It is powered by 12 lift fans for vertical flight and one propeller for horizontal flight. Cora has achieved experimental airworthiness certification from both the New Zealand Civil Aviation as well as the United States Federal Aviation Administration and has logged more than 1,000 test flights so far. Wisk partners with NASA on the safe integration of autonomous aircraft systems into UAM [25], [26].

Lilium. Founded in 2015 and reportedly valued worth a billion dollars in 2020 by Baily Gifford, a venture capital firm, Lilium is one of the most prominent yet controversially discussed ventures in the UAM sector [27]. Lilium, which has raised over 375 M$ as of early 2021, is developing a five-seat vertical aircraft, powered by 36 tiltable, electrically powered, ducted fan propellers. The company demonstrated its ability to vertically take-off and land, as well as to perform slow forward flight. However, a demonstration of a full transition to aerodynamic flight is still pending. Two prototypes of the five-seat aircraft have been developed, one of which was lost in a thermal runaway incident. Much of the public debate on the feasibility of the configuration focuses on the promoted maximum range of 300 km initially communicated by the company. As of today, Lilium has refrained from further promoting technical specifications, like the range or the maximum speed of 300 km/h on its website. In an interview, founder Daniel Wiegand set the initial profitability bar for Lilium's business model to a minimum of 150 to 180 km. According to Wiegand, this bar be distinctly exceeded by the first vehicles in service. Batteries capable of providing energy for the promised 300 km were being tested by the company already today [28][5].

Joby. One of the earliest players in UAM and arguably the closest to bringing a eVTOL aircraft to the mass market is Joby Aviation. Founded in Santa Cruz in 2009, the company had raised over 800 M$ by 2020, lately through technological partnerships with car maker Toyota and ride-hailing company Uber's *Elevate* department [30]. Joby recently announced its merger with Reinvent Technology Partners, a SPAC, to capture

---

[5]Lilium has announced a merger with Special Purpose Acquisition Company (SPAC) *Quell* in April 2021 and has announced to develop a seven-seater aircraft for ranges of up to 240 km. As this thesis was in the editorial phase by April 2021, the author deliberately refrained from major adaptions of the assumptions and data. Instead, singular remarks to this thesis are made, where appropriate [29]

another 1.6 B\$ in early 2021 [31]. Joby's current aircraft, dubbed *S4*, is a fixed-wing configuration with six electrically powered, tiltable propellers and is designed to carry four passengers and one pilot over a maximum range of 240 km at a cruise speed of 320 km/h. The company has conducted test flights on various smaller prototypes, like the earlier *S2*, designed for two passengers, including manned flights. Joby claims to achieve certification by 2022 and offer the first commercial flights in 2024.

2.1.2 Challenges and limitations

Techno-economic perspective: Several researchers have been designing eVTOL aircraft to assess technological viability, the potential of competing configurations, and expected costs. Among the earliest to publish on the matter were Sinsay et al., who in 2012 estimated that battery technology available by presumably around 2030 would enable short-hop ranges and lead to feasible aircraft designs [12]. Despite advances in battery technology, Sinsay et al. point out that those eVTOL aircraft will be significantly heavier than their turboshaft equivalents but may become economically viable depending on prospective costs of fuel and electricity [12].

Johnson and Silva of NASA Ames and Silva et al. have since put considerable effort into developing a technical baseline within NASA's computational framework NDARC[6]. Based on a specific UAM mission accounting for the geography, population density, and existing infrastructure in 28 U.S. cities, Johnson and Silva, as well as Silva et al. performed sizing and analysis of various configurations, including electric Quad-Rotor, Side-by-Side, and Lift & Cruise aircraft. Facilitating the chosen UAM mission range of 120 km, they assume an effective battery specific energy of 400 Wh, clearly identifying the battery energy and power capability to be the primary gatekeeper toward applying eVTOL technology in UAM scenarios. Referencing their previous works on low emission rotorcraft, they argue that battery-powered aircraft do not meet long-term efficiency goals, given the high U.S. electric grid emissions [7], [32].

Notably among works on the status of technology is the comprehensive technology assessment published by Datta et al., who summarize in a technical report several topic articles by subject matter experts of the *Transformative Vertical Flight* (TVF) initiative [33]. Besides outlining eVTOL concepts currently under development and a simple UAM mission analysis, the report reviews critical technologies. The central relevance of the performance metrics *lift-to-drag ratio* and *power loading* is discussed, and empirical data of both parameters is provided. Furthermore, current and next-generation battery technology is briefly assessed. Datta et al. also outline the current state and high technological readiness of hydrogen fuel cell technology. They state how the Proton-Exchange Membrane Fuel Cell (PEMFC) is a promising alternative to batteries as the primary energy carrier [33].

Stressing how trades in vehicle design are interconnected with the mission profile to be served by eVTOL aircraft, Shamiyeh et al. analyze two different vehicle classes: A Multi-Rotor configuration and a Lift & Cruise concept, both with varying levels of payload.

---

[6] An introduction to the framework NDARC is provided in Section 2.2

They find how the specific energy consumption per traveled passenger-kilometer is highly dependent on the operational scheme. Shamiyeh et al. identify the flight altitude as a proxy for time spent in energy-intense, hover-like flight states and the off-design range as opposed to the maximum design range to be highly influential. The strong dependence of specific eVTOL performance is similarly reported by Clarke et al., who study variability in UAM mission profiles as interdependencies of vehicle components based on the SUAVE framework[7] [34].

Studies featuring an assessment and discussion of the costs of operating eVTOL aircraft have been published by Fredericks et al., Duffy et al., and Brown and Harris [35]–[37]. Electrification of aircraft is generally seen as a chance to lower carbon emissions associated with aviation and significantly reduce cost. Duffy et al. analyze and confirm the general economic feasibility of UAM and find that the total operating cost of eVTOL is lower compared to aircraft powered both by a turbine and by a piston engine [36]. Fredericks et al. account this mostly to comparably lower prices of electricity over aviation fuel (in the U.S.) and a reduction of labor and maintenance cost as a result of a simplified drivetrain architecture [35]. Brown and Harris provide a detailed study on the feasibility and economic viability of UAM and break down the total cost per passenger-kilometer into capital and operating expenses. For a reference mission in New York City, they determine total trip costs of between around 160 $ and 260 $, which is within the same order of magnitude as upscale ride-hailing services. They report how the cost of the battery dominates capital expenses per mission due to the battery's limited cycle life. In contrast, they find that the price of electricity only slightly affects the operational expenses, which are strongly driven by pilot wages. Brown and Harris further confirm and stress the assessment of Johnson and Silva, that a specific battery energy density of 400 Wh/kg is critical for enabling value for UAM [37].

Operational perspective: Besides technological concerns, an array of considerations regarding operational limits of UAM exist. Vascik et al. investigate potential operational constraints that could arise during the implementation or scale-up of a UAM system. With respect to various reference missions in different city settings, they conclude three major scalability limitations for UAM ecosystem: (1) Aircraft noise, impeding public acceptance of a potentially loud and intimidatory new vehicle class. (2) The availability and placement of take-off and landing areas, i. e. vertiports, within already developed urban areas, dictating how well the novel transportation mode is embedded in proficient power grids as well as in the transportation network. This point is further discussed in a study by Postorino and Sarné [38]. (3) And the challenge of air traffic control (ATC) arising through hundreds or thousands of piloted, and potentially autonomous, aircraft flying over populated ground [11]. Besides those three, Vascik et al. list safety and reputation, the availability of pilots, network operations logistics, and all-weather operations as decisive but more manageable for the scale-up of UAM. To outline the emergent embedding of the novel transport mode in cities early on, Thipphavong et al. of NASA provide high-level concepts of operation for UAM [15].

---

[7]An introduction to the framework SUAVE is provided in Section 2.2

On the demand side, Plötner et al. analyze the potential demand of UAM as a supplementary mode of transport in the greater Munich area [39]. Using agent-based simulations, they demonstrate how UAM demand could concentrate on short routes, with a maximum range of 40 km covering 84% of requested routes. A maximum range of 110 km could suffice to serve 90% of demanded routes. Those supposedly short ranges imply a low sensitivity of UAM demand toward the required flight speed. However, Plötner et al. assume rapid recharging or swapping of batteries in between missions legs. They further do not include intercity demands in their model. As for the energy carrier, Plötner et al. discuss how hydrogen could be a technological alternative to batteries but argue that hydrogen's required infrastructure may crucially limit its application on the discussed short urban routes. On the contrary, Plötner et al. discuss how hydrogen might be beneficial to meet noise emission requirements, as it allows for lighter aircraft and a reduced disk loading of eVTOLs in hover. Finally, Plötner et al. point out research gaps like the impact of noise-induced routing, the role of security processes on the operational scheme, and induced demand due to a novel transport mode [39].

Environmental perspective: Assessments on the sustainability of eVTOL and UAM have not been published until recently when Kasliwal et al. [40] and André and Hajek [41] reported that eVTOL might become environmentally competitive to ground-based mobility. Kasliwal points out the large impact of mission distance [40]. Correspondingly, André and Hajek demonstrate the influence of the operational mission profile and application scenario, reporting how the environmental footprint is largely determined by the relative share of hover flight, the grid carbon intensity, the seat-utilization, the circuity factor, and the battery's cycle life [41]. Building on those results, Melo et al. review modeling approaches and discuss the requirements toward an integrated Life Cycle Engineering (LCE) framework of future air transportation systems [42]. They stress the importance of advances in battery technology and state how Lithium-Sulfur Batteries (LSB), with increased capacity and lifetime, could help to reduce eVTOLs carbon footprint. Most recently, Mudumba et al. [43] confirm the afore identified regionally available grid carbon intensity and the detour ratio (i. e. road circuity) as substantial drivers of UAM's carbon impact. In a macroscopic approach to modeling UAM's influence on urban transportation's carbon emissions, Pukhova finds little difference between scenarios with and without the operation of eVTOLs [44]. However, Pukhova's study is based on one particular Multi-Rotor configuration model developed by Shamiyeh et al. [45] and focuses solely on the vehicle's energy consumption [44].

2.2 Vertical Aircraft Conceptual Design

The design process of an airplane or rotorcraft always begins with a set of requirements, typically lined out by the customer or user of the aircraft. Ever since the Wright brothers first took flight in 1903, those requirements toward aircraft design have been subject to change. Throughout the past century, aircraft and helicopters were designed to serve increasingly varying missions and carry ever-heavier payloads, while continuously improving their flight envelope, capabilities, stability, and safety. The core mantra

of aircraft development in aviation's first decades was "Higher, Faster, Farther", resembling this strive for an increased capability and flight envelope [46]. The 1990s showed a shift of this paradigm towards the mantra "Better, Cheaper, Faster", representing the aim to maximize aircrafts' life cycle value through increased performance (*better*) at decreased cost (*cheaper*) at shorter development times (*faster*) [46]. With direct operating costs as the primary goal, and a significant contribution to those stemming from development and manufacturing of the aircraft, designs would be improved toward cheap manufacturing instead of decreased fuel consumption [47]. This left opportunities for improved environmental metrics only on an incremental basis [46], [47]. However, the past two decades led to a perception of climate change as an existential threat for societies and economies. Based on the global public pressure toward a more sustainable economy, some believe that the development of eVTOL heralds yet another paradigm shift in aircraft design. UAM's promise to provide a zero-emission transportation mode on the one hand and the undertaking of global leading aircraft companies like Airbus to develop hydrogen-powered aircraft on the other [48], demonstrate the importance of sustainability to the sector. With an ever-increasing need for higher efficiencies and higher capacities to manage the expected demand growth, sustainability has become an essential requirement in aircraft development [49].

2.2.1 Challenges in conceptual design

The process of designing an aircraft consists of the three phases conceptual design, preliminary design, and detailed design [50]. With a gradual increase of modeling fidelity over the phases they cover the scheme of translating the customer's requirements toward an aircraft into a vehicle design that can be manufactured, tested, certified, and ultimately utilized. Definitions on the specific tasks within each phase may vary between authors and are subject to the developer's capabilities, i. e. the computational power, which has significantly advanced over recent decades and facilitated the use of higher-fidelity analyses into earlier development stages. Sinsay thoroughly reviews rotorcraft advanced design and provides definitions of the design phases [51]. He states that the aim of conceptual design is to define an aircraft configuration to meet the system-level requirements, which are subject to constraints on economic and technology considerations [51]. Aware that vast uncertainties may be present in the conceptual design state, he constitutes that those economic and technological uncertainties "must be small enough to have high probability that requirements will be met" [51].

   Classic rotorcraft conceptual design is building on empirical methods to achieve high predictive accuracy in the early stages of the development process [51]. Empirical or semi-empirical methods have been traditionally used by authors such as Prouty and Layton [52], [53], but also more recently by Tishchenko et al., Rand and Khromov, Lier, Raymer, and Johnson [54]–[58]. Wirth points out how regression-based analyses are used to determine fundamental polynomial sizing laws, linking characteristic rotorcraft parameters to design parameters [10]. An example is estimating a helicopter's main rotor radius or empty weight by initially assessing the design gross mass, where the design gross mass itself is found through a multiple of the required useful load. He argues that

implicit definition of the configuration type and number of main rotors often reflects the design organization's expertise and proves effective and reliable if the envisioned configuration builds on tried-and-tested technology, but may lead to significant and potentially uncontrollable uncertainty in design space exploration beyond viable bounds [10].

Mavris et al. and Schrage first pointed out the limitations of traditional, deterministic design based on regression of historical data [59], [60]. Schrage states that "if new technologies, either product or process, are required for innovative or out-of-the-box designs then these historical databases must be replaced with more relevant data" and explicitly includes models outside the design domain, like Economic Life Cycle Cost Analysis [60]. Both mention higher-fidelity methods such as Computational Fluid Dynamics (CFD) or Finite Element Analysis (FEA) as potential ways to improve the design process and explore novel technologies, thereby predicting the trend towards more sophisticated and computationally expensive analyses persisting ever since [59], [60]. Today, it is arguably agreed within the aeronautical community that further evolutionary improvement is insufficient to meet future requirements regarding aircraft. For instance, Pornet et al. point out the need for disruptive technologies and revolutionary configurations [61]. Moore and Frederiks were among the first to consider and advocate such disruptive technologies in their work on the suitability of electric propulsion in aircraft [62]. They argue that, besides apparent limitations like the specific energy of batteries, designers and researchers have to consider the additional degrees of freedom facilitated by novel approaches [62].

Sinsay approves the call to make greater use of physics-based analyses in rotorcraft design, putting the problematic reliance on empirical approaches in rotorcraft design into a broader perspective [51]. He points out how building on existing solutions and mature technology with the aim for evolutionary progress has led to a divergence of capability advances and costs. On the one hand, the rate of progress regarding capability metrics in airplane and rotorcraft development has continuously decreased over the decades, as shown by McMasters and Cummings [63]. On the other hand, new configurations lack to sustain a further capability increase at rates that justify the respective increase of prices [51]. Sinsay argues that while novel configurations may break free from the evolutionary and limiting nature of regression-based design, the associated risks and uncertainties due to a lack of a priori knowledge could imply a substantial increase in prices and thus remove the economic case for designing [51]. Several authors advocate to reduce uncertainties in early stages by using higher-fidelity physics-based models facilitated by computational power, but early design stages often lack the data required for such models [10], [51], [63]. Sinsay expresses this dilemma of today's decision-makers, who are "left with the undesirable choice between pursuing novel designs, with greater uncertainty, which could meet or exceed requirements at an improved cost, or taking an evolutionary path with greater certainty, but with smaller potential improvement in performance and cost" [51]. The extraordinarily high funding of the many startups pursuing the development of eVTOL aircraft somewhat reflects the Sinsay's first option of choice from an UAM investor point of view. Given the presumed market potential, many are willing to take the risk that the development, operation, and acceptance of novel aircraft configurations may eventually fail. In contrast, the rather careful strategies pursued by

established rotorcraft companies of gradually developing technology demonstrators to assess technological readiness while using designs closer to their expertise clearly reflects Sinsays second option.

2.2.2 Methodological design approaches and trends

With new requirements comes the need for respective models in the design process and the need to embed those models in design frameworks [49]. Price et al. and Wirth advocate for an integrated design and analysis approach, in contrast to conventional, sequential development [10], [49]. Integrated Product Development (IPD), initially proposed by Olsson in the 1960s [64], is considered one of the best-known integration approaches to support product development [65]. Various comprehensive introductions to IPD have been provided, notably the works of Ehrlenspiel and Mehrkamm, and Vajna [65], [66]. IPD is a multidisciplinary and holistic approach to product development, which considers the product's complete life cycle. The main idea is to sustainably provide cost-effective products by including feedback from life cycle stages subsequent to the actual development. Embedded in the tension field between time, cost, and quality, IPD can substantially reduce costs due to shorter development times, more efficient production, and reduced quality issues [65]. The schematic depiction of life cycle costs in Figure 2.2 shows how costs, although largely incurring at later life cycle stages, are committed in the earliest development stages. Consequently, conceptual design offers the highest potential to save costs. One may logically conclude that the same applies to the environmental life cycle impact of a product, like GHG emissions.
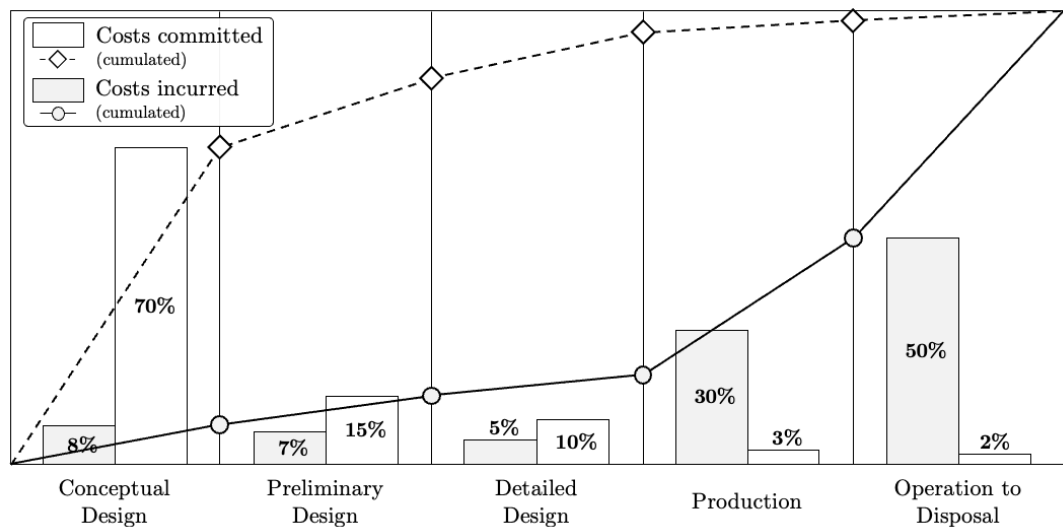
Figure 2.2: Committed and incurred cost of a product over its life cycle. Depiction adapted from [65]. Data from [67].

Wirth points out that, while integrated design methodologies have traditionally been applied in the space sector and find growing acceptance in the airplane industry, rotorcraft

development processes are slower to adopt such approaches [10]. However, one counterexample to this development is Schrage of the Georgia Institute of Technology, who developed, taught, and documented Integrated Product and Process Design (IPPD) for rotorcraft development [60]. Both Schrage's IPPD methodology and Wirth's approach to preliminary rotorcraft design, outlined later in this section, build on ideas of system decomposition and multidisciplinary analyses [10], [60]. As such, they overlap with Sinsay's proposed approaches to the design of vertical flight aircraft in light of the outlined challenges. Therefore the following provides a brief introduction to the ideas of Systems Engineering and Design Thinking, with a subsequent distinct introduction to Wirth's approach of the hierarchical, model-based preliminary design of rotorcraft.

Systems Engineering The complex task of aircraft design is often facilitated through Systems Engineering (SE). Several references provide overviews, introductions, and guidelines to the methodology, among those National Aeronautics and Space Administration (NASA), the International Council on Systems Engineering (INCOSE), and the International Organization for Standardizations (ISO) [67]–[69]. While NASA defines SE as a "methodical, multi-disciplinary approach for the design, realization, technical management, operations, and retirement of a system", INCOSE stresses SE's universality by providing multiple definitions and linking SE to systems thinking as well as keywords such as *interdisciplinary*, *iterative*, *socio-technical*, and *wholeness* [67], [68]. SE aims at fulfilling the needs of a system's stakeholders. To this end, SE describes hierarchies of and within systems throughout the complete life cycle of a product, comprising all stages from exploratory research to retirement of the product. It aims to manage complexity and change and thus gain control over Life Cycle Costs (LCC) development processes of complex products.
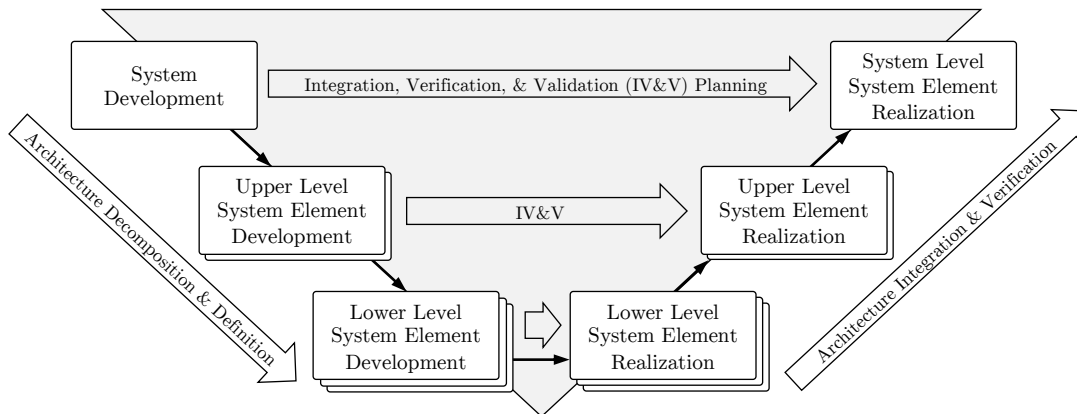
Figure 2.3: The V-Model in Systems Engineering, adapted from [67].

A common representation of the development process of a system within SE is the V-model, which is depicted in Figure 2.3. It depicts the systematic decomposition of a

system into its sub-systems, i. e. the definition and development of the systems architecture, on the descendant left side, followed by the system integration and verification on the ascending right side. The system requirements feed into the V-model at the top left. The system realization in the form of a final aircraft is in the top right. As Wirth points out, SE aims not only at finding a design capable of meeting its requirements, but also expands those requirements toward overall objectives such as cost-effectiveness of the system [10]. The design optimization toward cheap manufacturing as opposed to fuel efficiency in large aircraft developments of the 1990s, outlined by Kundu, is an example of an economic objective [47]. Exchanging the pure economic objective with an environmental one, like a low life cycle impact on climate change, exemplifies the application of SE in the scope of the thesis.

**Design Thinking** Design thinking is "a discipline that uses the designer's sensibility and methods to match people's needs with what is technologically feasible and what a viable business strategy can convert into customer value and market opportunity", according to Brown of Ideo, a design and innovation consultancy [70]. Instead of a well-documented outline and methodology like SE, design thinking reflects a mindset where developers find new designs facilitated by empathy, integrative thinking, optimism, experimentalism, and collaboration [70]. Nevertheless, as Sinsay points out, the concept of observing, understanding, synthesizing, and visualizing a problem, followed by the iterative design thinking core of prototyping, testing, and refinement shows similarities to the requirements decomposition, architectural breakdown and design, verification, and validation present in SE [51]. He points out the enormous potential of what he calls a "cut-and-try" approach in earlier aircraft developments, where the rapid prototyping and highly iterative development cycles led to successful, low-cost results [51].

Hierarchical, Probabilistic, Model-Based Design Motivated by the outlined challenges of the limited nature of classical, regression-based design approaches, the uncertainties associated with novel technical solutions, the need for higher-fidelity analyses in early design phases, and the necessity to provide for a structured multi-fidelity framework, Wirth proposes hierarchical, probabilistic, model-based design [10]. Building on SE ideas, he champions a harmonized decomposition and verification methodology to perform a deterministic system sizing through semi-empirical and model-based relations. The deterministic conceptual and preliminary design routines are embedded in a probabilistic scheme to form robust designs along increasing modeling fidelity, i. e. along the system's decomposition. The approach is largely motivated by Mavris' and deLaurentis' ideas to robustly predict technically viable and affordable aircraft systems through stochastic approaches, Schrage's work regarding the integrated product and process design (IPPD), as well as Krosche and Heinze's robustness analysis of the design of Short Take-Off and Landing (STOL) aircraft [59], [60], [71], [72]. The present thesis builds and extends on the work by Wirth; thus, this section elaborates further on (a) the different types and nature of uncertainties and (b) the approaches and ideas used in the preliminary works just referenced. As for (a), a comprehensive literature assessment is provided by Wirth. Building on the definitive work on uncertainty management pro-

vided by Walker et al. [73], Wirth concludes that engineering sciences lack a shared understanding of uncertainty [10]. Walker et al. give a structure to the matter of uncertainty, lining out that uncertainties appear in three dimensions: the *location*, *level*, and *nature* of uncertainty [73]. In that, the *location* resembles where the "uncertainty manifests itself within the model complex". Walker et al. describe that it may be beneficial to understand the location of uncertainty through generic maps, i. e. the context, the model itself, the model's inputs, or the parameters used to calibrate the model. Actual values are unknown in explorative scenarios like the assessment of future aircraft, which hinders a validation of the predicted values and determination of the prediction error. Walker et al. argue that the model's credibility can, nevertheless, be achieved by systematically describing the uncertainties. This can be done by categorizing uncertainties regarding their *level* from determinism to indeterminacy, along the stages of statistical uncertainty, scenario uncertainty, and recognized ignorance. Moreover, a distinction of uncertainties is possible by their *nature*, i. e. their cause. Epistemic uncertainty, caused by the lack of knowledge or data, can be mitigated by additional research and model refinement. Aleatory uncertainty, which is sometimes referred to as variability uncertainty and refers to the randomness of a system, cannot be reduced by the modeler [73], [74]. In his work, Wirth builds on the *nature* dimension and focuses on epistemic uncertainties due to their possible mitigation in the context of rotorcraft design. However, the task of designing and assessing future eVTOL configurations demands an additional emphasis on the *location* and *level* dimensions. Firstly, when modeling a multidisciplinary system at low fidelity, the modeler must understand how uncertainties within relatively small sub-systems can affect the overall result. Secondly, when combining disciplines of different breadth and depth, such as in eVTOL conceptual design and environmental assessment, the modeler needs to distinguish between statistical variability and different scenarios.
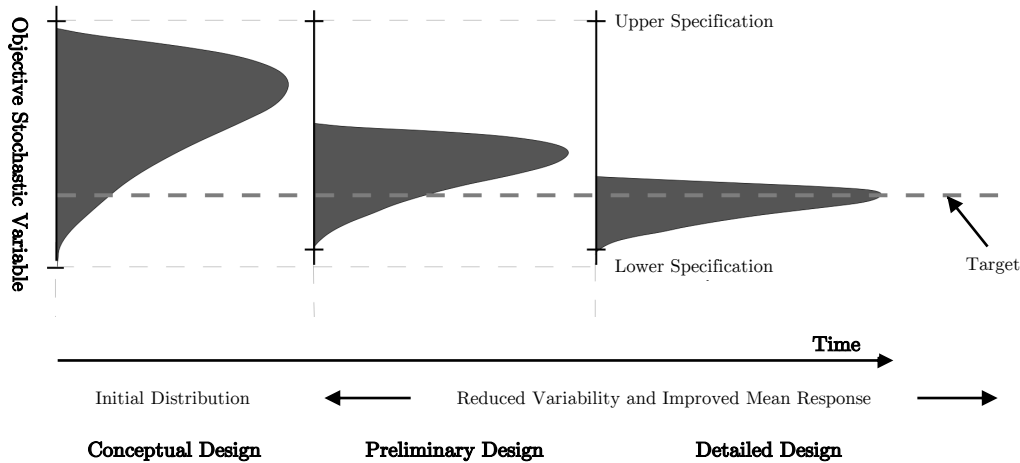
Figure 2.4: Evolution of product design objectives, adapted from [71].

As for (b), a core motivation of Mavris' and DeLaurentis' approach lies in reflecting not only traditional aerospace disciplines but also *life cycle* disciplines, such as economics, reliability, manufacturability, among others [71]. Methods and data within those disciplines exhibit various degrees of uncertainties, especially in early development stages, and amplified by innovation within and amongst the disciplines. Thus, Mavris and deLaurentis propose a probabilistic approach with a stochastic model that gradually reduces uncertainties concerning the system's objectives over its development stages and shifts its mean toward the targeted levels, as depicted in Figure 2.4 [71]. Schrage points out how the trend toward the inclusion of additional disciplines and probabilistic approaches, together with more computational effort in analyses, can quickly lead to a problem exceeding the scope and computational capabilities [60]. The framework developed by Wirth, which reflects the gradual uncertainty reduction outlined by Mavris and deLaurentis, executes a sizing job in seconds[8] on the conceptual fidelity level. If the model fidelity increases to the level of preliminary design, the same job can easily exceed hours or may not even be executable. A conceptual sizing and assessment methodology should therefore provide for an additional means of probabilistic analyses. Mavris and deLaurentis propose what they call "technology impact forecasting" to evaluate how technological advances may fare in future scenarios and support the idea by response surface equations. Response surface equations relate objectives like the emission of carbon equivalents to k uncertain input factors, providing the modeler with an option to identify influential factors that can be assessed through higher-level analysis or further sensitivity analyses [59].

2.2.3 Contemporary design tools, and applications

Many research institutions develop and apply conceptual design tools. The following provides a review of the most relevant endeavors and points out how the institutions draw on the approaches as mentioned earlier.

NASA Ames Research Center Arguably the most renowned and applied vertical aircraft conceptual design methodology is the NASA Design and Analysis of Rotorcraft (NDARC) framework, developed by Wayne Johnson of NASA Ames Research Center [58]. Besides the documentation and user manual, Johnson provides the theoretical groundwork behind the tool and architecture of the code [75] as well as validation and demonstration of the framework [76]. In an article published previously to the framework itself, Johnson and Sinsay discuss the requirements regarding a design and analysis framework to facilitate research and supporting rotorcraft acquisition from a government laboratory perspective [77]. They give special attention to the procedural placement of what they refer to as the information manager. The object holds all relevant information on the design, analysis, and optimization and ultimately executes the process. Only by such an information manager central to the various disciplines and tasks are multidisciplinary and multi-fidelity analyses enabled [77]. Building on the ideas of Johnson and Sinsay, NASA has integrated NDARC into a broader framework

---

[8]On a conventional quad-core desktop computer or notebook

of tools such as the Comprehensive Analytical Model of Rotorcraft Aerodynamics and Dynamics (CAMRAD) to establish a validated toolbox for multi-disciplinary design, analysis and optimization (MDAO) of vertical lift vehicles. Meyn presents the essence of the undertaking, reflected in the python-based software package RotorCraft Optimization Tools (RCOTOOLS), which incorporates NDARC and CAMRAD, within the multi-disciplinary optimization framework OpenMDAO [78]. Several publications on the technological capabilities of eVTOL aircraft in UAM use NDARC or RCOTOOLS.

The Boeing Company An early example of an integrated multidisciplinary design tool is the Rotorcraft Conceptual Design and Analysis (RCDA) tool suite developed within the Boeing Integrated Vehicle Design System (BIVDS) program [79]. As an early example for an MDO framework, it built on heritage methodologies within the distinct domains of the design and analysis problem. Based on the RCDA suite, Hirsh et al. perform parameter studies and demonstrate the ability of multidisciplinary analyses to cut development time by at least an order of magnitude if compared to traditional methods of passing data among the disciplines' designers [79]. Furthermore, Duffy et al. have developed a multidisciplinary design analysis & optimization (MDAO) tool to explore eVTOL and perform comparative cost assessments of electric and conventional eVTOL aircraft [36]. As a case study using the tool, they demonstrate the cost-saving potential of a potential Boeing eVTOL powered by future battery technology compared to state-of-the-art helicopters using piston and turboshaft engines [36].

German Aerospace Center (DLR) Building on the ideas of Lier, who proposed the formulation of an empirical basis for rotorcraft conceptual design, the German Aerospace Center (DLR) developed a toolbox capable of reflecting the rotorcraft conceptual and preliminary design process [56], [80], [81]. The multidisciplinary design process draws on many of DLR's computational tools and capabilities to facilitate the assessment of novel aircraft configurations [81]. However, based on DLR's latest publications, the framework remains heavily reliant on its empirical rotorcraft database to estimate basic geometric parameters. It does not allow to explore electric powertrains or distributed electric propulsion systems. It is thus deemed irrelevant to the thesis' scope.

The French Aerospace Lab (ONERA) Over the past decade, and as a collaboration between six research departments within ONERA, Basset et al. have developed the multidisciplinary rotorcraft design framework C.R.E.A.T.I.O.N. [82]. The "Concepts of Rotorcraft Enhanced Assessment Through Integrated Optimization Network" is similar [83] to the multi-fidelity approach laid out by Johnson and Sinsay in that it comprises the required modules within a framework over various levels of modeling fidelity. According to Basset et al., C.R.E.A.T.I.O.N.'s primary aim is to assess factors that limit a broader application of rotorcraft in urban areas, i. e. the environmental footprint of rotorcraft and the noise emitted in operation [84]. The tool is designed to be computationally lean by deriving surrogate database models. It intends to present the user with what Basset et al. describe as a "creation capability" in that it has a pseudo-random rotorcraft architecture generator, and features acoustics models already in early design phases [84]. Notably, Basset et al. perform sizing and analysis of a reference helicopter and tandem

configuration for an urban transport mission together with a comparative LCA. They report significantly reduced noise emissions and fuel consumption if the configuration is well adapted to the specific mission requirement. Current activities of ONERA are the extension of the numerical workshop toward designing eVTOL focusing on flight conditions in the case of failure of one more multiple thrusters [85]. Moreover, Russel and Basset provide a comparison of the ONERA framework to NASA's NDARC [83].

Stanford University SUAVE (Stanford University Aerospace Vehicle Environment) is an open-source, multi-fidelity conceptual design environment developed at Stanford University [86]–[88]. The framework is designed to analyze and optimize both conventional and unconventional designs by augmenting relevant correlations with physics-based methods instead of fixed empirical correlations [86]. Lukaczyk et al. outline the core principles and organization of the framework [86]. MacDonald et al. dive into the incorporation of higher-fidelity methods [87] and multi-fidelity use at constrained computational resources [88]. SUAVE's core motivation is to overcome legacy methods based on empirical correlations to model aircraft beyond what is "tried-and-tested", while at the same time reducing uncertainties as early as possible when exploring and developing novel configurations. SUAVE intends to give researchers the ability to contribute to today's explorative aircraft concept development, which is enabled by novel technologies and configurations [86]. Lukaczyk et al. point out three essential features of SUAVE:

1. An energy-carrier-agnostic powertrain formulation

2. An object-oriented code architecture implemented in Python to ensure arbitrary configurations and a collaborative effort of various researchers

3. An infrastructure that allows for integrating higher-fidelity modules if needed

By the latter, Lukasczyk et al. argue, SUAVE can use "the right fidelity at the right time", thus tackling the core of the rotorcraft design challenge outlined by Sinsay [51], [86]. Applications of SUAVE are the works of Clarke et al., who demonstrate the importance of identifying and quantifying the behavior of design variables and constraints at early design stages, and of Vegh et al. who compare and contrast the design frameworks SUAVE and NDARC [34], [89]. Clarke et al. perform a conceptual design and optimization task of Wisk's Cora concept. They add mission requirement parameters to the optimization design space to account for the outlined importance of the UAM design space. Various objective functions are evaluated, and lead to considerable variations in the mission design space variables depending on the optimization goal. They propose to include the mission profile early on in the design process and suggest a parallel optimization of eVTOL and mission design [34]. Vegh et al. perform the comparison of SUAVE and NDARC by modeling and analyzing the Cora configuration [89]. They report considerable differences in resulting aircraft geometries, system weights, and aerodynamic performance. To improve sizing result accuracy, they suggest higher fidelity analyses to boost model calibration and propose further work on aircraft design programs [89].

Massachusetts Institute of Technology Several aircraft conceptual design studies with a focus on either UAM [90], [91] or multidisciplinary design optimization [92], [93] have

utilized GPkit, a Python-based toolkit for geometric programming developed at the Massachusetts Institute of Technology (MIT), and presented by Burnell et al. [94], [95]. GPkit provides a model interface that translates this model to a numerical representation, solves the convex optimization problem, and parses the solution to return it to the modeler [95]. The key advantage of geometrical programming is its guarantee of finding a global solution, which comes at the expense of requiring formulations that may prove too restrictive for specific conceptual aircraft design problems. Kirschen et al. thus elaborate on GPkit's extension toward signomial programming, a related form of geometric programming [92]. Using signomial programming, York et al. propose a novel methodology for physics-based aircraft multidisciplinary design optimization (MDO). They prove the approach to be faster than competing MDO tools in solving a set of benchmark problems and demonstrate the method's reliability to evaluate both traditional and nontraditional aircraft configurations [93]. Regarding UAM, Gnadt et al. use GPkit in their design and analysis of a hybrid turbo-electric STOL aircraft [91]. Brown and Harris perform trade studies of different eVTOL configurations, searching for operating cost minima, extended by posterior semi-empiric noise assessments [90]. They find higher lift-to-drag ratios and higher disk loadings, i. e. a high efficiency in cruise flight and lower hover efficiency, to imply a lower weight and reduced operational cost. Vice versa, lower disk loadings at the expense of a reduced cruise efficiency yield lower noise emissions. As for costs, Brown and Harris identify the most decisive cost drivers to be pilot salary and battery amortization [90].

Other research institutions A wide variety of researchers put effort into the design, assessment, and optimization of novel aircraft configurations, such as eVTOLs, electric airplanes, and hydrogen-powered drones and aircraft: Among the most notable contributors to research on conceptual design of eVTOL in Europe are Bacchini and Cestino, of the Politecnico di Torino, Italy, who analyse eVTOL configurations [96] and discuss key aspects of eVTOL design [97]. Bacchini and Cestino provide a comparison of existing eVTOL configurations by estimating performance parameters using basic methods like Prandtl's lifting line theory and rotorcraft momentum theory [96]. They conclude that "winning" concepts may only be identified if the respective mission is fixed: While short ranged missions of up to 30 km are contested by Wingless, as well as Lift & Cruise configurations in terms of consumed energy and flight time, longer missions may best be served by Vectored Thrust configurations [96]. Bacchini further provides a comprehensive investigation of vertical aircraft, including early-era eVTOL, like the Harrier Jet and V-22 Osprey, and current developments including various alternative energy carriers, as well as a wind tunnel study on the effect of retractable lift propellers, in this doctoral thesis [98]. To this end, he develops a toolset based on analytical equations from momentum theory and elementary physics, which he refines by experimental data on electric ducted fan propulsion [98]. In his wind tunnel tests, he finds drag reductions for retractable propellers around 30%. He concludes that such a system may be well suited to increase cruise speed and range despite the respective additional mass of the required mechanical system and structure and the eventually higher battery mass [98]. To perform topology studies within the vast design space of eVTOL aircraft, Kränzler et al. develop and pro-

pose the simulation tool *AirCAD*, featuring aerodynamic analyses using blade element theory [99]. They compare Multi-Rotor, Lift + Cruise, and Tilt-Wing configurations at state-of-the-art technological readiness and find a minimum of the range specific energy requirement of all configurations at ranges around 20 km and 50 km for the Multi-Rotor and lifting surface configurations, respectively [99]. Regarding the development and optimization of STOL vehicles, Finger et al. [100] argue in favor of a hybrid propulsion system to meet the fundamentally differing system requirements of the distinct flight states, namely high power requirement in short take-off and lower but lasting power requirement in forward flight [101]. They show how the conventional design optimum at minimum installed *power-to-weight*, which results in the lightest aircraft, differs from optima in primary energy consumption and cost for hybrid STOL aircraft.

2.3 Sustainability of Aircraft

2.3.1 On sustainability

The thesis title prominently introduces the topic of sustainable aircraft development. But what is sustainability? In its 1987 report, the United Nations (UN) Brundtland Commission defines sustainability as "meeting the needs of the present without compromising the ability of future generations to meet their own needs" [102]. The 2004 UN General Assembly defines three "interdependent and mutually reinforcing pillars" of sustainability: *Economic development*, *social development*, and *environmental protection* [103]. Informally, the three are referred to by profit, people, and planet, respectively.

Figure 2.5: The United Nations Sustainable Development Goals.

Today's most prominent sustainability definition is reflected in the UNs 17 sustainable development goals by the United Nations Member States in 2015 as "a universal call to action to end poverty, protect the planet and ensure that all people enjoy peace and

prosperity by 2030" [3]. Of the 17, goal 13, *Climate Action*, is to harness policy, investment, and technology to limit a further increase of the global mean temperature to a maximum of two degrees above pre-industrial levels. However, other goals also reference climate in their sustainability context. For instance, goal seven, *Affordable and Clean Energy*, addresses the currently small share of renewable powers in the world's energy demand (17.5% as of 2017) and portraits how defining more rigorous policies could prevent over 40% of global emissions. Goal nine, *Industry, Innovation and Infrastructure*, points out the importance of renewable energy in light of increased urbanization, new industries, and information technology. Goal eleven, *Sustainable Cities and Communities*, further substantializes this, displaying how cities, while occupying only 3% of Earth's land, account for over 70% of carbon emissions [3]. Mitigating and ultimately stopping global warming is a core objective of the world. Despite the wider and varying definition of the term sustainability, the scope of this thesis thus understands sustainability in the outlined climate context and measures it by emissions of greenhouse gases (GHG). This reflects two of the four basic dimensions of sustainable mobility defined by Holden et al. [104]. However, an unequivocal quantification of whether a product or process is sustainable can not be provided, as no threshold exists below which an emission per functional unit is considered sustainable [104], [105]. Instead, the thesis uses the term in a deliberately qualitative way and in line with the idea of Holden et al.: An eVTOL may be considered sustainable if it satisfies a basic transport need without compromising long-term ecological sustainability [104]. The latter applies if its emission's order of magnitude is equal or lower than in ground-based transport modes.

2.3.2 Life Cycle Assessment

Life Cycle Assessment (LCA) is a methodology to analyze and quantify the environmental impact of a product or service throughout its life cycle. It is a *cradle-to-grave* perspective, including effects from the extraction of raw materials and product manufacturing and the product's use to its end-of-life treatment, i. e. recycling and final disposal [106], [107]. As such, LCA comprehensively assesses the effects of products or services on nature, human health, and resource consumption [106]. Besides the international standard, a range of secondary literature provides comprehensive information on the method [108]–[110]. Figure 2.6 depicts LCA's the four procedural phases according to the international standard: goal and scope definition, inventory analysis, impacts assessment, and analysis [107].

The first studies to perform LCA were published in the 1970s, often with a specific comparative aim to assess *product A vs. product B* [111]. Since the 1990s, fundamental methodological developments, international recognition, standardization, and a surge in the number of LCA studies took place [111], [112]. The past decade has seen a shift from purely environmental analysis toward a *planet-, people-, and profit*-oriented perspective to determine the overall sustainability of the assessed subjects [113]. Finkbeiner et al. and Guinée et al. proposed to move from a product-oriented focus to including an economy-wide perspective and couple LCA with LCC, thus performing Life Cycle Sustainability Assessment (LCSA) [111], [113]. Another widely regarded publication by
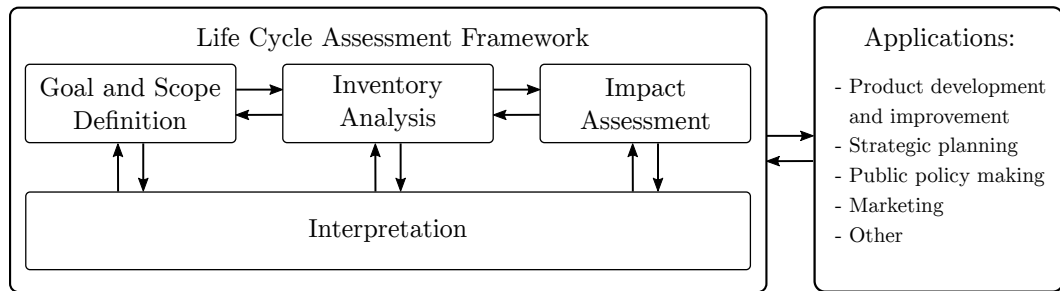
Figure 2.6: The Life Cycle Assessment framework. Adapted from [106].

Finnveden et al. reviewed trends and challenges and serves as a basis in this state-of-the-art section [112]. The remainder of this section will outline variations and challenges of LCA along the procedural phases shown in Figure 2.6.

Goal and scope definition. The first LCA phase requires decisions by the LCA practitioner, which substantially impact the results of the study [112]. While the goal should comprise the study's stakeholders and their intended use of results, the scope includes information on the product or service, its boundary, functional unit, allocation procedures, impact categories, as well as assumptions and limitations [106]. Finnveden et al. conclude three major differentiators within this phase: The distinction between *attributional vs. consequential* LCA, the importance of *scenarios*, and the role of *system boundaries and allocation* [112].

Attributional LCA yields a description of environmentally relevant physical flows over the system's boundary, while consequential LCA adds the perspective on how these flows may change through decisions caused by the LCA [112], [114]. The economic dimension of consequential LCA can be exemplified through Wright's 1936 study on the cost of aircraft, according to which a decision to invest in a technology will have effects on the future cost of the technology [115]. Other dimensions, such as the influence of average vs. marginal data, or the elasticity of supply and demand, can be found in the review by Finnveden et al. [112] and studies cited therein. Consequential LCA can thus become complex in their setup. However, multiple studies conclude that both attributional and consequential LCA are suited used to assess systems, especially if the systems in scope are yet to emerge in the future. [116], [117].

When modeling such a future system, the choice of scenario becomes relevant [112]. Börjeson et al. differentiate *predictive*, *explorative*, and *normative* scenarios, depending on whether the study aims to determine what will happen, what may happen, or how to achieve a specific target, respectively [118]. Predictive scenarios are either forecasts or what-if analyses; Explorative scenarios consist of external and strategic views; Normative scenarios may be viewed in light of their preserving or transforming nature [118]. In line with the thesis' aim and challenges, forecast-type scenarios and external explorative scenarios provide a practical perspective. Forecasts usually provide a defined set of data points or results, e. g. "low" or "high", but in contrast to what-if scenarios do not incorporate dependencies on other potential events in the future. External scenarios

typically focus on describing a situation further in the future and span the range of possible results, which may occur. Energy outlooks are a typical example. Forecasts and external scenarios both explicitly exclude potential actions at the hand of the study's user [118].

Three types of system boundaries are distinguished by Guinée et al.: A separation of a product from its environmental background; A separation of significant from insignificant flows; And a separation between the system in scope from related, but out-of-scope systems [119]. Finnveden et al. stress that while drawing a boundary between a product and the environment is usually straightforward, the associated life cycle inventory should always include all life cycle phases. Thus, if a battery, together with its associated flows of resources and emissions, is input or output to the system, the study should be referred to as *partial* LCA [112]. Defining the system boundary to separate significant from insignificant flows is generally considered difficult and poses the question, why available but insignificant data would not be included in a study for the sake of completeness [112]. For instance, studies on the sustainability of eVTOLs explicitly exclude impacts from the UAM infrastructure or vehicle production, arguing that they do not substantially alter the result [40], [41]. The third boundary type, a separation of systems in scope from outside systems, refers to the correct allocation of flows and impacts and is debated in several LCA studies [120]–[123]. The two styles of allocation in multi-functional systems, or *co-products*, are (1) the allocation of flows based on physical properties and (2) system expansion [120]. The main challenge allocating flows, i. e. of multiple inputs and outputs of a system, is to choose the determining parameter. Existing options are based on physical means like the associated mass and energy of the flow, or on economic means like the revenue of a product [124]. An example within the thesis' subject may add context: Compare a system where eVTOL batteries, after their effective capacity has decreased below a practicable threshold, go to a second life application in stationary energy storage, with a competing hydrogen-powered eVTOL where the batteries for the same stationary energy storage have to be produced or sourced from other inputs. Allocation of the battery system (option 1) would imply that the battery's production and end-of-life impacts are split over the eVTOL and stationary storage applications based on an appropriate allocation key. The assessment of the competing hydrogen-powered eVTOL would not be affected. A full system expansion (option 2) would require a consideration of possible battery sources for the stationary energy storage in the hydrogen eVTOL case. According to the cited literature and the author's best knowledge, there is no agreed-upon view in the LCA community as to whether and when allocation or system expansion should be preferred.

Inventory Analysis. The second phase of LCA aims at determining and quantifying the elementary flows into and out of the system. Its output is an inventory of flows which serves as a basis in the subsequent impact assessment step [110]. It is also possible to skip impact assessment and move directly to the interpretation, which is referred to as Life Cycle Inventory Analysis (LCI), or to combine the inventory analysis and impact assessment as suggested by Guinée et al. [106], [111]. Suh and Huppes distinguish six

approaches to compiling life cycle inventories [125]: Two process-based LCI, through setting up a flow diagram or an inventory matrix; One method using economic Input-Output Analysis (IOA); And three hybrid methods, combining process-flow LCI and IOA [125]. The remainder of this section lines out process-based LCI, as they are most common in LCA, and provides a brief introduction to IOA and views on when to use which type.

Setting up a life cycle inventory is considered a crucial yet cumbersome step in LCA [112]. Besides the collection and iterative refinement of data, the system at hand must be modeled to represent the respective flows [108]. Heijungs and Suh provide a comprehensive guide to the compilation, i. e. the algebraic representation of a basic inventory model and various kinds of extensions in LCA [108]. Within the comprehensive work of Hauschild et al., Bjørn et al. suggest a six-step approach to perform the inventory analysis [110]:

1. **Identify processes for the LCI model:** Relevant processes within the defined system boundary are collected and detailed to link them to databases or quantitative models. Starting from the reference flow in scope of the study, all required upstream and downstream flows are identified and depicted. Multi-functional flows are allocated or expanded, as outlined before.

2. **Plan and collect data:** Based on the study's scope, data for each identified flow is collected. Data specificity, i. e. accuracy, is best determined by the required importance of the flow in the analysis. Data sources can be measurements, models, scientific literature, database results, and expert judgements. Numerous databases are being developed and maintained by official entities as well as private companies.

3. **Construct unit processes and check quality:** In the third step, LCA practitioners should check collected flow datasets for completeness, i. e. the correct representation of inputs, outputs, and data quality, e. g. through verification of flow quantities.

4. **Construct the model and calculate LCI results:** Modeling a virtual and quantitative representation of the assessed system is typically performed by using specific LCA software, which is often available in connection with proprietary databases. This liberates LCA practitioners from implementing the underlying mathematical model.

5. **Prepare a basis for uncertainty management:** The use of Sensitivity Analysis (SA) and Uncertainty Quantification (UQ) methods helps to ensure statistical robustness of the study's results. As discussed, the topic is central to the thesis' methodology.

6. **Report:** To ensure quality and reproducibility, Bjørn et al. propose to follow a reporting scheme containing six dimensions: The LCI model at system level, the unit processes, metadata, the LCI results, assumptions regarding the life cycle stages, and documentations on the uncertainty management.

As mentioned before, a different approach to inventory modeling besides process-based LCI is to apply economic IOA or combinations of process-LCI and IOA, i. e. hybrid LCI [112], [126]. IOA bases on precompiled Input-Output tables that comprise monetary flows between an industry's sectors, thus linking industry sector interactions far upstream of the reference flow. Adding information on resource use and emissions to the sector's tables allows to approximate a product's or process's impact [127]. Finnveden et al. argue that pure IOA is often no alternative to conventional LCI due to a too coarse sector resolution [127]. According to Suh and Huppes, IOA provides a first estimate at best. They further limit the applicability of IOA to three factors: IOA allows assessments only at pre-consumer stage; It requires the amount of imported commodities to be negligible; And it only provides results on processes in the past, as it takes 1-5 years to collect and publish the respective Input-Output tables [125]. To counter those limits, hybrid approaches combining the broad perspective of IOA and product-centric view of process flow LCI have emerged [125], [128]. However, like pure IOA, hybrid IO-LCI are regarded unfit to provide a full picture for stand-alone applications and are considered the most time- and labor-intense types of inventory compilation methods [112], [125].
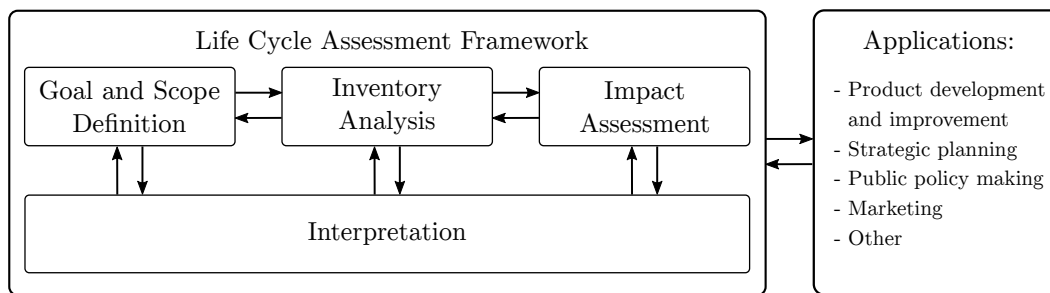
Figure 2.7: Life Cycle Impact mechanism. Adapted from [129].

Impact Assessment. In the third procedural step of LCA, the system's flows are assessed regarding their environmental consequence [106]. According to the international standard, Life Cycle Impact Assessment (LCIA) comprises the selection of impact categories, the classification of LCI result to those categories, and the calculation of indicator results, as well as optional actions regarding the scope and quality of the assessment [106], [107]. A brief review of the stages, based on the comprehensive work of Hausschild and Huijbregts on LCIA, is provided in the following [130]:

1. **Selection**: Impact categories, category indicators, and characterization models are selected in accordance with the scope and aim of the study. Impact categories are e. g. acidification, climate change, ecotoxicity, land use, water use, and particulate matter formation, among others. Within those categories, category indicators reflect the point of impact along the environmental pathway, depicted in Figure 2.7. In the case of climate change, early midpoint indicators are the measurable atmospheric concentration increase of greenhouse gases, the radiative forcing, or

the atmospheric temperature increase. In contrast, endpoint indicators are the loss of human life and ecosystem damage. The latter always resemble a choice of the *areas of protection*: Human life, Natural Environment, and Natural Resources. Lastly, characterization models provide the algebraic implementation of the impacts indicator, i. e. the amount of carbon equivalents in the case of atmospheric GHG emissions.

2. **Classification**: Results of the previously performed LCI are mapped to the selected impact categories.

3. **Characterization**: Flows from the LCI are amplified according to the category indicator. Simply put: The emission of $1\,\mathrm{kg}$ methane resembles $25\,\mathrm{kg}$ of carbon equivalents (CO_2e), and the characterization step is necessary to perform the respective multiplication.

4. **Optional steps**: To facilitate the subsequent interpretation phase, LCIA offers several optional steps. *Normalization* may be applied to bring scores of different impact categories to comparable levels, e. g. through an expression of the score in person equivalents per year. *Weighting* allows to compare reference products and processes in trade-offs, e. g. suppose fossil fuels are compared to bio-fuels under consideration of both climate change and water use. Weighting requires a manual setup of category factors based on the knowledge and preference of the practitioner.

The distinction between midpoint and endpoint categories is debated over within the LCA community: Aiming for an endpoint impact may appear much more tangible in some impact categories, like human toxicity, but undeniably increases the associated uncertainty of results by additional modeling [112]. Due to the high importance and ubiquitous discussion about climate change, this impact category is almost exclusively reported in the amount of GHG emissions, measured in carbon equivalents (CO_2e). Many LCA tools and databases allow access to integrated results for LCI and LCIA, like the swiss EcoInvent database [131]. Besides databases, scientific publications have become an important source of LCA data and are to the authors experience often more comprehensible than databases. They usually report LCIA results.

Interpretation. As the fourth and final step of LCA, the Interpretation phase aims to draw conclusions concerning the scope and goal of the performed study and give recommendations to the practitioner and reader [106]. According to the international standard, the interpretation phase should depict the relativity and reliance of results on utilized models and proposed assumptions [106]. As such, the importance of the assessment of uncertainties and the results sensitivities to input variation is evident. Hellweg et al. warn that especially the aim of completeness causes over-simplifications and uncertainties. They point out how, in future studies, refined resolution of regional data and accuracy can lead to more relevant and meaningful LCA results [132].

A variety of studies is exemplary for the handling and assessment of uncertainties in LCA [110], [133], [134], with a dedicated section provided by Finnveden et al. [112]. Notably, Finnveden et al. suggest that three distinct approaches may tackle uncertainties in LCA: The *scientific* approach, i. e. refining the model-fidelity and gaining access to data of higher accuracy, is regarded most valid but often not practicable, for instance when resources, such as the lead time toward a decision, are limited. The *social* approach, i. e. the discussion of uncertainties and unknowns with the LCA's stakeholders, can at best increase boost cooperation within the scientific community, but at the worst, give way to a higher valuation of opinions over facts. Therefore Finnveden et al. opt for a third option, the *statistical* approach, which does not alleviate uncertainties but incorporates them into the study. This is comparable to the robustness measures in rotorcraft conceptual design, that have been outlined in the previous section. The approach is applied by many practitioners [110], [133], [134], and has been adopted by secondary literature on the matter: Within the LCA handbook by Hauschild, Bjørn et al. suggest using Monte Carlo experiments using statistical distributions within the model's parameter ranges to account for uncertainties [110].

2.4 Electrochemical Energy and Power Sources

Three technological options exist for developing electrically powered vertical aircraft: Batteries, which are most popular in ongoing projects, fuel cells, and supercapacitors [135]. Several references introduce and compare electrochemical power sources [136], [137]. An easy-to-digest comparison of the potential of electrochemical power sources is the Ragone plot, as depicted in Figure 2.8. The ease comes at the expense of blending the fuel's chemical potential with the technological readiness of the respective means of energy storage and conversion, which is discussed in greater detail in Section 4.1. For now, the Ragone plot provides an overview of the two most critical parameters of power sources in aircraft applications. The *specific energy* determines the available energy per aircraft weight and is the limiting factor of flight endurance and range. The *specific power* determines the required weight of the powertrain architecture to provide the required power. While both are important in conventional and short take-off and landing aircraft, the latter is even more decisive in vertical aircraft, as the power requirement in vertical flight exceeds that in horizontal flight by far.

Figure 2.8 vividly demonstrates the supreme characteristics of combustion engines, like turboshaft or piston aggregates, using hydrocarbon-based fuels, i. e. kerosene. Both the specific energy and specific power of kerosene-powered combustion engines exceed that of current state-of-the-art electrochemical power sources. However, only a small minority of eVTOL intend to use this ostensible advantage in hybrid propulsion systems. The author is aware of research addressing potentially sustainably kerosene substitutes and additives like bio-fuels and electro-fuels [138]–[140]. However, as this thesis deliberately focuses on eVTOL aircraft and Distributed Electric Propulsion (DEP), such alternatives are neglected in the following.
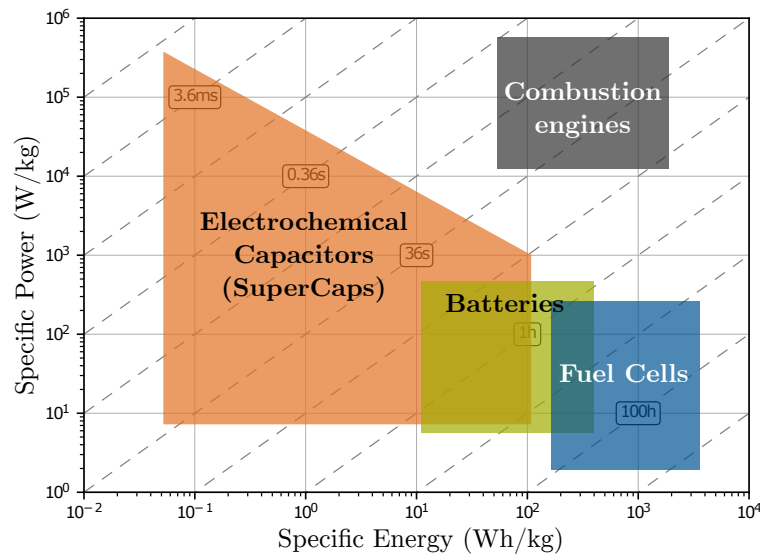
Figure 2.8: Ragone plot. Adapted from Winter and Brodd, and Misra [135], [136].

A sound classification of electrically powered aircraft concepts requires elaborating on the information comprised in the Ragone plot. Firstly, electrochemical power sources are still evolving and growing in capabilities despite rapid developments in recent years. Secondly, characterizing an application's power source alternatives requires to understand the implications and efficiencies within the application's technical system: Comparing fuel types to one another should be done on the level of effective technical specific energy, not on the level of chemical. Third, markets may change their decisive metrics over time, and applications of electrochemical power sources are determined by their technical capability as well as external factors like material and infrastructure availability. The following sections introduce and review the two most promising options for sustainable eVTOL aircraft: lithium batteries and hydrogen fuel cells.

2.4.1 Lithium batteries

The Lithium-Ion Battery (LIB) has become increasingly popular and a driver in the electrification of the transport sector due to its increase in specific energy (Wh/kg), energy density (Wh/L), and its decline in cell cost over the past decades [137], [141]. While the first commercially successful LIBs in the 1990s had a specific energy and energy density of around 80 Wh/kg and 200 Wh/L, respectively, those values have increased to 256 Wh/kg and 697 Wh/L in 2015 [141]. In the same period, cell prices have decreased about tenfold, from over 2.000 \$/kWh to around 250 \$/kWh in portable electronics and mobility applications [142]–[144]. The growth in specific energy of LIBs currently reaches its limits, with further gains limited to 30 % [142], [145]. Depending on size and application, prices for LIB cells are expected to further decline, possibly below 100 \$/kWh due to continued growth in cumulative battery production [143]. This section provides a brief introduction to common and next-generation cell chemistry types suited for eV-

TOLs and reviews the environmental impact of LIBs. It aims to provide a thorough understanding of the available and expected technology and its potential and challenges regarding its application in vertical flight aircraft.

Working principle and cell chemistries of state-of-the-art LIBs. Like all battery types, LIBs consist of two electrodes in contact with an electrolyte solution. Chemical energy is released via redox reactions at the anode and cathode, respectively the negatively and positively charged electrode [136]. The electrodes are separated by an ion-permeable membrane and are put into circuit by copper and aluminum current collectors. During discharge, positive lithium ions, stored within the anode grid, cross the separator toward the cathode, while electrons move through the conductor and produce an electric current. Commercial, state-of-the-art (SOA) LIBs consist of a graphite or graphite-silicon anode, a porous, lithium metal oxide cathode, and a liquid electrolyte to conduct the lithium ions. Various cathode types have evolved in recent years, providing different technical characteristics, like higher energy, power, or cycling stability [146]. They differ in their composition of lithium metal oxides:

Lithium cobalt oxide (LCO) cells, developed as early as 1980, commercialized in 1991, and considered the economically most successful type, are primarily used in electronics due to their high specific energy, good cycling stability and low-self discharge [145]. LCO cells are prone to thermal runaway. They are expensive due to the high amount of cobalt and are thus not suited for larger-scale applications like Electric Vehicle (EV)s and eVTOLs [144]–[146]. **Lithium manganese oxide** (LMO), also first commercialized in the 1990s, has a higher cycle stability of around $1,000$ to $1,500$ cycles, is less prone to thermal runaway, and is significantly cheaper than LCO, but provides less specific energy [145], [146]. Due to its reliability, it is used in current EVs, such as the Nissan Leaf, as well as in e-bikes, power tools, and medical devices [144], [146]. **Lithium iron phosphate** (LFP) is known for higher power density, higher thermal stability, and excellent cycling stability. However, LFP has the lowest energy density compared to other cathode materials [145], [146]. Like LMO, LFP cells do not contain the expensive and scarce cobalt, which makes them comparably affordable [144], [146]. Thanks to its high cycling stability of up to $2,000$ cycles, LMO cathodes find applications in batteries for e-scooters, e-bikes, and power supply systems [146]. Like LCO, **lithium Nickel Cobalt Aluminum oxide** (NCA) cells show high specific energy, but at lower cost, due to a reduced amount of cobalt. NCA is suited for automotive use and has been the choice in Panasonic's batteries for Tesla [145]. However, the high nickel content led to increased reactivity with electrolytes at higher temperatures. Thermal stability can be increased by adding manganese into the cathode material, as in **lithium Nickel Manganese Cobalt oxide** (NMC) cells. As NCA cells, NMC cells have a reduced cobalt share and are cheaper compared to LCO cells. They are manufactured in different element compositions and are used in EVs due to their high performance.

It is questionable whether any of the described cell chemistries provide the full range of requirements set by eVTOL engineers in terms of energy and power density, by certification agencies in terms of thermal stability, and by operators and investors in terms of business case infliction due to limited durability. Besides using state-of-the-art LIBs

in prototypes and technology demonstrators, it is likely that eVTOL configurations will largely build on novel cell chemistries as soon as they are commercialized [32].

Next generation battery chemistries. Several authors review and discuss potential advances of next-generation batteries, sometimes referred to as post-lithium ion batteries (PLIBs) [141], [145], [147]–[149]. In general, two approaches to advancing the current state LIB capabilities exist: First, by increasing capacitive performance through novel active electrode materials. Second, by using solid or gel electrolytes in contrast to liquid electrolytes, to facilitate more flexible and stable devices [147]. As for the first option, Berg et al. consider a combination of lithium and sulfur as cathode materials with high specific charge anode material, such as metallic lithium, as most promising to reach practical applications within the coming decade [145]. Table 2.1 provides an overview of expected cell types using a metal anode and various cathode chemistries, as collected by Cheng et al. [148]. The listed battery types are referred to as Lithium-Metal Battery (LMB) which reflects innovative anode material. As one representative of LMB, the most prominent next-generation cell chemistry is based on lithium metal and sulfur (Li-S). Today, a variety of issues put limits practical the application of LMB cells. One is the formation of dendrites on the lithium metal anode, which crucially cuts the battery's cycle life [149]. Realistically estimating the expected performance in terms of specific energy and energy density of various PLIB technologies is tied to standardized cell setups and consistent measurement protocols among PLIB researchers [141]. Placke et al. even rendered it unclear whether any of those technologies will succeed [141]. In contrast, manufacturers of LMBs, like OxisEnergy and Cuberg, claim to soon be able to provide the transportation sector, and especially the eVTOL industry, with LMBs capable of both high power and high energy density [150], [151].

	Li-intercalation cathode battery	Li-S battery	Li-O_2 battery	Refs.
Theoretical e_{spec} (Wh/kg)	<1,200	2,600	3,505	[148]
Practical e_{spec} (Wh/kg)	350	600	800	[137]
Cathode technology maturity	high	medium	low	[148]
Implementation duration after handling of Li-Metal issues	immediately	short time	long time	[148]

Table 2.1: Lithium-Metal battery types. Complemented from Cheng et al. [148].

The second option, often referred to as the development of all-solid-state batteries (ASSB), is believed to yield more safe, stable, and flexible energy storage devices [147]. However, as ASSBs do not use liquid electrolytes, a challenge arises from a comparably low ionic conductivity and interfacial electrode-electrolyte contact, ultimately resulting in lower power densities and a shorter cycle life [147]. A recent publication in nature energy by Randau et al. provides a comprehensive review of ASSB of different solid electrolytes and a variety of active electrode material combinations, including graphite and lithium-metal anodes, as well as lithium intercalation and lithium-sulfur cathodes. [152]. They report that, so far, no ASSBs reach energy density values comparable to

state-of-the-art LIBs. Moreover, ASSBs with lithium-metal anodes, which are considered a potential next-generation cell type, still lack sufficient power density: Even low currents lead to the aforementioned dendrite formation and the internal shorting of the cell [152]. Nevertheless, venture capital-backed company QuatumScope, aiming to supply electric cars with novel battery cells, claims to have solved the present challenges and promises to soon provide cells of up to 500Wh/kg energy density [153].

Environmental impacts of lithium batteries. Batteries allow electrically powered vehicles to operate free of local GHG emissions. However, the production of electricity itself and the production of batteries can cause considerable GHG emissions, which have to be included in the environmental assessment of electric vehicles. This section covers the latter through a brief review of literature that assesses and discusses GHG emissions associated with the life cycle of batteries, taking into account both scientific references as well as policy-oriented studies. A report by the World Economic Forum (WEF), prepared by consultancies McKinsey & Company and SystemIQ, points out the currently high environmental impact of the battery value chain. However, the report suggests that the associated GHG intensity can potentially be halved until 2030, despite the expected sharp growth in annual battery demand [154].

Philippot et al. perform an LCA based on the dismantling of a specific battery cell and find that the battery manufacturing process's electricity mix is most impactful regarding GHG emissions. Thus, they argue that high production capacity and an electricity mix with low carbon intensity can lead to a reduced impact, with a potential minimum as low as $39.5 \, \mathrm{kgCO2e/kWh_c}$ [155]. However, emission values of existing battery cells and production systems are usually much higher: In their 2011 LCA study, Majeau-Bettez et al. determine GHG emissions of NMC and LFP cell types at around 200 and $250 \, \mathrm{kgCO2e/kWh_c}$, respectively [156]. Those values are confirmed by Le Varlet et al., who report GHG emissions of NMC at $201 \, \mathrm{kgCO2e/kWh_c}$, LFP at $217 \, \mathrm{kgCO2e/kWh_c}$, NCO (with graphite anode) at $225 \, \mathrm{kgCO2e/kWh_c}$, and LMO at $220 \, \mathrm{kgCO2e/kWh_c}$ [157]. Emilsson and Dahlhöf as well as Regett et al. argue that the assessment must account for the potentially decreased carbon intensity of the used electricity and heat, and for a better production plant capacity [158], [159]. Based on various scenarios using renewable and fossil-fuel-based electricity mixes, Emilsson and Dahlhöf report a range of GHG emissions in NMC-type battery production from 61 to $106 \, \mathrm{kgCO2e/kWh_c}$. They verify the result by various other sources, such as studies by Kelly et al., who report $65 \, \mathrm{kgCO2e/kWh_c}$ based on a European supply chain and $100 \, \mathrm{kgCO2e/kWh_c}$ with a Chinese supply chain [160]. Regett et al. confirm the lower end with a GHG emission value of $62 \, \mathrm{kgCO2e/kWh_c}$ for an industrial battery plant run with renewable power, and $112 \, \mathrm{kgCO2e/kWh_c}$ the same plan run on coal, but point out how smaller-scale plants can lead to impacts of up to$212 \, \mathrm{kgCO2e/kWh_c}$ [159].

The referenced studies do not include effects from the end-of-life of batteries but perform deliberate *cradle-to-gate* analyses. Here, Emilsson and Dahlhöf reference the *Final Product Environmental Footprint Category Rules* of the European Commission, which state that 12 % of the GHG emissions of LIBs occur at the end-of-life stage [158]. The WEF report referenced at this section's beginning predicts that, by 2030, a total 54 % of

batteries could be recycled, but with only 7 % of raw materials substituted by recycling outputs [154]. However, as Bobba et al. of the European Commission Joint Research Center (JRC) analyses, many batteries used primarily in electric vehicles will find second-life applications. This can significantly reduce the GHG emission accountable to the use in the primary application [161]. The apparent variations and dependencies in the environmental assessment of batteries underscore the complexity of performing an LCA of a system that has yet to emerge. Concerning the assessment of eVTOLs, the thesis will therefore develop distinct scenarios based on the presented studies and imply significant uncertainties within those.

2.4.2 Hydrogen fuel cells

Of all known fuels, hydrogen has the highest specific energy $(33.3 \, \text{kWh/kg}^9)$ and is regarded as a clean, safe, and economically viable option for transportation and even energy storage [162], [163]. The working principle of a fuel cell was first described in 1839 by german scientist Christian Friedrich Schönbein [164]. Sir William Grove, a Welsh lawyer and scientist and today referred to as the "Father of the Fuel Cell", developed the first working prototype by 1842 [164]. The german-baltic chemist Friedrich Ostwald pointed out the technology's advantage over thermal engines, whose thermodynamic efficiency is inherently limited by the Carnot cycle. In 1894, he stated that "the path which will help to solve this biggest technical problem of all [...] must be found by the electrochemistry" [164]. However, it took until the US' spacecraft programs in the 1960s for the technology to find application. Batteries used by NASA in the Mercury program were deemed too heavy, thus critically limiting the payload, and were replaced by a Proton-Exchange Membrane Fuel Cell (PEMFC) in the subsequent Gemini missions.

Fuel cells have since found application in stationary power plants, submarines, and portable power systems [165]. Many mainstream sectors however did not pick up the technology beyond experimental scale until recently, when fuel cell technology increased in specific power and lifetime, while showing a decline in prices [166], [167]. The advance of fuel cell systems into new applications is prominently reflected in the automotive industry: Asian carmakers released Fuel Cell Vehicle (FCV) models Mirai, of Toyota, and Nexo, of Hyundai, while German automotive companies performed extensive research on the technology in concept vehicles [165]. Railway operation is another potential application of hydrogen fuel cell technology, especially since around 50 % of the German railway infrastructure is not yet electrified [168]. Hydrogen railroads have already been tested: Two trains manufactured by rail transport company Alstom have successfully serviced routes in the german state of Lower Saxony from 2018 to 2020 [169], [170].
A variety of projects focus on hydrogen-electric aviation: As for small-scale eVTOLs, researchers have developed and tested PEMFC-powered demonstrators and shown the potential to increase endurance significantly [171]. Other research comprises small passenger aircraft, like the project Hy4 of the German Aerospace Center (DLR) [172]. The project's spin-off *hy2fly*, as well as startups like the U.S.-based *Skai*[10] and the announce-

---

[9]Lower heating value
[10]See Section 2.1

ment of Airbus' hydrogen program *ZEROe* show the eagerness to bring the technology into commercial businesses [19], [48], [172]. This section introduces the basic working principle of hydrogen fuel cells, hydrogen storage, and the environmental impacts with the production of fuel cells and hydrogen. Interested readers find comprehensive reviews on the subject matter i. e. in the works of Abdalla et al. and Baroutaji et al. [171], [173].

Fuel cell type	Operating temperature (°C)	Ion	Applications
Alkaline (AFC)	50 - 200	OH^-	Space vehicles (e. g. Apollo, Shuttle)
Protone-exchange membrane (PEMFC)	30 - 100[11]	H^+	Vehicles, mobile applications and small stationary systems
Phosphoric acid (PAFC)	~ 220	H^+	Stationary, combined heat and power systems (CHP)
Molten carbonate (MCFC)	~ 650	CO_3^{2-}	Medium to large-scale CHP (up to MW)
Solid oxide (SOFC)	500 - 1,000	O^2-	All sizes of CHP (kW to MW)

Table 2.2: Hydrogen fuel cell types. Adapted from Dicks [164]

Working principle and challenges of fuel cells. Fuel cells are galvanic cells that convert chemical energy into electricity, i. e. a low-voltage direct current [164]. The process does not require additional mechanical work or thermal activation energy, but only fuel and oxidant supply to initiate the reaction. Fuel cells work similarly to batteries, with the fuel and oxidant resembling the electrodes, while the electrolyte may be either liquid or solid. Fuel cells are usually classified based on the used electrolyte. Various types have developed over time to satisfy distinct fuel cell specifications and applications. Table 2.2 comprises the types of hydrogen fuel cells. The Alkaline Fuel Cell (AFC) and PEMFC usually operate at lower temperatures and considered suitable for mobile and portable applications. The Phosphoric Acid Fuel Cell (PAFC), Molten Carbonate Fuel Cell (MCFC), and Solid Oxide Fuel Cell (SOFC) operate at much higher temperatures and typically power stationary applications [164].

In PEMFC, a solid polymer membrane allows the flow of hydrogen protons. The protons stem from a redox reaction of hydrogen at the fuel cells anode, which is initiated by a metal catalyst. At the cathode, oxygen reacts with electrons from the electrode and hydrogen protons from the electrolyte to form water. The two electrodes are connected, leading to a low-voltage direct current. This mechanism results in electric currents well below $1\,\mathrm{V}$. Thus it is common practice to *stack* fuel cells and put them in series. As the operating temperature of PEMFC is low compared to other fuel cell types, they rely on sophisticated catalysts to activate reaction at the anode. Historically, the catalytic potential in PEMFC is achieved by a high amount of platinum. Due to cost pressure, the platinum content was be gradually reduced in recent years. Accordingly, Wilson et al. of the US US Department of Energy (DOE) report the decline of fuel cell system

prices from 145 \$/kW in 2006 to 50 \$/kW in 2017. They estimate the ultimate stack price goal per *kW* at 30 \$ [174]. Whiston et al. assessed the cost, stack durability, and specific power of PEMFCs based on the elicitation of 39 experts [175]. They report that most experts regarded the DOE target of 30 \$/kW to be met by 2050, agreeing that the high platinum group metal loading poses a barrier [175]. Concerning ground-based mobility, Gröger et al. review and discuss in detail the cost contributions of components and confirm that platinum reductions will continue to reduce fuel cell prices significantly [176]. Regardless of the platinum content in PEMFC, Wilson et al. further point out a high sensitivity of prices to production volume [174].
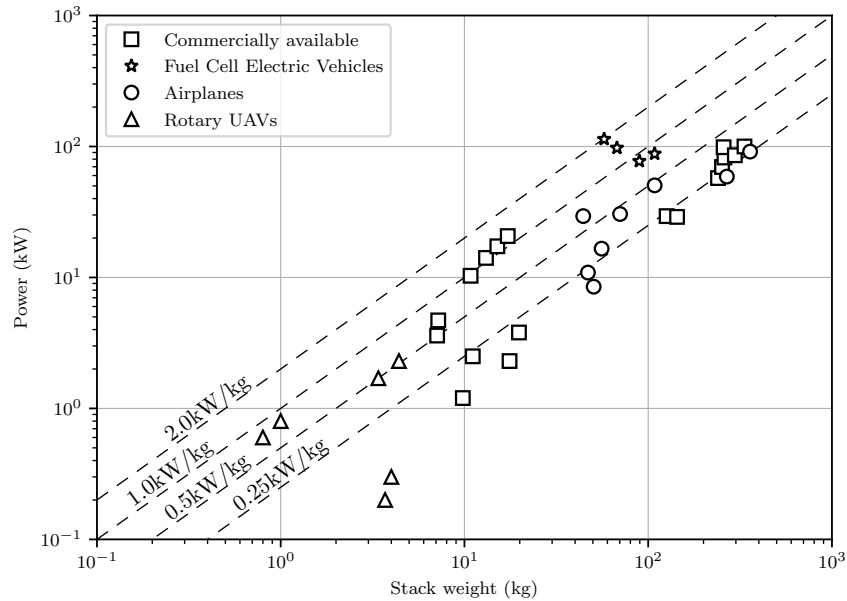
Figure 2.9: Power relative to stack weight of various fuel cells. Adapted from [177].

Challenges in hydrogen-powered PEMFC in aircraft are, besides general challenges such as cycle durability and cost, the system's weight and volume [171], [178]. Ng and Datta have collected data on the specific power of PEMFC for a range of cells that are either commercially available or used in various applications [177]. Figure 2.9 reproduces their collection. As shown, fuel cells are comparably heavy relative to their output power. For one, this is due to the fuel flow channel's and current collector's materials, mostly graphite and metals. Those components usually account for around 90% of the stack weight [179]. Furthermore, like batteries, fuel cells need auxiliary equipment to function, such as power and heat management systems, and pumps [180]. The difference between module-specific and system-specific power due to auxiliary devices is highlighted by Minnehan and Pratt of Sandia National Laboratories, a technology research institution [181]. According to their 2017 report, the highest specific power in commercially available PEMFC on module and system level are 2.97 kW/kg and 1.02 kW/kg, respectively [181]. However, note the respective module and system weights of 33.1 kg and 98 kg, implying limits regarding scalability [181]. Ning et al. mention a maximum specific

power of 2.0 kW/kg for a PEMFC stack declared by car company Toyota [180]. According to industry experts, the main challenges to improving specific power arise from high activation losses at the cathode and platinum-electrolyte O_2 transport resistance [175]. US-based company HyPoint claims to have demonstrated an integrated stack system in airborne applications with an effective power density of 1.0kW/kg. HyPoint aims to double this value with their next stack generation. As outlined before and due to higher platinum contents to achieve high specific power, prices for such a system will be around 100 to 500\$/Wh [182].

Storage of hydrogen. Arguably the most significant challenge in using hydrogen fuel cells in airborne applications is hydrogen storage. Hydrogen has a density of around $0.089 \, kg/m^3$ at atmospheric conditions. Reviews to common storage approaches of hydrogen are provided within the works of Abdalla et al., Baroutaji et al., and Rivard et al. [171], [173], [183] and within the publications of Bartélémy et al. on hydrogen storage and of Prewitz et al. on hydrogen in large civil aircraft [184], [185]. Storage of hydrogen can be fundamentally grouped into physical and chemical storage. Physical methods are the storage of gaseous hydrogen in high pressure tanks, usually either around 350 bar or around 700 bar, or the storage of cryogenic hydrogen [184]. Chemical methods comprise hydrogen storage in sorbents, metal hydrides, and chemical hydrides [186]. As of today, such chemical approaches are considered unfit for aircraft due to their slow unloading process, complicated heat management handling, and required treatment of by-products. However, researchers have demonstrated potential hydrogen mass fractions of 7.6 wt% to 18.4 wt%, and shown the technologies general viability, using a sodium borohydride to store hydrogen for a micro air vehicle [171], [185].

Like with chemical methods, many studies also question the ability of pressurized gaseous storage to provide the energy and volume density required by large civil aircraft [184], [187]. Baroutaji et al. report hydrogen mass fractions of 6.0 wt% to 6.7 wt% for gaseous storage at 350 bar and 700 bar, respectively. In the automotive sector, Hyundai Nexo, Honda Clarity, and Toyota Mirai reportedly accomplish 7.18 wt%, 6.23 wt%, and 5.70 wt%, respectively [178]. Rivard et al. stress the dependency of the actual mass fractions on the tank specification and application, pointing out the large gap between current technology readiness and the theoretical maximum fraction of 13 wt% reported by Züttel for a cylindrical tank at 200 bar [183], [188]. On the optimistic end is Val Miftakhov, CEO of the hydrogen aircraft company ZeroAvia, who states to use pressurized gaseous hydrogen with a mass fraction of 10 to 11 wt% [21]. He outlines how the alternative, the storage of liquified, cryogenic hydrogen at -253 deg Celsius adds unwanted complexity and leads to a potentially even lower storage fraction on system level. However, he believes that the achievable mass fraction of liquid storage is around 30 wt% on the tank system level. The actual density of liquid storage of hydrogen is highly dependent on the tank size, used tank material, and operational conditions, as Verstraete et al. find [187]. Their study on liquid hydrogen fuel tanks for large aircraft reports theoretical gravimetric storage densities of up to 70 wt% for a single, large tank. They point out how this theoretically high density is easily compromised by smaller tanks, as would be needed for eVTOL, or if effects like a holding period

before take-off are accounted for [187]. The technical publication of Sirosh of the U.S. DOE, published in 2002, reports a tank fraction of as little as 7.5 wt% for a tank that stores 5 kg of cryogenic hydrogen, giving a perspective the apparent differences [189]. Nevertheless, UAM company Skai claims to develop their hydrogen-powered eVTOL with liquid hydrogen storage [19]. Both the gaseous and liquid storage approaches, as well as uncertainties associated with tank mass fractions and required auxiliary devices are considered in the modeling of hydrogen-powered eVTOL configurations in this thesis.

Environmental impact of hydrogen. Converting hydrogen's energy into power in a fuel cell emits nothing but water and heat. However, hydrogen production, transport, compression, and storage can have a significant environmental impact, depending on the used feedstock and method [190], [191]. Traditionally, hydrogen has been produced from fossil fuels through i. e. steam reforming [173]. Today 76 % of annual hydrogen stems from natural gas steam reforming and 23 % from coal [162]. Conversely, around 6 % and 2 % of global natural gas and coal are used to produce hydrogen [162]. Nevertheless, hydrogen can be produced sustainably through electrolysis powered by solar or wind energy, and gasification of biomass [173]. The current share of renewable H_2 production is small but the number of clean production projects is increasing [162].

In an LCA of hydrogen-powered cars, Burkhard et al. find the GHG emissions associated with gaseous hydrogen from renewable wind power, compressed to 900 bar, including all relevant upstream processes, at $1.92\,kgCO_2/kgH_2$. Of those, 41% accounted for the construction of the wind turbine. Other upstream processes like electrolysis, compression, storage, and dispensing reflect 19%, 12%, 27%, and 1%, respectively, of GHG emissions. Burkhard et al. assume the electrolysis, compression, and dispensing as an integrated hydrogen refueling station, operated locally with only excess renewable power. They state that increasing the electrolyzer workload from 3.000 hrs to 6.000 hrs annually could reduce the total GHG emissions by 30% to $1.34\,kgCO_2/kgH_2$ [192]. In a similar assessment, Spath and Mann found a lower baseline impact of $0.97\,kgCO_2/kgH_2$. The lower impact is linked to the tank pressure of 200 bar instead of 900 bar and a smaller material consumption during the construction of the turbines. Spath and Mann argue how a reduction of the wind power system mass could further reduce GHG emissions for hydrogen production (i. e. $0.76\,kgCO_2/kgH_2$ if masses are reduced by 22%) [193]. In a study assessing hydrogen from solar-powered electrolysis, Cetinkaya et al. find total GHG emissions of $2.41\,kgCO_2/kgH_2$, of which 63% are due to the construction of the photovoltaic panels [194]. For the currently employed hydrogen productions from natural gas and coal, Cetinkaya et al. report emissions of $11.9\,kgCO_2/kgH_2$ and $11.2\,kgCO_2/kgH_2$, respectively.

3 Methodology

3.1 An Integrated Approach to eVTOL Design and Assessment

The core of this thesis is a framework capable of integrated conceptual design, analysis, and environmental assessment of eVTOL aircraft. This section serves as a primer and introduction to the methodology and incorporated models. It provides the reader with a view on modeling fidelity, an understanding of the architectural domains, and an introduction to the procedural framework of the method.

3.1.1 Preliminary considerations based on previous work

The computational framework developed for this thesis bases on the ideas described by Wirth [10]. Wirth proposes a hierarchical, model-based, probabilistic preliminary design framework for rotorcraft and eVTOLs. Fundamental adaptions of Wirth's approach provide a baseline for the thesis' methodology, with an added environmental assessment scheme to serve the thesis' objective. This section elaborates modeling considerations based on a sensitivity analysis of Wirth's conceptual design approach and results.
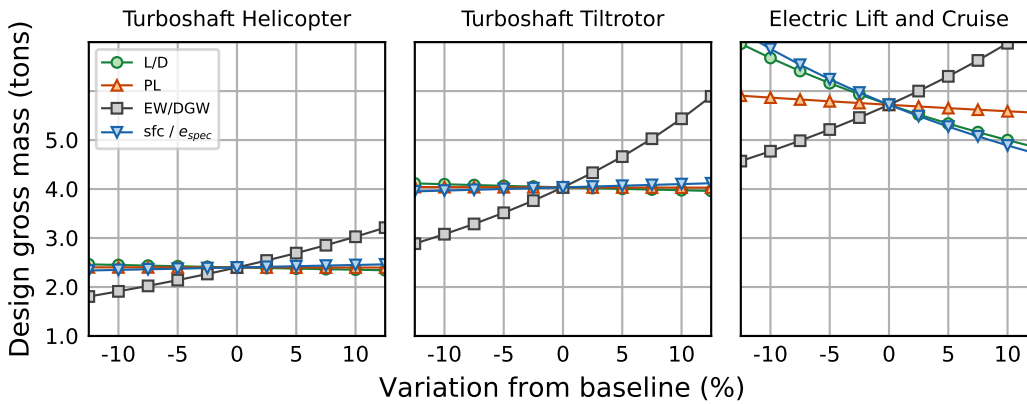
Figure 3.1: Sensitivity analysis of system-level metrics on design gross mass.

Figure 3.1 visualizes input sensitivities of system-level metrics on the Design Gross Mass (DGM) for a Helicopter and a Tiltrotor configuration powered by turboshaft engines, and a Lift and Cruise configuration powered by DEP. For the three configurations, the system-level metrics are the fraction of empty weight (EM/DGM), the power loading (PL) in vertical flight, i. e. hover, and the optimum lift-to-drag ratio (L/D) in horizontal flight. The turboshaft configurations are further determined by the specific fuel

consumption sfc. In contrast, the corresponding parameters for the DEP configuration are the cell-specific energy (e_{spec}) and the overall efficiency of the battery system (η_{total}). Of the latter two, Figure 3.1 only contains e_{spec}, as the sensitivities of both inputs mathematically coincide. Wirth refers to this model hierarchy as Tier 0, representing the lowest system decomposition level in his SE-based framework [10].

The sensitivity analysis builds on Wirth's UAM mission scenario but makes specific adaptions [10]. Payload mass increases to 444 kg resembling four passengers of 88 kg each and one crew member of 92 kg, according to a report prepared by EASA [195]. It resembles Wirth's payload mass of 442 kg from two passengers (2·90 kg), cargo (2·6 kg), and fixed useful load (250 kg). Flight time in hover reduces to 2 min from the 8 min suggested by Wirth. This assumption is considered valid as no minimum hover time is specified for eVTOLs within EASA's Special Condition [196]. It is further in line with reference works and eVTOL companies' publications, as outlined in Section 4.1. Publicly available eVTOL test flight videos suggest that transition to wing-borne flight is feasible within seconds. The design mission range is 150 km with a reserve of 20 min at cruise velocity. Table 3.1 lists design input parameters for the three reference configurations. In line with Wirth, the baseline values for L/D and PL represent the performance at atmospheric standard conditions of ISA+20 K [10]. The depiction in Figure 3.1 bases on one-at-a-time sampling around the parameters' baseline values.

Parameter	Symbol	Unit	Baseline Value		
			Helicopter	Tiltrotor	Electric
Cruise lift-to-drag	L/D	-	3.1	5.3	11.0
Hover power loading	PL	N/kW	46.5	37.5	40.5
Empty mass fraction	EM/DGM	-	0.735	0.809	0.47
Specific fuel consump.	sfc	kg/kWh	0.365	0.415	–
Cell specific energy	e_{cell}	Wh/kg	–	–	141.7
Propulsive efficiency	η	-	–	–	0.68

Table 3.1: Input parameters to Wirth's conceptual design framework [10].

Figure 3.1 supports Wirth's conclusion that the DGM of the Helicopter, Tiltrotor, and DEP configuration increases, respectively [10]. It further provides a new perspective on the high spread of the DGMs' distribution reported by Wirth. Based on his probabilistic approach, Wirth finds the statistical distribution of the DEP configuration's DGM highly spread, with the largest values over 8.000 kg. He accordingly states that eVTOL configurations are the least robust design candidate to serve the outlined mission. However, this must be accounted to the employed modeling fidelity. Adding up DGM deviations from one-at-a-time sampling with equidistant sampling intervals unambiguously increases the respective distribution's bandwidth. While the Tiltrotor's sensitivity to the EM/DGM ratio is noticeably higher than for the Helicopter, the DGM of the DEP configuration exhibits higher sensitivity towards not only the EM/DGM ratio but also to L/D and the cell-specific energy e_{cell} and propulsive efficiency η. Figure 3.1 motivates three requirements for the adaption of Wirth's framework:

1. **Refine modeling quality for the design's empty weight:** Figure 3.1 reveals a dominant influence of the configurations' empty mass fraction on their DGM. The regression-based preliminary design approach restricts eVTOL design, as novel configurations and alternative energy carriers are not reflected in conventional empty weight regression models. Furthermore, the empty weight of conventional configurations may be impinged by a mission-specific fixed useful load. In addition, the modeling simplicity and high baseline values of the empty weight fraction, roughly accounting for 50 % of DGM, implies how the sizing outcome is highly sensitive to the parameter. Therefore, modeling by empty weight fraction needs an appropriate data baseline. If such data is not available, a more detailed breakdown of a concept's empty mass needed, as is argued by Finger et al. as well as by Moore and Fredericks [62], [100].

2. **Refine data quality of the lift-to-drag ratio:** Figure 3.1 further shows how the DEP configuration's DGM exhibits a high sensitivity regarding the configuration's cruise efficiency L/D. In the conceptual design framework developed by Wirth [10], L/D is an input parameter, determined by the designer to his best knowledge and varied within an assumed uncertainty interval. The apparent high sensitivity of the DGM to L/D demands substantiation of L/D using physical models or empirical data. If both can not be provided at the chosen modeling fidelity, further sensitivity analyses to evaluate the uncertainty's implication on the result are imperative.

3. **Integrate appropriate-fidelity models for alternative energy carriers:** The sensitivity study presented in Figure 3.1 indicates notable differences in the relative influence of parameters among configurations differing in energy storage and conversion technology. As outlined, the DEP configuration exhibits a high sensitivity regarding parameters representing its powertrain, while turboshaft configurations show minor sensitivity on variations in specific fuel consumption. The implementation of alternative energy carriers into the present model thus needs to be carefully aligned with the choice of appropriate modeling fidelity.

As discussed, Figure 3.1 shows how the DEP configuration's DGM is sensitive toward L/D and e_{cell}. The battery mass is determined by its total capacity, which in turn is required to provide enough energy to deliver the specified mission envelope. Extending the conceptual design framework towards alternative energy carriers while maintaining a high level of generality thus demands a perspective on sensitivities regarding the objective mission: How do an increased time in hover flight or a shorter design mission range play out in different configurations? The SA in Figure 3.1 is performed with a fixed set of range, reserve, and hover time requirements. When seeking a robust configuration in conceptual design, SA must include variations of the design mission profile.

To this end, Figure 3.2 complements the SA by displaying the resulting DGM of the respective configurations for varying mission ranges and hover flight times. Range variations are displayed on the x-axis, while the curves represent mission hover times from 1 min to 3.5 min, shown by respectively brightening shades of blue. The orange x marks the baseline DGM for each configuration. Design input parameters are held
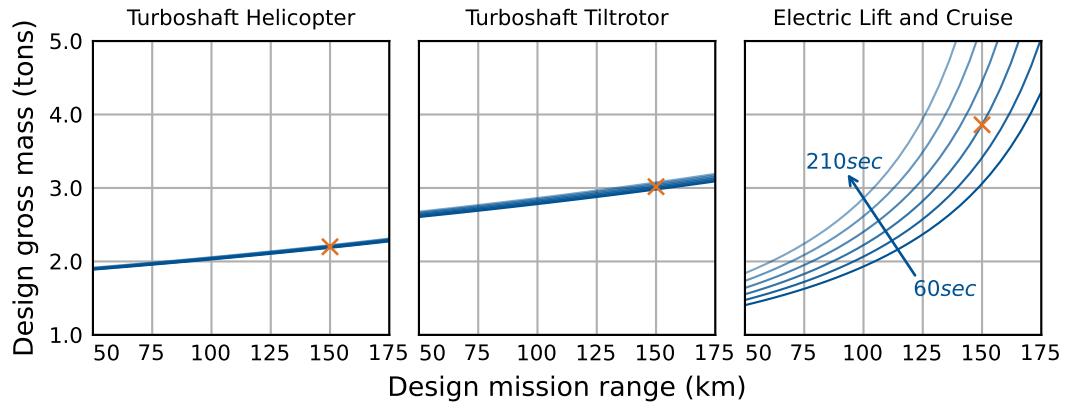
Figure 3.2: Sensitivity contour analysis of mission requirements on design gross mass.

at their respective baseline values, as listed in Table 3.1. As documented by Wirth, Figure 3.2 shows an increase of the baseline DGM over the three configurations from left to right. All three configurations show an increase of DGM with increasing range. While this increase appears to be relatively linear for the Turboshaft Helicopter and Tiltrotor, the Electric Lift & Cruise configuration exponentially grows with increasing range requirement. Variation of the required hover time has almost no effect on the Turboshaft configurations, while the electric version shows considerable changes in DGM. Notably, if the range requirement is decreased compared to its baseline, the Electric Lift & Cruise configuration turns out to converge at lower DGM than the conventional rotorcraft configurations. This is the case below a break-even at around $R = 0.5R_{baseline}$ and $0.8R_{baseline}$, for Helicopter and Turboshaft, respectively. Besides differences in the configurations' design parameters, the strongest differentiator of concepts is the fuels' specific energy. The exponential growth of DGM due to an increased battery mass at high range requirements indicates that the sizing point is close to the edge of what is physically possible with this configuration type and energy carrier. As the first result of this analysis, the findings of Wirth's study regarding the technical feasibility of eVTOL may be put under scrutiny. Secondly, two further considerations regarding the conceptual design and assessment of eVTOL are made:

4. **Recognize parameter uncertainties:** The apparent sensitivity of results toward parameter uncertainties in constantly changing inputs, such as the available cell-specific energy of batteries, demands considering and quantifying impacts of those uncertainties.

5. **Rethink mission requirements:** The choice of configuration and energy carrier is interdependent with mission requirements. Specifying a set of mission requirements and subsequently determining the ideal configuration is an unfit approach in a yet evolving and yet-to-be commercialized technology.

3.1.2 Architectural domains

It has been outlined by Wirth how Systems Engineering makes use of distinct architectural views [10]. Price at el. list five architectural views to engineering systems: The *requirements architecture*, comprising the customers' demands towards the system's capabilities; The *functional architecture*, resembling the system's functions to enable its requirements; The *physical architecture* as a representation of the relationship between entities within the system, i. e. how the sub-systems interact to fulfill the system's functions; The *technical architecture*, providing information on the interconnection and interdependence of elements of the system; And the *dynamic operational architecture*, which describes how the system's entities interact over time [197]. Wirth uses the former four of those five architectural views in his probabilistic design approach while collapsing the requirements and functional architecture [10]. The methodology developed in this thesis adapts the idea. In contrast to reproducing the classic domain definitions, this study deliberately defines its domains to represent the various parameter spaces within the broad scope of conceptual design and environmental assessment. The domains and the parameter sets they comprise are outlined and introduced in the following. The procedural framework, which organizes the domains' parameters and their model-based relations, follows subsequently.

The **requirements domain** holds information on what the stakeholders expect the eVTOL system to be capable of. A non-extensive list of requirements includes the system's technical capability to carry out a specific mission quantified by payload mass, range, velocity, time spent in hover flight, atmospheric conditions, and flight altitude. Legal entitlement to perform the mission through type certification is needed. Operators expect profitability, thus the cost of buying, operating and maintaining the system are included. As for public acceptance, noise emission levels are a crucial requirement. Ultimately, as motivated at the core of this thesis and central to the promise of UAM to provide clean transportation, one of the most crucial demands toward eVTOLs is the environmental impact caused over the system's life cycle. At its very core, the *job-to-be-done* by eVTOL aircraft is to transport a payload, mostly the customers, from one place to another, within a shorter amount of time than competing and mostly ground-based modes of transport. It is further a key requirement and even manifested in the vehicle classes name, that the eVTOL should be able to hover for a given amount of time. As such, the defining parameters describing the requirements domain in this framework are the *payload* (m_{pay}), the design mission's *maximum range*[1] (R_{req}), the needed *hover time* for a mission leg ($t_{hov,req}$), i. e. the time required in one take-off and landing cycle, the cruise flight *velocity* (v_{crs}). By default, no additional mission segments than a basic hover and cruise flight are assumed. However, users of the framework will find it procedurally easy to implement potential climb, descend, and maneuvering phases. A more detailed parameter set within the requirements domain implies the need for a similar modeling fidelity in other domains, otherwise the significance of the added data can hardly be validated. Clarke et al. emphasize the importance of detailed mission requirements and the high sensitivity of eVTOL aircraft's performance metrics toward mission parameters.

---

[1] An additional 20min loiter for emergency procedures may be included, see Section 4.1

The **design domain** provides the main interface to the system's designer. It comprises information on the aircraft configuration as well as on the energy storage and conversion type. As such, the design domain defined the configuration by a set of system-level design choices and associated parameters: The aerodynamic efficiency in cruise flight is described by the *lift-to-drag* ratio (L/D). Efficiency in hover flight is indicated by the *power loading* (PL), meaning the ability of the rotor or distributed propellers to generate a certain amount of force with a given amount of power. The *structural mass fraction* (f_{Struct}) defines which share of the aircraft's mass is necessary within the systems structure, i. e. the fuselage, wings, rotary lifting devices, empennages, nacelles, and so forth. Information on the weight of all other sub-systems, like avionics, controls, wiring, cabin, and auxiliary systems, is provided for through the *other mass fraction* (f_{Oth}).

The **technological domain** manifests design choices within the technical system based on technological readiness. In the context of the low-fidelity modeling approach used in the thesis, the technological domain depicts the energy storage and power conversion system characteristics. It covers the cell-specific energy (e_{spec}) of battery cells, their maximum possible degree of discharge (f_{DoD}), a factor describing weight losses due to packaging and management of the battery system (f_{BMS}); The fuel cell efficiency (η_{stack}) and hydrogen tank fraction ($f_{w\%t}$); And an empiric relationship between electric motor weight and the efficiency of the electric powertrain (f_{mtr}). Note that a mutually exclusive association of parameters to domains poses a challenge. The structural mass fraction, for instance, contains information on (a) the designers choice of configuration, i. e. whether the aircraft should feature lifting surfaces, as well as on (b) the technological readiness of materials and manufacturing capabilities, i. e. how lightweight the structure may be built, to still qualify for certification. Technically, the parameter could be divided into two parameters, one for each domain, to maintain mutual exclusiveness of the model's inputs. Rotorcraft design tools like NDARC provide this option, as they let the designer chose a wide range of *Tech Factors* to modulate sub-system weights. In alignment with the scope and right fidelity approach of this work, the author suggests refraining from unnecessarily increasing complexity for the sake of domain separation.

The **operational domain** contains information on the operation of the aircraft within the bounds of the maximum design mission. It holds the payload, number of passengers (n_{pax}), and the average seat utilization (f_{util}). Moreover, the domain allows analyzing how the aircraft performs if applied in an off-design mission, i. e. at higher or lower mission ranges (R_{ops}) and hover times ($t_{hov,Ops}$). In earlier publications, this thesis' author, as well as Brown and Harris, and Shamiyeh et al. stress how an eVTOL's performance, power requirement, and cost depends on such off-design conditions [37], [41], [45]. For instance, aircraft specifically designed for longer ranges, like *Joby* or "*Lilium*", can significantly divert from their average power design point due to a high share of power intense vertical flight if operated on shorter routes.

The **background system** covers all relevant information for the environmental assessment of the aircraft in scope, such as underlying energy grid carbon intensities ($\iota_{Electricity}$), hydrogen sourcing impacts ($\iota_{Hydrogen}$), the aircraft material's sourcing impacts or the aircraft's life expectancy.

3.1.3 Procedural framework

Figure 3.3 depicts the procedural framework of the developed methodology. Five steps comprise the scheme, two of which may be omitted if analyses require no statistical evaluation. Users of the code may adapt and extend the framework to their needs. Code development follows a stringent data container structure and interfaces definition, facilitating future use and adaption.
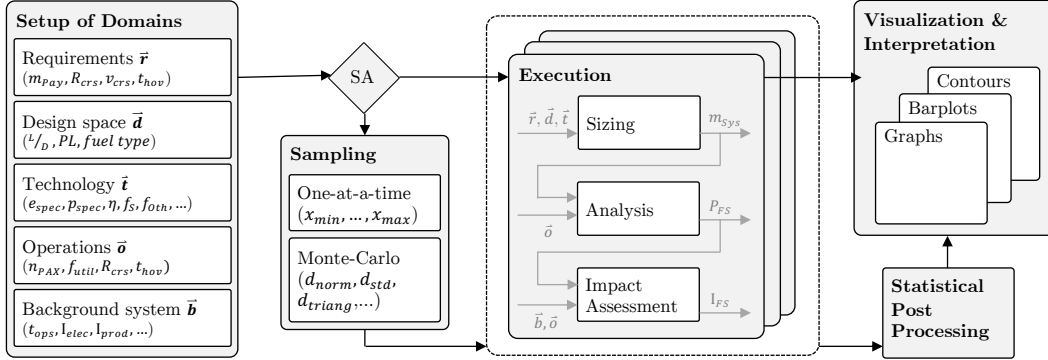
Figure 3.3: Procedural representation of the developed methodology.

- **Setup of domains.** The five domains that describe the system are instantiated and initialized. The domains cover the requirements toward the aircraft capabilities, the design space for the aircraft designer, technological capabilities and constraints, operational settings and schemes, and information on the background system. Not all domains are mandatory in every execution of the framework, depending on the intended execution modules. For instance, an isolated sizing, i. e. conceptual design task does not require information on the operational scheme and background system. Analogously, an impact assessment task of a known configuration does not need previous sizing and analysis of the concept. It is sufficient that the data container holds the parameters required for the demanded task.

- **Sampling.** Running the framework to perform either sensitivity analyses or to evaluate core tasks in a probabilistic fashion requires a sampling of parameters before the execution. Two sampling types are distinguished: One-at-a-time sampling schemes function as a wrapper around the deterministic core of the model. They perform a repetitive execution by alternating one parameter to a distinct value and resetting the parameter to its baseline. Monte-Carlo sampling methods perform hundreds our thousands of model evaluations with random parameter draws based on the distribution type (i. e. uniform, normal, triangular) and predefined distribution interval. The number of system executions can quickly grow to large sets and can induce performance problems depending on the fidelity level of implement models. As Wirth demonstrates, quasi-Monte-Carlo methods such as latin hypercube sampling can compensate an increased effort.

- **Execution.** The three models at the framework's core perform sizing, analysis, and impact assessment tasks. They build on the results of one another. For instance, the analysis module requires data on system masses, and the impact assessment requires data on the aircraft's power consumption in its flight states. It is certainly possible to independently execute the modules, given that the domain data containers provide the required parameters. The sizing module's nucleus of finding a mass equilibrium of an eVTOL's systems and yield the eVTOL's DGM is outlined in the following section. However note, that the framework can yield the system's equilibrium for any other parameter within the domains. The user may determine the maximum cruise range based on the eVTOLs DGM or the minimum cell-specific energy required by a predefined eVTOL to perform a given mission.

- **Statistical Post Processing.** The framework supports statistical evaluation methods to facilitate evaluating the model's probabilistic execution. As the framework is implemented in *Python*, multiple libraries are available to support and visualize this statistical distribution. This thesis evaluates median values as well as 95% confidence intervals.

- **Visualization & Interpretation.** A defined set of plotting routines supports visualization of the results of the method's execution, each build to function in a plug-and-play manner. The visualization of statistical distributions in this thesis uses bar plots for median values and error bars to display the impact of uncertainties by confidence intervals.

3.2 Conceptual Design

3.2.1 System decomposition and performance

At its core, the methodology solves the model-based mass equation of the aircraft's systems, as outlined in Equation 3.1. Numerous scientific publications dealing with the conceptual design of eVTOL perform similar approaches, among them Wirth and Hajek, Brown and Harris, and Ng and Datta [10], [37], [198], [199]. The aircraft's design is obtained at the equilibrium of its DGM and the sum of its system's masses, which are functions of DGM. The aircraft's systems are its structure, including the fuselage, wings, rotors, propellers, and empennages; The powertrain group, including all means of power conversion, such as engines, electric motors, fuel cell stacks, and drive systems; Other components, such as flight controls, instruments, avionics, and the cabin; The energy storage system, which consists of either a battery pack including a Battery Management System (BMS), packaging and cooling, or of a hydrogen power system including the tank and the fuel itself; And the useful load, comprising payload, i. e. passengers and baggage, and crew. Respectively, the systems' masses are m_{Struc}, m_{Ptr}, m_{Oth}, m_{Ener}, and m_{Pay}. This segmentation follows the system decomposition of Johnson, which is performed by NDARC [58].

Solving Equation 3.1 requires inputs from the requirements domain, design domain, and technical domain. Mission requirements, i. e. the maximum range, cruise speed, and

hover time of the aircraft, dictate the concept's power and energy requirements. Technological readiness defines to which extent the aircraft's system can fulfill those energy and power requirements. Design choices determine how well the technological potential is leveraged to fulfill the mission requirements. Through models, those domains' parameters yield the system's masses.

$$m_{DGM} = m_{Empty} + m_{Ener} + m_{Pay} = m_{Struc} + m_{Ptr} + m_{Oth} + m_{Ener} + m_{Pay} \quad (3.1)$$

Empty weight modeling fidelity. The state-of-the-art approach to modeling the aircraft's empty mass as a fraction of the total mass by utilizing legacy concepts through the empirical empty mass fraction has several shortcomings, as discussed before. Therefore, this thesis breaks down the empty mass into structural mass, powertrain mass, and other components mass, see Equation 3.1. It aims to limit the sensitivity of the aircraft's mass toward uncertainties, allow a representation of various energy carriers in modeling, and account for use case-appropriate component weights.

The thesis builds on the approach outlined by Ng and Datta, who suggest a refined, yet also empirical formulation for the structural and other masses [198], [199]. Structural mass is calculated as $m_{Struc} = f_{Struc} \, m_{DGM}$. The mass of other components is compiled by $m_{Oth} = f_{Oth,Pay} \, m_{Pay}$, thereby deviating from Ng and Datta's formulation $m_{Oth} = f_{Oth,EW} \, m_{Empty}$. The rationale is to fully decouple the mass of other components from unrelated influences of i. e. the batteries' specific energy and describe it purely in terms of the underlying business case: the transportation of passengers at a certain level of convenience. Ng and Datta themselves reference Harris, who suggests $f_{Struc} = 0.24$ for modern, weight-optimized helicopter configurations. They further assume $f_{Oth} = 0.3$ [177], [200]. Using the structural weight fraction of *best-in-class* helicopters for a novel aircraft configuration is still imprecise. Uncertainties regarding the structural masses fraction are mitigated by comparing the factors to mass fractions resulting from the next higher fidelity level frameworks. Table 3.2 comprises values for the two parameters based on eVTOL reference models provided by Moore and by Silva et al. through NASA [32], [201], and developed by Vetter in a student thesis supervised by this thesis' author [202]. NDARC calculations use the referenced models that can be downloaded from NASAs website. In addition, Table 3.2 provides the calculated fraction of other component masses in relation to the useful load (m_{Oth}/m_{Pay}), to project the actual weight of other masses in electric eVTOL configurations.

At values ranging from 0.252 to 0.306, the structural mass fractions shown in Table 3.2 are slightly higher than the proposed $f_{Struc} = 0.24$ for *best-in-class* helicopters. Comparing the four configurations introduced by Moore and Silva et al., one finds approximately 5% higher fractions for fixed-wing aircraft NASA [32], [201]. The *"CityAirbus"* model developed by Vetter also results in a relatively high fraction of 29.2%. Of course, the underlying NDARC models, i. e. the NASA AFDD mass formulations for components, are empirical themselves. At 0.135 to 0.223, the depicted empty weight-based fractions of *other* masses in NDARC configurations are lower than the assumed 0.3. Respective

Subject	m_{Struc}/m_{DGM}	m_{Oth}/m_E	m_{Oth}/m_{Pay}	References
Assumption Ng & Datta	0.24	0.3	-	[198], [199]
NDARC *Uber eCRM*	0.305	0.223	0.617	[201]
NDARC *Lift+Cruise*	0.306	0.135	0.554	[32]
NDARC *Quadrotor*	0.254	0.152	0.579	[32]
NDARC *Side by Side*	0.252	0.187	0.534	[32]
NDARC *Quad-Coax*	0.292	0.188	0.711	[202]

Table 3.2: Assumed and calculated structural weight and other weight fractions.

values of the payload-based other masses fraction range from 0.534 to 0.711. The indicated value intervals will serve as a baseline in the application of the methodology. However, correctly predicting system masses, especially on lower fidelities, is acknowledged to be highly prone to error. Therefore, the provided data set is subjected to statistical uncertainties in its application in Section 4.1.

Vertical lift aircraft system efficiencies. The aircraft's energy carrier and powertrain are determined according to the vehicle's power requirement in its flight states, the time spent in the individual flight states, and the systems' efficiencies. Power requirements for flight in hover and cruise are calculated based on the aircraft's system-level metrics. Those are the power loading (PL) and the lift-to-drag ratio (L/D) as outlined in Equation 3.2.

$$P_{hov} = \frac{m_{DGM}\ g}{PL}, \ P_{crs} = \frac{m_{DGM}\ g\ v_{crs}}{L/D} \tag{3.2}$$

Power requirements of the individual flight states are possibly combined to an average power consumption based on the relative time share spent in hover-like flight f_{Hov}. The average power consumption is of specific interest if off-design operation conditions are analyzed, as it may strongly influence results referenced to a certain functional unit.

$$P_{avg} = P_{hov}\ f_{Hov} + P_{crs}\ (1 - f_{Hov}) \tag{3.3}$$

Some eVTOL concepts use ducted or shrouded fans, which can significantly alter the required induced power in hover flight. Building on the simplifying assumption that the required hover power of such Ducted Vectored Thrust configurations largely equals the induced power, the effect of a fan shroud is accounted for by the wake contraction ratio a_w as outlined by Leishman [203]. The hover power is corrected according to Equation 3.4.

$$P_{hov,shroud} \approx P_{hov}\ \frac{1}{\sqrt{2\,a_w}} \tag{3.4}$$

3.2.2 Electrochemical energy and power sources

Electric motors. The formulation of the electric motor weight follows an evaluation performed by Ng and Datta [198], who examined 17 different AC permanent magnet

synchronous motors developed for application in aircraft. They report the relation shown in Equation 3.5.

$$\ln m_{Motor}(\text{kg}) = -0.89 + 0.89 \cdot \ln P(\text{kW}) \tag{3.5}$$

They show how the motor weight of aerospace motors is within a 30% error band from the given relation and that weights are generally lighter than motors developed for non-aerospace applications [198]. However, they do not discuss the potential effects caused by required redundancies in aerospace applications.

Batteries. The mass of a battery system is determined by the required electric capacity C, the voltage U, and the specific energy e_{Batt} of the battery cell.

$$m_{Batt} = \frac{C_{Batt}U}{e_{Batt}} \tag{3.6}$$

Capacity is defined as the capability of a cell to provide a current i over a time t, and denoted in *ampere-hours* (Ah). The effective capacity of a battery depends on the current draw, called the C-Rate ζ_{Batt}, and on the battery's cycle age and temperature: C_{batt} declines with increasing cycle count and at higher current draws. The latter effect is referred to as Peukert's law [204], [205] and the effective capacity may be described by Equation 3.7, where τ is the battery rating, and n is the type-, age-, and temperature-variant discharge parameter.

$$C_{Batt} = i \, \tau \, \left(\frac{t}{\tau}\right)^{1/n} \tag{3.7}$$

In any given flight state, the capacity must suffice to provide the required power over the time t spent in that flight state, without exceeding its maximum discharge current expressed by the $C - Rate$ [198]. That is, both the respective power and energy have to be provided by the battery. Inserting Equation 3.7 into 3.6 for all k flight states, while accounting for the discharge current constraint and for power losses during discharging η_{dis} and at the electric motor η_{mtr}, leads to Equation 3.8. Fully discharging the battery would be highly detrimental to its cycle life and is usually avoided [206]. The depth of discharge f_{DoD} parameter is introduced to account for the surplus battery mass.

$$m_{Batt} = \frac{1}{e_{Batt} \, \eta_{dis} \, \eta_{mtr} \, f_{DoD}} \sum_k \max\left(P_k \, \tau \, \left(\frac{t_k}{\tau}\right)^{1/n}, \frac{P_k}{C - Rate} \right) \tag{3.8}$$

The battery mass calculated by Equation 3.8 represents the mass of the integrated battery system, comprising single battery cells, combined to modules and battery packs, equipped with a BMS. The used effective specific energy of the battery is determined from the cell-specific value and the BMS' efficiency through $e_{Batt} = e_{spec} \, f_{BMS}$.

Hydrogen fuel cell systems. The hydrogen fuel cell system consists of the fuel stack, its cooling system, and a power distribution unit. The mass of the PEMFC, together with its support units, is calculated based on the specific powers of the three systems as presented in Equation 3.9.

$$m_{PEMFC} = m_{stack} + m_{cool} + m_{pdu} = \frac{\max\left(P_{crs}, P_{hov}\right)}{p_{fc,eff}\,\eta_{mtr}} \tag{3.9}$$

Hydrogen is stored in tanks and reduces in mass during operation, which is expressed using Breguet's range equation to determine the required fuel mass. Hydrogen fuel masses for a given mission of range r, based on the aircraft's gross takeoff weight at the beginning of a mission m_{DGM} is calculated using Equation 3.10. In that, the hydrogen's specific energy is expressed by e_{H_2} (kWh/kg) and efficiencies include the electric motor η_{mtr} and the fuel cell stack η_{fc}.

$$m_{H_2,crs} = m_{DGM}\left[1 - \left(\exp\frac{r\,g}{e_{H_2}\eta_{fc}\,\eta_{mtr}{}^{L/D}}\right)^{-1}\right] \tag{3.10}$$

Similarly, Equation 3.11 describes the calculation of hydrogen fuel mass consumed in hover and hover-like flight states. Like in cruise flight, the onboard mass of the fuel reduces with every time unit spent in hover; thus, the equations are inaccurate in that they slightly overpredict the required hydrogen mass in hover flight. However, hover times in the context of a UAM mission are expected to be short compared to cruise times. Further, as Rudzki showed in his thesis supervised by this work's author, the beneficial effect of the system weight's decrease over a mission is comparably small, as hydrogen is very light compared to the time-invariant tank weight [207].

$$m_{H_2,hov} = \frac{P_{hov}\,t_{hov}}{e_{H_2}\,\eta_{fc}\,\eta_{mtr}} \tag{3.11}$$

Concluding the model formulation on the hydrogen powertrain, Equation 3.12 determines the tank weight. The tank mass is typically calculated based on the required fuel mass and a fraction representing the fuel-to-fuel system ratio.

$$m_{tank} = m_{fuel}\left(\frac{1}{f_{w\%t}} - 1\right) \tag{3.12}$$

3.2.3 Powertrain hybridization

Despite the numerous advantages of batteries and hydrogen fuel cells, they share a challenge: Relative to their weight, they are either suited for high power output or for high energy output. However, eVTOL require sufficient power to vertically take-off, hover, and vertically land, as well as sufficient energy to fulfill their flight envelope. Therefore, power sources are likely to be combined in hybrid powertrain architectures [101]. Most eVTOL developers use batteries and combine cell with a high specific energy, most likely NMC and NCA types, with a high specific power Lithium-Polymer Battery

(LPO). Companies usually do not provide data on essential design decisions like the power system architecture. Stahl et al. recently published a study on the modeling and performance of hybrid battery architectures [208]. They analyze various hybrid architectures and conclude how dual systems which use a high-power battery with an attached power management system and a high-energy battery are potentially fit for eVTOLs. They report that the advantage of hybridization strongly varies depending on configuration and payload mass [208]. Using hydrogen fuel cells will likely also require being complemented by high power sources, like supercapacitors or high specific power batteries. As Ng and Datta conclude from their studies, eVTOL configurations using only a fuel cell might not even be able to vertically take-off due to a prohibitively heavy stack [177], [199]. Given the limited specific power and energy, the framework allows to design and assess configurations that use hybrid powertrain architectures. This section outlines the implemented Degree of Hybridization (DoH), tests the approach, and discusses the significance of uncertainties regarding real-world powertrain data.

$$f_{DoH} = 1 - \frac{P_{HES}}{P_{HES} + P_{HPS}} = 1 - \frac{P_{crs}}{P_{hover}} = 1 - \frac{v_{crs} \, PL}{L/D} \tag{3.13}$$

Equation 3.13 defines the DoH as the share of support of a power generating High Energy System (HES) by a High Power System (HPS). The HES needs to be capable of powering the time dominant flight state, which is cruise flight. In combination, HES and HPS meet the required maximum power, i. e. hover flight in most cases. It is up to the practitioner to either provide the framework with a distinct value for f_{DoH} or to let the framework evaluate a power-optimum DoH. The latter is done by assigning flight states to the respectively active power generating systems. It is then possible to determine the DoH based on the flight states' power requirements as shown in Equation 3.2.
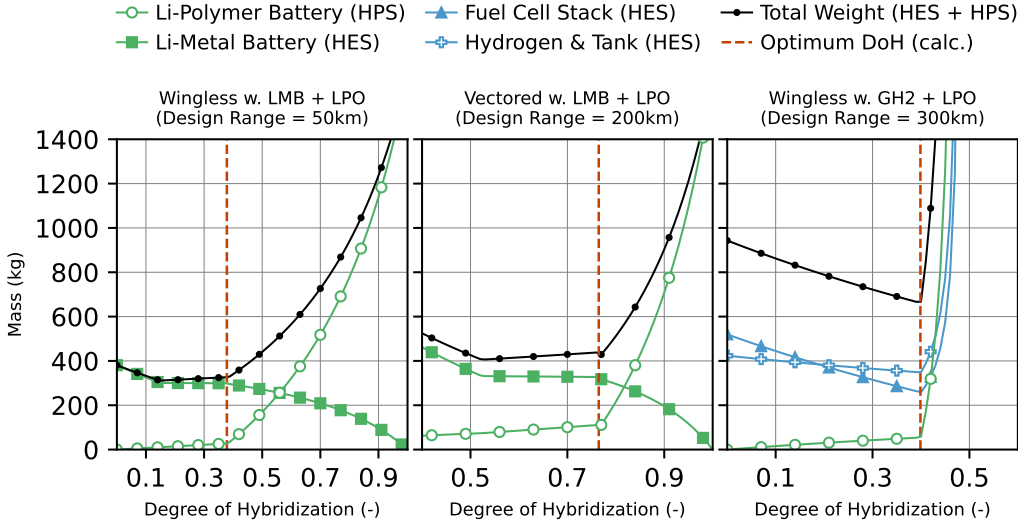

Figure 3.4: Component masses of various powertrains over DoH.

Figure 3.4 shows powertrain component masses of three different configurations. The two configurations on the left side have *battery-hybrid* powertrains, with an LMB for high energy and an LPO for high power. The plot on the right side resembles a *hydrogen-hybrid* powertrain with Gaseous Hydrogen Storage (GH2). The configurations are a wingless concept, i. e. Multi-Rotor, in the left and right plot, and a Vectored Thrust concept in the middle. The **Multi-Rotor** subplot on the left shows how, at $f_{DoH} = 0.0$, the configuration is solely powered by the HES system, as its mass coincides with the total weight. For $f_{DoH} = 1.0$, the Multi-Rotor is powered solely by the LPO, i. e. the HPS, which leads to an accordingly high total battery weight. The dashed vertical line resembles the calculated optimum hybridization degree according to Equation 3.13. However, one finds how the calculated optimum meets the second-lowest discontinuity in the total weight curve. The deviation of the actual optimum is relatively small and thus accepted concerning the methodology development. Nevertheless, it points to a shortcoming of the approach, which is further discussed below. The **Vectored Thrust** configuration shows a similar behavior but increases in HES mass later, i. e. at a much higher $f_{DoH, opt}$, due to the low specific power of the LMB and smaller power loading of the configuration. For $f_{DoH} > f_{DoH, opt}$, the LPO has to provide energy for horizontal flight, leading to a rapid increase of battery mass due to the low specific energy of the LPO. This behavior due to limited LPO specific energy also explains the steep increase of total powertrain weight for $f_{DoH} > f_{DoH, opt}$ in the **GH2-powered Multi-Rotor** configuration on the right side. Compared to the Vectored Thrust concept, the required design range is another 100 km longer, thus increasing the required HPS battery capacity if the optimum DoH is not met. For $f_{DoH} < f_{DoH, opt}$, the hydrogen-hybrid configuration converges at higher masses due to increased fuel stack weights, which can be explained by the limited specific power of the fuel cells. In contrast, the required hydrogen and tank mass only gradually increase.

The hybridization model described in Equation 3.13 has two limitations:

- First, the model constructs the optimum DoH based on power requirements, not on energy requirements. The time spent in a particular flight state is not incorporated in the model. For instance, if specifications require a long time in hover mode, the HPS may effectively be sized by an energy requirement (capacity) instead of the power requirement (rate of discharge). This would neglect that the model calculates DoH as a function of power.

- Secondly, the model identifies the optimum DoH based on configurations system-level metrics, not on the powertrain metrics. For instance, the model will find an optimum $0 < f_{DoH} < 1$ in a *battery-hybrid* system, in which the HES is a future battery cell with a high specific power. However, the potentially high discharging capability of the future cell might make hybridization altogether obsolete, implying an optimum hybridization of $f_{DoH} = 0$.

Nevertheless, Figure 3.4 demonstrates that the presented approach is suitable within the scope of this thesis and given the current technological capability of the available energy carriers.

3.2.4 Verification of the conceptual design approach

Brown and Harris have developed and applied a framework to conceptually design eVTOL configurations and assess the expected costs of aircraft and their operation, as was outlined in Section 2.2 [37]. At a similar modeling fidelity level, their work provides a suitable baseline for verifying this thesis' conceptual design framework. Brown and Harris perform their analysis on four different battery-powered eVTOL configurations: a Lift & Cruise, a Compound, a Tilt-Wing, and a Tilt-Rotor configuration. Figure 3.5 replicates their results of system sizing and flight state analysis and presents them with bar plots. In the mass plot on the left, the absolute bar height resembles the maximum take-off weight. The three smaller bars resemble the masses of airframe, battery, crew, and passengers, from left to right. As for the right plot, the lower bars reflect the power required in a cruise flight, while the higher bars show the power requirement for hover. Symbol markers display results estimated with the framework developed in this thesis. Respective error bars show the 95% confidence interval from uncertainties present in the underlying data.
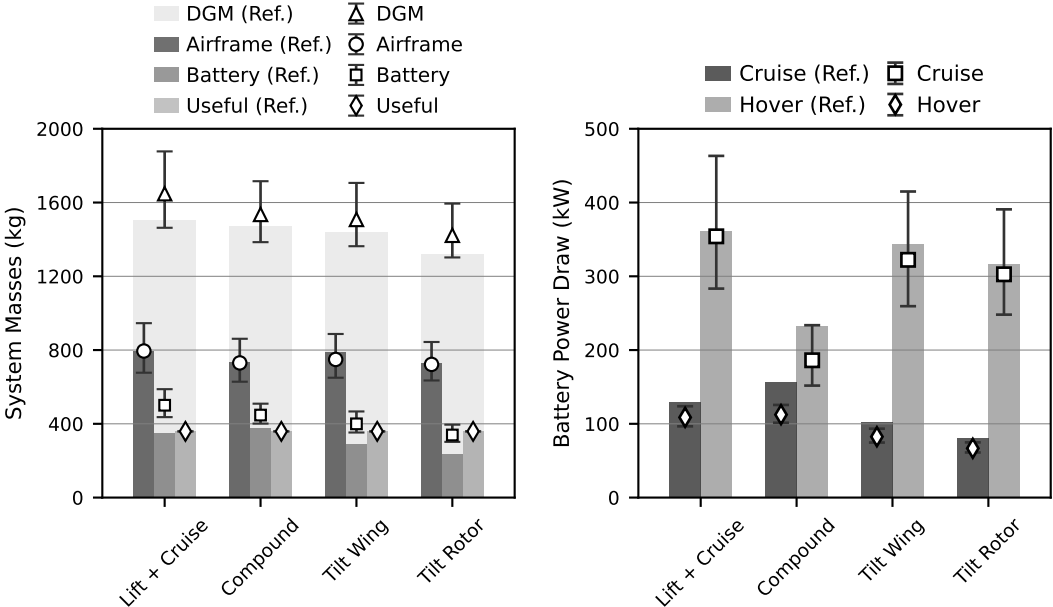
Figure 3.5: Verification of design masses and powers determined by the methodology.

Parameters describing the aircraft, the required mission, and the battery are assumed based on the data provided by Brown and Harris. However, Brown and Harris use empty mass fractions instead of structural mass fractions and disk loading instead of power loading. Therefore, the verification uses the framework's stochastic variant and compiles the structural weight based on statistical distributions resembling the structural mass fractions. While Brown and Harris use empty mass fractions of 0.43, 0.53, and 0.55 for the Compound, Lift & Cruise, and Tilt configurations, respective structural mass

fractions are distributed *normally* around baseline values of 0.24, 0.26, and 0.26, each with a standard deviation of 10%. As for the rotor efficiency, the suggested disk loadings of $215\,\text{N/m}^2$ (Compound) and $718\,\text{N/m}^2$ (Lift & Cruise, Tilt-Wing, and Tilt-Rotor) are transformed into respective power loadings of $0.081\,\text{N/W}$ and $0.046\,\text{N/W}$, based on respective figures of merit assumed by Brown and Harris. Like the structural fraction, baseline values of PL are impinged with a standard deviation of 10%. Comparison of the results described by Brown and Harris (the bar heights) with this methodology's outcomes (markers and 95% error bars) shows that both the absolute result values as well as trends across configurations are reflected. While the spread of error bars around up to 400kg in take-off weight and over 150kW in hover power can be accounted to the assumed standard deviation of 10% in structural mass fraction and power loading, it yet shows a considerable sensitivity of the developed design and analysis models toward those system-level metrics. Thus, Section 4.1 puts particular emphasis on the analysis and discussion of those trends.

3.3 Sustainability Assessment

The fundamental capability of this thesis' methodology is to determine the environmental life cycle impact of eVTOL aircraft. Therefore, it assesses GHG emissions measured in carbon equivalents. This section discusses how the LCA framework is applied within this thesis and lays out the underlying intentions and modeling decisions.

3.3.1 Application of the Life Cycle Assessment framework

The primary step in LCA is the definition of goal and scope: The work's nature as a doctoral thesis does not inherently limit the possible range of *stakeholders* of study. However, the subject matter itself (UAM) and the focus of the thesis (configuration-agnostic conceptual design of eVTOL) primarily target researchers and engineers in the aerospace and mobility community. Besides the methodological focus to provide readers with an understanding of uncertainties, the studies *results* shall help to (a) assess how eVTOL environmentally fare as a transport mode and (b) which configurations are preferable in terms of their climate impact. Aspects regarding the LCAs **scope** comprise the following:

Product or process in scope. The subject of the assessment are eVTOL configurations as yielded by the design task of the methodology and their operation in UAM scenarios.

Boundary definition. The system's *boundary* separates the aircraft from the environmental background system, representing the most straightforward form of boundary according to Guineé et al. [111]. Strictly following this representation implies to refer to the study as partial-LCA due to limited detail in depicting sub-systems with a distinct life cycle, like batteries and fuel cells. In addition to this system-to-background boundary, the thesis distinguishes significant from insignificant flows. Flows are insignificant if the expected contribution to the overall impact is considered negligible, based on previous studies. Examples like the exclusion of engineering and administrative services for

the development and operation of eVTOL will be discussed in the subsequent section. Potentially significant flows are defined as out of scope if their effect could promote a misleading interpretation of the study's results. Such is the case for the construction, maintenance, and operation of infrastructure. Arguably lower emissions of eVTOL compared to cars and trains may base on including high emissions associated with the construction of roads and railways. According to Lord Adair Turner, economist and lecturer at the London School of Economics, the comparison of eVTOL and i. e. trains is only valid if consumers have a real choice between competing modes. This scenario would require enough eVTOLs to potentially substitute a significant share of existing and future train rides, thereby suspending the need to construct new railways. Since railways already exist and will continue to be built regardless of eVTOL, the only relevant comparison can be made based on the marginal impact [209]. To complete the boundary definition, system expansion is excluded with reference to the effects of second-life applications of batteries. Second-life applications can significantly reduce the potential carbon impacts, as they allow to distribute impacts from production and end-of-life over a longer cycle life. The beneficial effect on the batteries' impact can be represented by a simple factor in system expansion's stead.

Functional unit. The standard functional unit for the production of eVTOL aircraft is *per vehicle* (#/eVTOL). Operational impacts and life cycle impacts are normalized to a *passenger-kilometer traveled* (#/PKT). Handy functional units to perform conversions and normalizations in are *per consumed energy*[2] (#/kWh), *per mission*, and *per vehicle-kilometer traveled* (#/VKT).

Allocation procedures. The performed LCA is attributional by nature. UAM has yet to become a reality and predictions on the implementation timeline have no scientific foundation. A valid estimation of the study's impact on associated investment or policy decisions, or the development of the sector as a whole, cannot be achieved. LCA-based indications for or against the sustainability of UAM may influence individuals in their choice of transportation mode. However, quantifying this effect is hardly possible, exceeds the defined scope, and contradicts the thesis' objective. A consequential LCA would require a more holistic perspective and should arguably be performed from a different scientific angle. Nevertheless, consequential LCA could use this work's findings as an input or even incorporate the framework due to its modularity.

Scenario type. Building on the scenario definitions of Börjeson, the study combines a predictive-forecast-type scenario with an explorative-external-type scenario [118]. The energy landscape in 2030 is described by an expected *standard* scenario and a possible *green* scenario (predictive-forecast-type). Both scenarios may be impinged by an uncertainty factor to span the range of possible results and compare the sensitivity due to such scenario uncertainties with the uncertainties present within the design and technological domains.

---

[2]At propeller shaft

Impact categories. In line with the aim of this work, the framework is solely applied to determine the impact on climate change through GHG emissions measured in carbon equivalents. It can be easily extended to provide analyses on other impacts in future studies. Section 2.3 outlined how sustainability assessment has developed from a pure environmentally-focused discipline toward a more comprehensive task in recent years. As such, the framework could mirror advances towards Life Cycle Sustainability Assessment to include assessments of energy costs, operational costs, or total cost of ownership.

3.3.2 System inventory definition and elementary flows

Following the setting and discussion of the scope of the LCA-type impact study, Figure 3.6 outlines a schematic representation of the eVTOL and UAM system and elements. The system's life cycle is represented by the three characteristic phases *Sourcing & Production*, *Operations*, and *End of Life*.
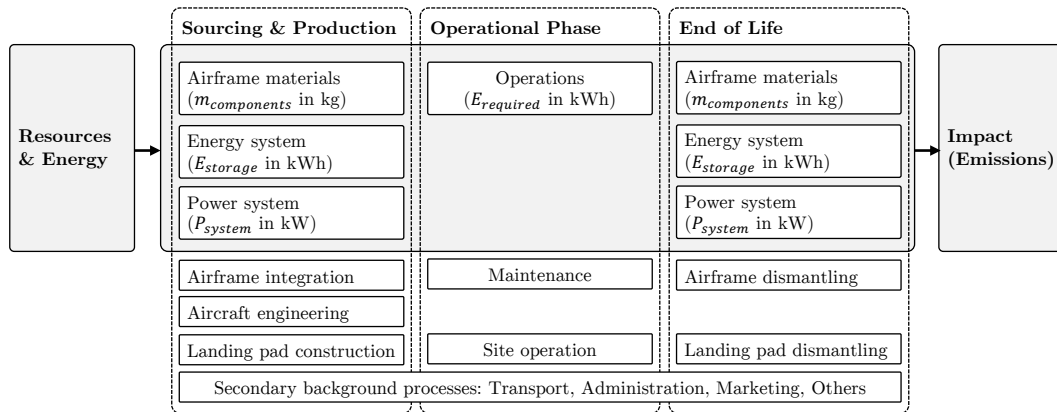
Figure 3.6: Life cycle phases and inventory of eVTOL aircraft.

Elements in scope of assessment within the **Sourcing & Production** phase are the required resources and energy to build the aircraft's frame, energy storage system, and power unit. The respective resources and energy, and the according impact or emission caused, are determined based on the airframes materials and components, the energy storage systems capacity, and the power units output power. This form of attributing the system's flows to its properties is advantageous over a possible pure attribution by masses, in that it is customized to the availability of the element's flow data. While data on the resources and impacts of $1\,kg$ of carbon fiber reinforced plastic is readily available from databases, batteries are usually assessed based on their effective cell capacity. Similarly, fuel cell stack assessments in literature are provided based on the power provided by the stack. Out of scope of the **Sourcing & Production** phase are the airframe integration, engineering efforts in research and development of the system, and the construction of operational infrastructure, most prominently the pads required for take-off and landing. Other background processes directly or indirectly associated

with the system, such as flight testing during development, administrative efforts in UAM companies, or marketing campaigns, are excluded, although they arguably have an environmental impact. The decisions to cast elements out of scope are motivated by various points. One is an expected low or negligible impact of an element and thus a nonexistent significance of this element's impact within the study's scope, even if the element is contributing to the systems overall impact: Examples for this cause are the airframe integration, research and development efforts, and test flight campaigns. Johanning, who performed an LCA of an Airbus A320, found the contribution of the three elements to the total impact at around $0.1\,\%$, $1 \cdot 10^{-8}\,\%$, and $1 \cdot 10^{-6}\,\%$, respectively. Another reason is the limited validity of the subsequent comparison of the system's result with other competing systems on a macroscopic level[3].

The **Operation** phase's representing element is the energy consumption of the aircraft within operation. As preliminary studies have shown, and as this thesis will confirm, it is the dominant contributor to the environmental impact of UAM and the determining factor of a sustainability advantage of eVTOL configurations over one another. The elements maintenance and site operation, i. e. the energy required to run vertiports, are out of scope for the LCA for the same reasons as outlined before.

Systems in scope of the **End-of-Life** phase resemble those in scope of the sourcing & production phase, as those elements are physical assets and need to be taken care of after the system is retired. In an earlier publication, the author discussed how the environmental impact of a eVTOL aircraft's end-of-life is about one order of magnitude smaller than the impact of the sourcing phase, and about two orders smaller than the impact from operation, if the assessment includes end-of-life treatments such as the incineration of materials [41]. However, effects occurring at the end-of-life of a system have potentially beneficial effects to a systems life cycle impact. At best, reusing and recycling sub-systems, components, and materials can reverse the detrimental of the primary sourcing and manufacturing of the system. Batteries, as a major contributor to the life cycle impact of eVTOLs, are a vital example of this circumstance: Political regulations aim to set fixed collection rates and recycling efficiencies of batteries and propose to hold economic operators accountable for complying within their scope [210]. Another likely option is that companies find, leveraged by policy and technological advances, an economic case in second-life applications of batteries. With respect to the assessment of the powertrain sub-system in eVTOL operation, the author regards a quantitative and reliable representation of this apparent combination of statistical and scenario uncertainties hardly attainable. Therefore, the framework chooses to model the potentially beneficial or detrimental effect of the end-of-life phase via a simple factor. By alternating scenarios and setting reasonable bounds for that factor, statistical analyses may (a) lead to an assessment of the importance of appropriate end-of-life strategies and (b) help to determine a likely need for refined modeling of end-of-life options.

---

[3]Refer to the earlier paragraph on **Boundary Definition**

3.3.3 Impact assessment

This section describes how the developed framework performs an impact assessment on the inventory outlined before. As outlined, the assessment includes impacts from the aircraft's structural and powertrain sub-systems and the aircraft's operational impact. Figure 3.6 showed that the impact associated with each sub-system is provided with respect to a different functional unit. While the impact from the sourcing of airframe materials is expressed per required mass of the material (i. e. per kg), energy impact is determined based on energy consumption during the operations phase (i. e. per kWh). The core task of impact assessment is to compile the sub-system's impacts with reference to a unique functional unit, to make them comparable and facilitate subsequent interpretation of the LCA. This methodology unifies the sub-system's impacts with respect to the functional unit of *one aircraft* (eVTOL) and *one flight hour* (FH) of this aircraft. LCA literature often refers to the former as a Cradle-to-Gate (CTG) analysis. The latter is, in an automotive context, often dubbed as a Well-To-Wheel (WTW) assessment. Transferring this denominative scheme to eVTOL aircraft, the author introduced the term Well-To-Shaft (WTS) analysis in an earlier publication [41]. The two functional units allow interpretation of the sub-system's physical contributions to the overall impact as well the actual contributions in a life cycle perspective. Based on the functional unit FH, further conversions to a passenger-kilometer traveled (PKT) are possible to provide the reader with a means to compare the impact of eVTOL to other transport modes.

Airframe impact / Cradle-to-Gate assessment. The determination of the impact based on the sourcing and production of the aircraft's materials is described by Equation 3.14. The Cradle-to-Gate (CTG) impact is found through summation of the j aircraft's components masses m, multiplied by the impact ι of the i used materials and the fraction f of each material in each component. The additional factor g described the respective end-of-life treatment of each component, allowing to increase or decrease the relative impact respectively.

$$\iota_{Airframe,CTG} = \sum_{i,j} \iota_i \cdot f_{i,j} \cdot m_j \cdot g_{re,j} \quad \left(\frac{impact}{\text{eVTOL}} \right) \tag{3.14}$$

The components in scope are the aircraft's structure, electric motors, *other* masses as defined in Section 3.2, and the powertrain system, which is either a battery pack or a combination of fuel cell stack and hydrogen tank. Input data of the materials' sourcing impacts and the materials' fractions in components is provided in Tables 4.5 and Table 4.6. To provide a life cycle perspective on the impact from the production of the materials of an eVTOL, it is necessary to exceed the CTG scope and transforming the calculated impact value to the functional unit of flight hours (FH) in operational life. As described above, this stage further provides the methodology's user to analyze the impact of various end-of-life scenarios for the materials' impacts on a global level.

$$\iota_{Airframe,LCA} = \frac{\iota_{Airframe,CTG}}{FH} \cdot g_{re} \; \left(\frac{impact}{\text{FH}}\right) \tag{3.15}$$

Operational impact and energy system impact / Well-to-Shaft assessment. Operational impacts cover effects associated with physical flows enabling an eVTOL aircraft to perform its actual mission during what LCA literature refers to as the *Use Phase*. As such, the operational impact is, for one part, the impact associated with the sourcing of energy, and therefore the sourcing of either electricity or hydrogen. However, due to the low life expectancy of batteries in applications with a high power draw, the scope of operational impacts is extended. Although included in the afore outlined component-based impact summation, a thorough assessment demands to include recurring impacts from battery replacement throughout an aircraft's life cycle. The assumption to amortize the batteries' impact using its cycle life instead of its lifetime in hours is similarly performed by Brown and Harris [37].

Figure 3.7 outlines how each of the four mentioned contributors to operational impact, electricity production, hydrogen production, battery production, and fuel cell production, can be transformed so that their actual impact is available with respect to the energy consumed by the eVTOL aircraft. The eVTOL system and the background system are subject to inefficiencies. As such, 1 kWh of energy required by the aircraft to sustain a particular flight state for a given time does imply a higher amount of necessary primary energy. As for the impact of battery and fuel cell sourcing, Figure 3.7 depicts on a high level how the recurring, one-time effect of sourcing is transformed. In essence, the capacity and power capability of the two systems are to be expressed with respect to one 1 kWh of energy drawn by the aircraft power shaft. In batteries, the determining factors are the battery life cycle and the effective capacity, often referred to as the effective depth of discharge. The specific fuel cell impact is determined based on the operational lifetime of the stack system.
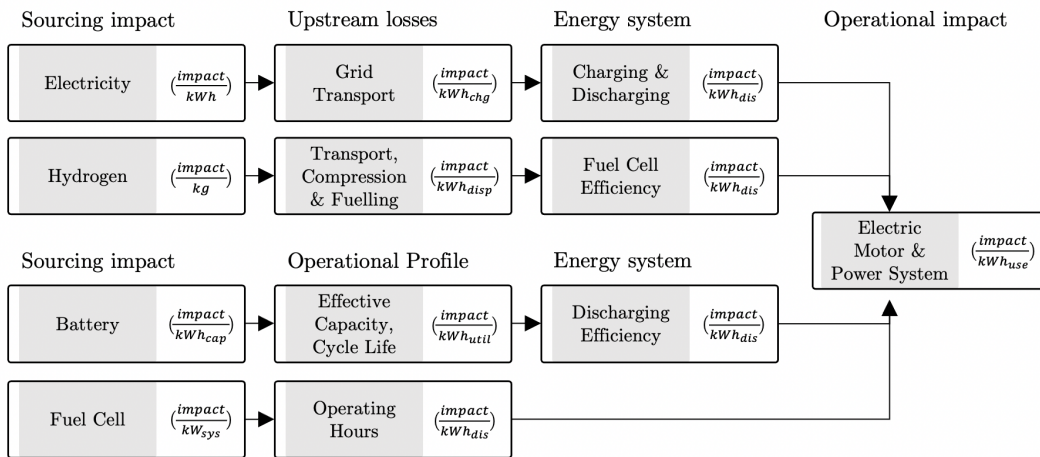

Figure 3.7: Sourcing impact and upstream efficiencies of powertrain systems.

The subsequent Equations 3.16, 3.17, 3.18, and 3.19 outline the respective mathematical representation of the logic shown in Figure 3.7. All four results are provided with the functional unit of 1kWh energy used by the aircraft.

$$\iota_{Electricity} = \frac{\iota_{Electricity,\,Sourcing}}{\eta_{grid}\,\eta_{chg}\,\eta_{dis}\,\eta_{mtr}} \tag{3.16}$$

$$\iota_{H_2} = \frac{(\iota_{H_2,\,Sourcing} + \iota_{H_2,\,Trans} + \iota_{H_2,\,Compr})}{e_{sp,H_2}\,\eta_{fc}\,\eta_{mtr}} \tag{3.17}$$

$$\iota_{Battery} = \frac{\iota_{Battery,\,Sourcing}\,g_{re}}{f_{DoD}\,n_{cyc}\,\eta_{dis}\,\eta_{mtr}} \tag{3.18}$$

$$\iota_{FuelCellSystem} = \frac{\iota_{Stack,\,Sourcing}\iota_{H_2Tank,\,Sourcing}\,g_{re}}{t_{ops}\,\eta_{mtr}} \tag{3.19}$$

Based on the provision of all operational impacts with respect to used energy, it is straightforward to calculate the impact of a flight mission based on the sum of the impact of respective flight segments. The latter is determined by multiplying the raw operational impacts of the sourcing of electricity, hydrogen, batteries, and fuel cells as yielded by Equations 3.16, 3.17, 3.18, and 3.19, with the required power and respective time. The logic is given in Equation 3.20. Special attention must be given to the hybrid nature of powertrains as outlined in Section 3.2. Based on the degree of powertrain hybridization, flight states may be sustained by one or multiple types of energy. Thus, the framework must associate the respective impacts with the flight states. This is accounted for within the framework.

$$\iota_{mission} = \sum_{i,j} \iota_i \cdot E_j = \sum_{i,j} \iota_i \cdot (P_j t_j) \left(\frac{impact}{MISS}\right) \tag{3.20}$$

Life cycle impact through functional unit harmonization. Lastly, it is demanded that functional units be unified to add up, compare, and analyze the impacts from the various contributors to each other and make the results tangible for readers. The functional unit *passenger-kilometer traveled* (PKT), chosen as a primary reference, is attained through the conversions outlined in Equations 3.21, 3.22, and 3.23.

$$\frac{impact}{PKT} = \frac{impact}{eVTOL} \cdot \frac{1}{t_{Life}(\text{h})} \cdot \frac{1}{V_{avg}(\text{km/h})} \cdot \frac{1}{n_{PAX}\,f_{util}(\text{-})} \tag{3.21}$$

$$\frac{impact}{PKT} = \frac{impact}{FH} \cdot \frac{1}{V_{avg}(\text{km/h})} \cdot \frac{1}{n_{PAX}\,f_{util}(\text{-})} \tag{3.22}$$

$$\frac{impact}{PKT} = \frac{impact}{MISS} \cdot \frac{1}{R_{mission}(km)} \cdot \frac{1}{n_{PAX}\,f_{util}(\text{-})} \tag{3.23}$$

4 Results and Discussion

4.1 Conceptual Design and Performance Analysis of eVTOL

A model-based methodology is only as good as the data that is fed into the model. As for eVTOL data, this implies a challenge. All previously outlined configurations are in the midst of their development, within stages like prototyping, testing, verification, and certification. Reliable aircraft parameters characterizing the concept's actual capabilities are hardly available and, arguably, often unknown to the aircraft's designer. An example of this is the aircraft's lift-to-drag ratio (L/D), also referred to as glide-ratio in fixed-wing aircraft, reflecting the aircraft's efficiency in cruise flight depending on the cruise speed. Methods like Momentum Theory and Blade Element Theory or the application of Computational Fluid Dynamics can provide somewhat accurate predictions on such aircraft characteristics. However, validating those predictions requires flying and testing the aircraft in an operational environment. This thesis incorporates uncertainties associated with a configuration's parameters and presents statistical distributions and confidence intervals instead of deterministic results. Moreover, it aims to understand how parameter changes influence those results and identify likely scenarios through sensitivity analyses. To this end, the developed sizing framework is fed with non-confidential data published by developers on their websites, parameters published by other researchers, and educated guesses if no other data source is available.

> **Note:** This chapter aims to demonstrate the implemented methodology and facilitate the reader's critical engagement with eVTOL configurations. Therefore, Sections 4.1 and 4.2 refer to real-world eVTOL configurations representing specific aircraft types developed by UAM companies. However, the thesis deliberately avoids retrofitting the assessed configurations to their actual weight (DGM) and performance. Instead, all configurations are designed, i. e. sized, based on assumed system-level metrics and specific mission requirements, both of which are subject to uncertainties. To prevent ambiguity errors of the actual eVTOL aircraft and their virtual representations, the thesis refers to the aircraft models by the respective *"eVTOL"* or *"Company"* name put in quotation marks. As such, *"Volocopter"* refers to the thesis' representation of the company's VoloCity aircraft. *"CityAirbus"* models the eponymous eVTOL developed by Airbus, *"Vahana"* represents the *beta*-prototype of Airbus' subsidy A^3, and *"Cora"* reflects the concept developed by Wisk Aero. *"Joby"* and *"Lilium"* refer to the five-seater aircraft models S4 by Joby and Phoenix by Lilium. *"Skai"* refers to the hydrogen-powered eVTOL configuration developed by Alaka'i Technologies.

4.1.1 Design mission requirements

The conceptual design models use data from the requirements, design, and technology domains. Table 4.1 comprises the requirements domain for the selected eVTOL configurations. Payload is calculated based on the seat capacity, where (n_{Seat}) includes one pilot seat. According to EASA, the weights of passengers and the pilot are assumed at 88 kg and 92 kg, respectively [195]. Cruise velocities and maximum range requirements comply with what eVTOL companies have published.

Requirement	Unit	Volo-copter	City-Airbus	Vahana	Cora	Joby	Lilium	Skai
n_{Seat}	-	2	4	2	2	5	5	5
V_{Crs}	m/s	27.8	33.3	52.8	44.0	89.0	83.0	39.7
	kts	54	65	103	86	173	161	77
R_{Crs}	km	36	50	100	100	240	300	644
t_{Hov}	min	. . .	. . .	. . .	1.0	. . .	. . .	. . .
		. . .	. . .	. . .	1.5	. . .	. . .	. . .
		. . .	. . .	. . .	2.5	. . .	. . .	. . .

Table 4.1: Design requirements toward selected eVTOL configurations.

The required hover time (t_{hov}) is assumed by the thesis' author. It is provided by a triangular distribution rather than a deterministic value. For all configurations, the mean hover time is set to 1.5 min, with a minimum of 1.0 and a maximum value of 2.5 min. The values reflect a likely range based on scientific and commercial publications but are lower than the required hover time of helicopters. Shamiyeh et al. assume a combined hover time of 1.0 min for the take-off and landing segments and a transition time of 2.0 min each for the climb and descent segment to a flight level of 300 m above ground [45]. Brown and Harris assume a total hover time of 2.0 min as a design requirement but deem a much lower hover time of 30 sec in revenue and deadhead missions possible [37]. Nathen of Lilium states a total hover power requirement of 102 sec per mission, consisting of 15 sec for take-off, 45 sec for landing, and 21 sec per transition [29]. Notably, Nathen argues that Lilium's seven-seater's theoretical maximum hover time is 384 sec, based on the battery capacity, but will not be practically reached due to overheating of the batteries [29].

The requirements domain further allows adding a reserve time for loiter or cruise flight in accordance with flight regulations. However, the present thesis regards the safety reserve to be implied within the range and hover requirements, which bases on the following: The definition of reserves is dependent on the vehicle class under which manufacturers certify their vehicle. If certified and operated under VFR conditions according to the US Code of Federal Regulations (CFR), eVTOLs have to be able to perform a 30 min loiter segment by day, and 45 min by night, at any given point during the mission. If certified and operated as a rotorcraft under VFR conditions, this time reduces to 20 min [211]. In case a specific eVTOL certification class is implemented, lower requirements are possible. The US General Aviation Manufacturer's Association

(GAMA) is advocating a 3.7 km diversion distance, arguing that eVTOL aircraft will be capable of landing in a large variety of areas [212]. EASA's Special Condition for small-category VTOL aircraft, as the world's first dedicated technical specifications for eVTOL aircraft, gives a qualitative measure by requiring "energy for a sufficient reserve based on a standard flight" [196]. The latter two formulations, together with both batteries' and hydrogen tank systems' available excess energy due to discharging and storage characteristics, allow to conclude that the above-made assumption is reasonable.

4.1.2 Aircraft configuration assumptions

Table 4.2 comprises the system-level metrics *lift-to-drag ratio* (L/D), *power loading* (PL), and *structural weight ratio* (f_{Struct}), which describe the design domain of the selected eVTOL configurations. For the remainder of this thesis, note that L/D describes the *lift-to-drag ratio* of a configuration at its typical cruise speed. Therefore, the values of L/D typically reflect a relatively high, if not the maximum possible, value of each configuration. The three parameters resemble the author's assumptions, based on scientific literature, student theses, and informed guesses. Like the hover time requirement depicted in Section 4.1.1, the resulting uncertainties are provided by triangular distributions rather than deterministic values. Each triangular distribution is displayed by its minimum, mode, and maximum values in the upper, middle, and lower row, respectively.

Parameter	Unit	Volo-copter	City-Airbus	Vahana	Cora	Joby	Lilium	Skai
		1.8	1.8	7.0	8.5	13.0	16.3	1.8
L/D	-	2.9	2.9	7.2	9.65	14.0	17.0	2.9
		5.3	5.3	7.4	10.8	17.0	18.26	5.3
		94	49	42	32	30	15	29
PL	N/kW	108	56	52	42	37	18	37
		122	64	63	51	44	23	46
		0.24	0.24	0.25	0.25	0.25	0.25	0.24
f_{Struct}	-	0.25	0.25	0.26	0.26	0.26	0.26	0.25
		0.27	0.27	0.30	0.30	0.30	0.30	0.27

Table 4.2: Assumptions of system-level metrics of the selected eVTOL configurations.

In addition to Table 4.2, those triangular distributions are visualized by their Probability Density Function (PDF) and Cumulative Density Function (CDF) in Figure 4.1. Mind that the y-axis covers a range of $[0,1]$ for the CDF, but has a unique range for each PDF according to the respective probability. For the sake of simplicity, all PDFs are illustrated as normalized functions. The used triangular distributions allow to cover likely input ranges of the parameters, as the limited availability of valid data does not provide an accurate statistical representation of configurations but yield minimum and maximum values. Note that the x-axes' intervals are of identical length for each parameter row in Figure 4.1 to illustrate the uncertainty of the underlying data of the configurations.
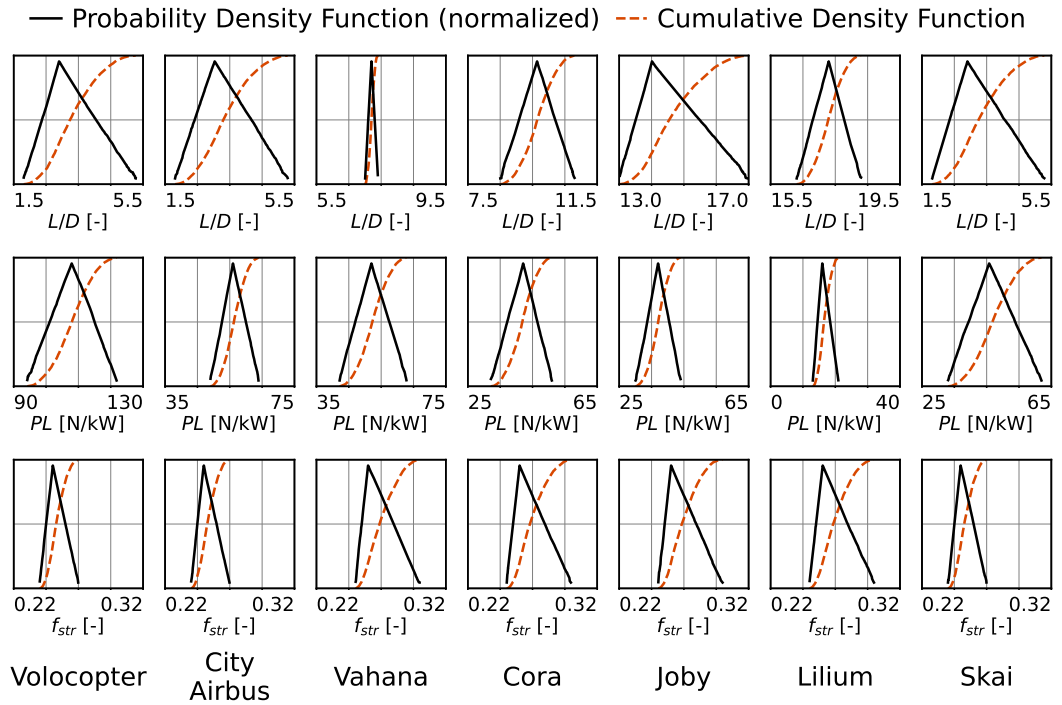
Figure 4.1: Density Functions of Triangular Design Parameter Distributions.

Especially the distributions representing $^L/_D$ are spread over varying ranges, i. e. if one compares the *"Vahana"* and *"Joby"* configurations. This must be considered when interpreting error bars and sensitivity analyses in the following sections. The following three paragraphs describe the underlying data of the presented triangular distributions.

Lift-to-drag ratio. The thesis assumes, that the aerodynamic efficiency of Multi-Rotor configurations in forward flight, which is reflected by their $^L/_D$, is within the same order of magnitude as for helicopters. Leishman depicts how the measured lift-to-drag of a Sikorsky UH-60 helicopter reaches its maximum value of around $^L/_D = 5.0$ only at a cruise speed of around $V_{crs} = 100$ kts. From 50 to 70 kts it shows distinctly lower values of around $^L/_D = 2.5$ to 4.0, respectively [203]. Datta et al. substantiate this value range based on measurements of several undisclosed conventional helicopter configurations [33]. As for eVTOLs, literature values of $^L/_D$ comprise 1.8 and 2.3 for CityAirbus and eHang, respectively (Brown and Harris [37] and Balli [213]), 2.8 to 3.4 for Multi-Rotor configurations of various DGM (Shamiyeh et al. [45]) and a maximum 5.3 of the four-seater quad-rotor configuration designed by Johnson et al. [7]. As for Tilt-Wing and Lift & Cruise configurations, the thesis assumes higher $^L/_D$ ranges. References contain values of $^L/_D$ between 7.0 and 8.5 through measurements of turboshaft-powered Tilt-Rotor configurations (Datta et al. [33]), calculated values of 7.4 for *"Vahana"* and 10.8 for *"Cora"* (Balli [213]), and 7.2 for the Tilt-Wing concept presented by Johnson

et al. [7]. Depending on the required payload, Shamiyeh et al. calculate $^L/_D$ ratios for Lift & Cruise eVTOLs between 9.8 and 12.8. Lift-to-drag ratios of electric Tilt-Rotor and Vectored Thrust configurations are assumed to be highest compared to other eVTOL configurations but are also subject to uncertainty. Kasliwal et al. perform their environmental assessment of flying cars with $^L/_D$ values ranging from 13 (min), to 17 (base-case), to 20 (max) [40]. Brown and Harris assume the $^L/_D$ of Tilt-Rotor aircraft like the *"Joby"* configuration at 14 [96]. Concerning Lilium's two-seater prototype, Bacchini and Cestino report a calculated value of 16.3 [37]. Lilium's co-founder Patrick Nathen calculates that the companies seven-seater will achieve an $^L/_D$ of 18.26 [29].

Power loading. The value ranges of PL build on the configuration's disk loading and figure of merit (FM) and are estimated based on the total disk area, the concept's DGM, and the rotor's FM, according to Leishman [203]. The used parameters are outlined in Table 4.3. Their values and triangular distributions are assumed as follows:

- **Design gross mass.** In cases where no upper and lower boundaries are depicted, the DGM values reflect officially communicated weight aims[1]. The DGM bounds of *Cora* are based on the comparison of SUAVE and NDARC by Vegh et al. [89]. The DGM intervals of *"Lilium"* and *"Skai"* are assumptions made by the author. Note that, as outlined in the introductory paragraph of this chapter, the purpose of the methodology's application is not to retrofit configurations. Therefore, the thesis avoids seeking convergence of the DGM values shown in Table 4.3 with the sizing's output DGM and regards Table 4.3 solely as an input.

- **Total disk area.** The configurations' disk area follows the number of rotors and their radius. It is primarily estimated based on visual references, i. e. by measuring photographs or sketches of the concept prototypes.

- **Figure of merit.** Estimations and assumptions of eVTOL FM are provided in the works of Vegh et al. (NDARC and SUAVE yield 0.673 and 0.601 for the Cora Wisk eVTOL, respectively [89]), Brown and Harris, who assume 0.78 for all configuration types in scope [37]), and Bacchini who assumes 0.7 for all configuration types [98]. As the figure of merit is prone to misinterpretation [203], this work assumes a simple triangular distribution covering the range of $[0.6, 0.8]$. The only exception is the *"Lilium"* configuration due to its ducted fan technology, which is granted the most optimistic end of FM estimations at $[0.8, 0.9]$. Note that this resembles a highly efficient rotor at a high thrust coefficient, low tip losses due to the shroud, and a reduced exit swirl due to the exit stator. Additionally, the *"Lilium"* configuration's hover power is corrected by a wake contraction parameter of $a_w = 1.3$ [29], [203].

Structural mass fraction. The assumptions of the structural weight ratios of the selected configurations build on the work of Harris and Ng and Datta, who report the lightest conventional state-of-the-art helicopter to have an f_{Struct} of 0.24. Based on the

---

[1]See Section 2.1

Parameter	Unit	Volo-copter	City-Airbus	Vahana	Cora	Joby	Lilium	Skai
		-	-	-	946	-	1,800	1,800
DGM	kg	900	2,200	815	979	2,177	2,000	2,000
		-	-	-	1,012	-	2,200	2,200
		-	-	0.80	0.65	1.18	0.25	0.95
r_{Rotors}	m	1.15	1.4	0.85	0.70	1.23	0.28	1.10
		-	-	0.90	0.77	1.28	0.32	1.25
		0.65	0.65	0.60	0.60	0.60	0.90	0.65
FM	-	0.75	0.75	0.70	0.70	0.70	0.925	0.75
		0.85	0.85	0.80	0.80	0.80	0.95	0.85
n_{Rotors}	-	18	8	8	12	6	36	6

Table 4.3: Assumed parameters for the estimation of the configurations' power loading.

framework's verification presented in Section 3.2, this value is adapted to 0.25 for Multi-Rotor configurations and to 0.26 for Tilt-Rotor and Vectored Thrust concepts. Lower and upper bounds are set according to the eVTOL models implemented in NDARC, whose f_{Struct} ranges from 0.25 to 0.3[2]. The value interval, as well as the apparent uncertainty, are substantiated by Vegh et al., who, for the Wisk Cora eVTOL, report $f_{Struct} = 0.24$ and 0.31, using the codes SUAVE and NDARC, respectively [89]. They find the most significant deviations between the models in the weight of the landing gear and point out that the weight model implemented in SUAVE assumes a large share of carbon fiber in the structure. Consequently, the positively skewed PDFs in Figure 4.1 resemble the author's assumption that an eVTOL's structure will be as lightweight as possible, with an uncertainty that its f_{Struct} might be higher than expected due to technological or regulatory constraints.

Not outlined in Table 4.2 but also required within the design domain is the mass fraction of *other components* f_{Other}, introduced in Section 3.2. As described, other components contain sub-systems such as flight controls, instruments, avionics, and the cabin, which are considered dependent on the configuration's useful load m_{useful}. Therefore and in line with the data collected from the works of Ng et al., Moore et al., Silva et al., and Vetter the other components' fraction is set to $f_{Other} = 0.6$ [32], [177], [201], [202]. The parameters describing the technology domain are provided and discussed in the subsequent section.

4.1.3 Powertrain characteristics

The assumptions and data concerning the technology domain, i. e. concerning batteries and fuel cell systems used in the thesis, are shown in Table 4.4. As outlined in Section 2.4, today's high-energy LIB cells, like today's hydrogen fuel cells, do not yield the necessary power for hover and climb flight states of eVTOL, which is why the thesis assumes hybrid

---

[2]See Table 3.2

Parameter	Unit	Lithium-Metal Battery			Hydrogen Fuel Cell			LiPo
		LB	Base	UB	LB	Base	UB	
e_{spec}	Wh/kg	300	325	350	-	33,322	-	160
p_{spec}	W/kg	750	812.5	875	500	750	1,000	4,000
f_{bms}	-	-	1.2	-	-	-	-	1.2
f_{DoD}	-	0.80	0.85	0.90	-	-	-	0.8
$f_{wt\%}$	-	-	-	-	0.27	0.30	0.33	-
$\eta_{discharge}$	-	-	0.95	-	-	-	-	0.95
$\eta_{f.cell}$	-	-	0.95	-	0.59	0.62	0.65	-
η_{motor}	-	0.93	0.95	0.97	0.93	0.95	0.97	-
n_{cycles}	-	600	800	1,000	-	-	-	800
$t_{op.hours}$	h	-	-	-	3,000	4,000	5,000	-

Table 4.4: Input parameters and variatons of alterantive energy carriers[4].

powertrain systems [199], [208][3]. Both powertrain types use a high-energy system based on an LPO. The parameters depicted in Table 4.4 reflect the author's assumptions based on the references collected and discussed in Section 2.4. In that, the assumption's underlying guiding principle is to authentically represent the expected technological capabilities and value ranges. Note that battery cells, for instance, are highly dependent on the utilization profile of the cell, even in a hybrid system where the battery is used in proximity to its nominal load. The LMB cell type listed in Table 4.4 is assumed to have a maximum discharge current of 2.5 C, limiting the available specific power. Higher peak discharge currents are possible but imply increased inefficiencies and heat generation, thereby posing risks to the thermal stability of electrolytes and deteriorating the battery's cycle life. According to Ellingsen et al., Lithium cells theoretically allow a cycle life of up to several thousand charging cycles if charged and discharged at around 1.0 C and utilized to modest discharging depths [206]. However, cells used at a higher $C - Rate$ have a significantly reduced cycle life. Severson et al. experimentally determined the cycle lives of 124 commercially available LFP cells and report an average cycle life of 806, at a $C - Rate$ comparable to fast charging conditions [214]. However, even higher discharge rates are possible and potentially required in power-demanding flight states, leading the cycle life to deteriorate further. Hence, Table 4.4 reflects a range of 600 to 1,000 cycles.

4.1.4 Conceptual design and analysis

This section depicts the conceptual design and performance analyses based on the outlined parameter ranges for eVTOL configurations. Figure 4.2 presents the Design Gross Mass (DGM) and the Consumed Specific Energy (CSE) per Passenger-Kilometer Traveled (PKT). Results are put into perspective by the maximum design flight range of the respective configurations, sorted by ascending range from left to right. The sizing methodology is evaluated **deterministically** and **stochastically**. The underlying pa-

---

[3]Refer to Section 3.2.3

rameter sets and triangular distributions are compiled in Tables 4.1, 4.2, and 4.4, and, as for the Design parameters, depicted in Figure 4.1. Once more note, that the thesis refrains from retrofitting real-world concepts but uses the configurations' names to descriptively apply the developed methodology[5].

Deterministic results of DGM and CSE are represented by grey and blue bar plots. Respective error bars show probabilistic results, denoting the medians of DGM and CSE, as well as the 95% confidence intervals. In cases where eVTOL-companies have published data on their configuration's DGM, those values are depicted by gray circles.

Stochastic results include calculations of 10,000 samples evaluated in a Monte Carlo scheme. Note that, due to the nature of the used triangular distributions, the medians of stochastic evaluations do not necessarily coincide with deterministic evaluations, which use the distribution's mode as inputs.
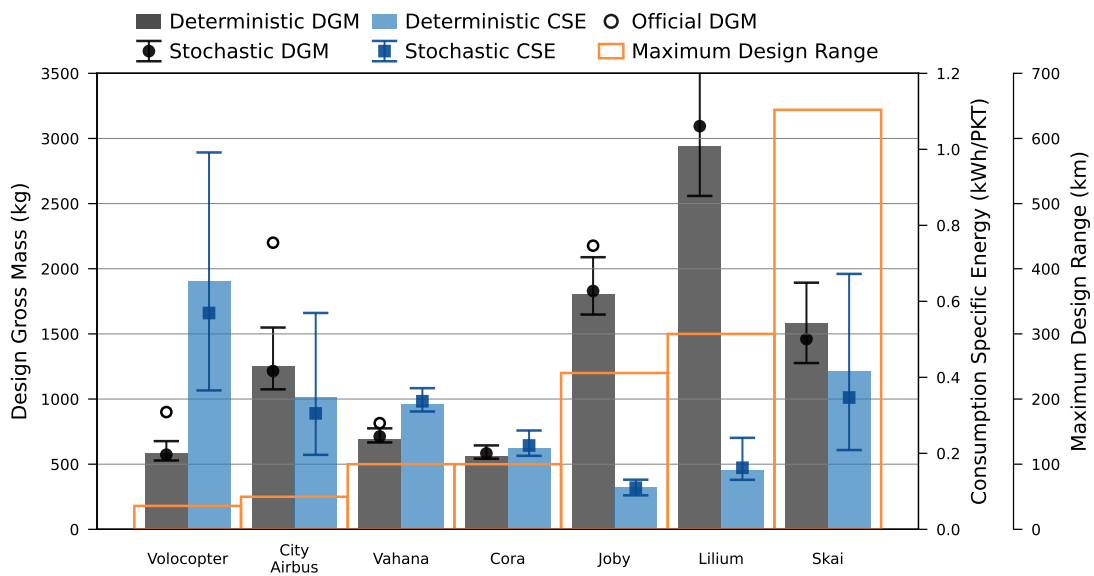
Figure 4.2: Design Gross Mass and Consumed Specific Energy of eVTOL concepts.

The first six configurations from the left resemble the battery-powered eVTOLs *"Volocopter"*, *"CityAirbus"*, *"Cora"*, *"Vahana"*, *"Joby"*, and *"Lilium"*. The configuration on the right side represents the hydrogen-powered *"Skai"* eVTOL. As outlined, both powertrain systems are hybrid systems. Thus the respective energy carriers are complemented by a high-power LiPo battery pack. For brevity's sake, this chapter will refer to the powertrain system only by its main energy carrier, i. e. batteries or hydrogen.

Discussion of DGM: The four left configurations, namely *"Volocopter"*, *"CityAirbus"*, *"Vahana"*, and *"Cora"*, are being developed for maximum ranges of 36, 50, and 100 km,

---

[5]Refer to the **Note** provided at this section's opening.

respectively, and resemble lower-range configurations in the eVTOL configuration spectrum. With a shown convergence of the conceptual design framework at a DGM of around 600 kg, 1.400 kg, 750 kg, and 600 kg, respectively, the configurations are also the most lightweight concepts within the study's scope. Recall that of the four, "CityAirbus", with its convergence-DGM of 1300 kg, is the only four-seater, while the other three are designed for two seats. The convergence-DGM of "Volocopter" and "CityAirbus" is distinctly lower than the officially communicated vehicle weights. This illustrates the outlined aim of the thesis to use real-world examples as a proxy for eVTOL configurations rather than retrofit actual concepts. As such, the results can improve the understanding of eVTOL-companies' design paradigms and assumptions. The significant DGM deviations of the proxies "Volocopter" and "CityAirbus" from the real-world vehicles' weight can be attributed to deviations in two input parameters and their respective domains:

1. The **requirements** domain of real-world eVTOL is subject to uncertainty. Most likely, eVTOL-companies differ in their **hover time specification**. Companies that develop Multi-Rotor configurations, like Volocopter and Airbus, arguably emphasize hover efficiency. Consequently, the author expects their eVTOL configurations to be designed for hover times longer than the assumed 1.5 min.

2. The framework assumes a similar **technological** domain for all configurations, with commercially available LMBs. The configuration proxies "Volocopter" and "CityAirbus" are sized using high **specific energy** LMB technology. However, their real-world counterparts are already undergoing extensive testing and thus rely on battery technology that is already available today, i. e. LIBs.

Following the first four designs in Figure 4.2 are the two battery-powered configurations resembling "Joby" and "Lilium", both at considerably higher maximum ranges and higher DGMs of 1.700 kg and 3.000 kg, respectively. Lastly, the hydrogen fuel cell-powered eVTOL "Skai", with a maximum range of around 640 km, converges at a DGM of around 1.500 kg. All three designs depicted on the right side of Figure 4.2 are developed for a capacity of four passengers and one pilot, or five passengers if operated autonomously. Of the three, "Joby" is the only one with an officially communicated DGM (2.177 km), which is also underestimated by the frameworks convergence-DGM. The results resembling "Lilium"'s configuration are at the verge of physical feasibility. The entire DGM confidence interval vastly exceeds the value of 1.500 km, stated by the companies' founder Daniel Wiegand in interviews. The thesis assumptions regarding *Lilium's* configuration are arguably optimistic, like its high figure of merit and optimistic lift-to-drag ratio presented in Table 4.2. However, this could be balanced by a potential overestimation of the structural mass and the required hover time. Referencing researchers of the Carnegie Mellon University, a recent Forbes article claims that *Lilium's* five-seater consumes around 1.2 MW in hover flight [215]. This framework finds the hover power consumption to be even higher, at around 1.4 MW. If one were to choose a lighter structural weight of $f_{Struct} = 0.19$ to 0.21 N/kW as input to the framework, the five-seater "Lilium" would converge at a DGM of $2,000$ to 2.500 kg and meet the 1.2 MW hover power. However, a reduction of the required hover time by 30 sec does not

lower this DGM range by much, indicating that the battery capacity is largely influenced by the high required discharge current[6].

Discussion of CSE: The Consumed Specific Energy (CSE) per passenger-kilometer traveled (PKT) shows a fundamentally different behavior over the configurations than the DGM. As seen in Figure 4.2, *"Volocopter"* has the highest median CSE of 0.6 kWh/PKT, despite being one of the most lightweight configurations. The other two lightweight two-seater configurations, *"Vahana"* and *"Cora"*, both sized for a maximum range of 100 km, consume around 3.5 and around 2.5 kWh/PKT, respectively. In contrast, the most heavyweight configurations resembling *"Joby"* and *"Lilium"*, which are developed for higher ranges of 240 and 300 km, require the least amount of energy per PKT with median CSEs of between 0.1 and 0.2 kWh/PKT. The *"Skai"* configuration exhibits, despite being the most heavyweight of the Multi-Rotor configurations, a median CSE of around 3.5 kWh/PKT. All three Multi-Rotor configurations (*"Volocopter"*, *"CityAirbus"*, *"Skai"*) show a significant spread in their 95 % confidence intervals. The described behavior is discussed in the context of two influential factors, but not limited to those.

1. **Cruise performance**: The required energy is calculated based on the power required by flight states and the time spent in those flight states. With a relatively short hover share, due to the uniform mode value of $t_{hov} = 1.5$ min, the total energy consumption is highly dependent on the cruise power. The cruise power equation[7] holds $^L/_D$ as the sole denominator and the cruise velocity V_{crs} in the numerator. Based on Tables 4.1 and 4.2, one finds the ratios of V_{crs} to $^L/_D$ (using the mode, i. e. most likely value) around 5.5 for Vectored Thrust configurations and around 10 for Multi-Rotor configurations. The low confidence of CSE results of Multi-Rotor configurations can be attributed to the uncertainty in the underlying $^L/_D$ data. At the minimum and maximum bounds of $^L/_D$, the above-described ratio results in values around 16.7 and 5.7, respectively.

2. **Functional unit**: The CSE is defined as the required energy per PKT. The functional unit PKT directly influences the quantity of CSE through the traveled distance and the number of passengers carried per mission leg. As such, the 600 kg, two-seat *"Volocopter"* consumes almost double the CSE than the four-seat 1.300 kg, four-seat *"CityAirbus"*. The impact of varying mission leg distances on CSE is hardly separable from other influential factors in Figure 4.2, as all configurations are operated at their design point, i. e. at their specified maximum cruise range.

Despite assumptions accounting for additional structural mass in Tilt-Rotor and Vectored Thrust configurations, i. e. for wings and empennages, such concepts seem most energy-efficient if operated at their design range. However, note the functional unit's potential influence, especially if eVTOLs are operated off their design point, i. e. in multi-legged missions.

---

[6]As outlined in Section 2.1, Lilium recently announced to pursue a seven-seater configuration and reduced the advocated range to 261 km, assuming a battery energy density of 320 Wh/kg [29].
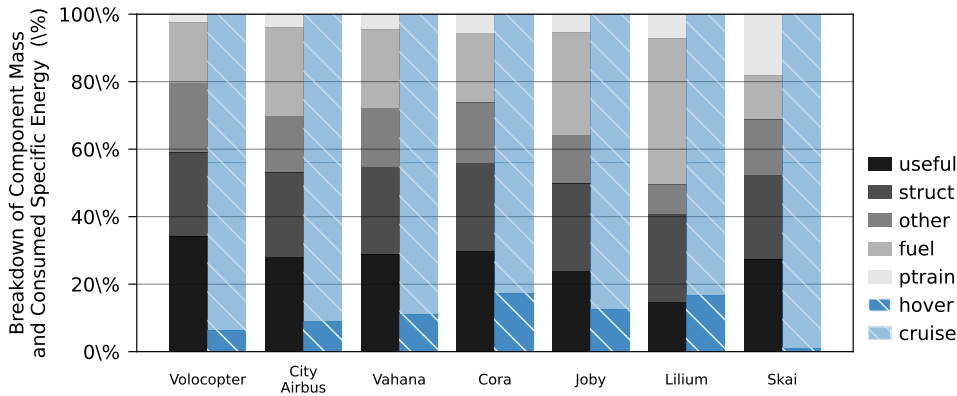
[7]Refer to Equation 3.2

Figure 4.3: Component break down of eVTOL mass and consumed energy.

Discussion of DGM and CSE breakdown: An additional view on the described DGM and CSE is provided in Figure 4.3, which shows a breakdown of the two quantities into their components. Respectively, the sub-system's masses and the main flight states accounting for the CSE are depicted by color scales of grey and blue, shaded from darker to lighter. Focusing on the battery-powered configurations, i. e. the first six columns from the left, a continuous decline of the relative shares of *useful* and *other* masses are discernible. In contrast, the mass shares of the *fuel* and *powertrain* consistently increase. In battery-powered versions, *fuel* resembles the entire battery system, including the battery management system (BMS) and cooling, while the *powertrain* value reflects the electric motor weight. The hydrogen-powered Skai configuration shows a different component mass breakdown, with a higher share of *useful*, *other*, and *powertrain* masses, and a distinctly lower share of the *fuel* mass category. Here, *fuel* contains the mass of stored hydrogen and the tank, while the *powertrain* accounts for the entire fuel cell system.

Concerning the flight states' breakdown, it is visible how hover segments consume comparably little energy but are increasingly significant with longer mission ranges in battery-powered concepts. In the hydrogen-powered *"Skai"* configuration, the contribution of hover energy is however almost negligible. The high power requirement of *Lilium's* configuration, which was discussed before, is impressively put into perspective. Although hover mode accounts for only 2.5 % of the flight time if operated on a 300 km mission, it consumes a staggering 20 % of the energy. In contrast, the *"Joby"* configuration uses around 12% of its total consumed energy for hovering. Again, note that results are based on the above-documented assumptions and consider how changes in single assumptions alter a concept's DGM. In summary, the findings indicate how configuration choices of eVTOL designers shape the vehicle's cost and impact performance.

4.1.5 Sensitivity analysis and discussion

The presented results are better understood in the context of their sensitivities towards modeling parameters of the respective domains. It was outlined in Section 4.1.2 how
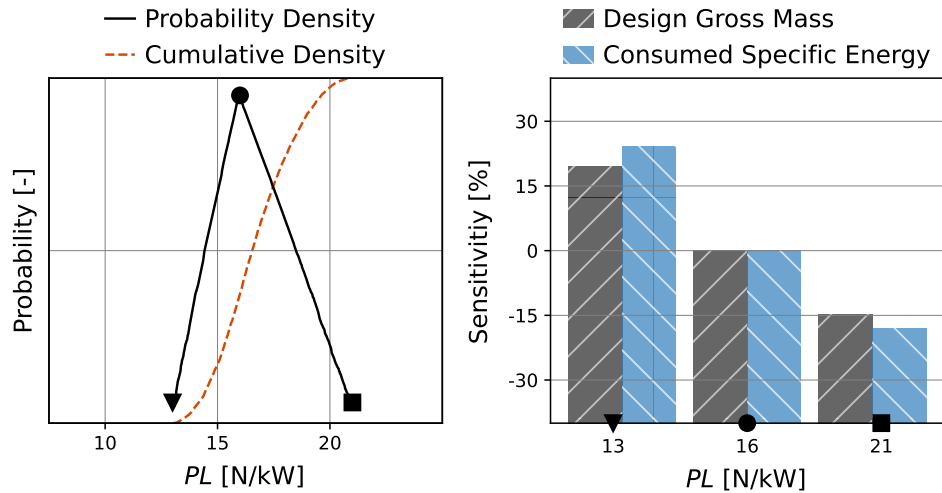
Figure 4.4: Triangular distribution and sensitivity analyses of *"Lilium's"* power loading

triangular distributions are used to represent those domains. Therefore, the Sensitivity Analysis (SA) in Figure 4.5 depicts how the DGM and the CSE change if the underlying parameters are set to their respective minimum and maximum value. Figure 4.4 illustrates this for variations of the power loading of the *"Lilium"* configuration.

The left subplot of Figure 4.4 shows the PDF and CDF[8] of the *"Lilium"* configuration's power loading. Distinct markers highlight the minimum, mode, and maximum values of PL. The right subplot shows the SA, i. e. it provides information on how sensitive the DGM and CSE react to changes of PL. The SA is performed with a one-at-a-time sampling of the distinct minimum, mode, and maximum values, which are again highlighted by the respective markers. The sensitivities of DGM and CSE are represented by gray and blue bars, respectively. It is discernible in the triangular distribution on the left that the distinct values are not distributed equidistant, implying that the distribution's mode, i. e. the *most probable* value, does not reflect the distribution's mean or median. Therefore, note that the bars depicting the sensitivities in the right are not placed equidistant either.

Figure 4.5 shows the SA of both the DGM and the CSE regarding the design, requirements, technology, and operations domains for all seven configurations analyzed before. Rows display the analysis' sensitivity by the input parameter, which is subject to uncertainty and therefore altered toward its lower and upper bound in the sampling. Columns reflect the analyzed eVTOL configurations, again in the order of increasing range requirement. The order of rows and displayed parameter variation follows the domains:

---

[8]Recall Figure 4.1

- The **requirements** domain is reflected by variations of the specified mission hover time (t_{hov}) in the **first row**. The row only shows grey bars, indicating that the normalized sensitivities of DGM and CSE on t_{hov} are equal.

- Sensitivities on the **design** domain are displayed by parameter variations of the lift-to-drag ratio (L/D), the power loading (PL), and structural weight fraction (f_{Struct}) in **rows two to four**. For f_{Struct}, the normalized sensitivities of DGM and CSE coincide, therefore row four shows only grey bars.

- The **technology** domain, represented by the battery cell-specific energy (e_{sp}) for battery-powered eVTOL and by the fuel cell-specific power (p_{spec}) for the hydrogen-powered *"Skai"* concept, is provided in **row five**. Again, the absence of blue bars indicates equal sensitivity of DGM and CSE.

- Concluding the SA, the influence of the **operations** domain, through shorter mission cruise ranges (r_{crs}) or longer required hover-like flight segments (t_{hov}), is shown in **rows six and seven**. Here, only blue bars are shown. In contrast to previous rows and domains, the operational domain does not influence the DGM. As grey bars would mark a normalized sensitivity of unity for every configuration, they are not depicted.

Discussion of DGM sensitivities: First, and unsurprisingly, Figure 4.5 indicates how increases in t_{hover} and f_{Struct} imply a DGM increase, while increases in L/D, PL, and e_{Spec} or p_{Spec} lead to a DGM decrease. It is discernible how input uncertainties towards t_{hover}, f_{Struct}, and PL, as presented in Table 4.2, are relatively low for the lightweight configurations *"Volocopter"*, *"CityAirbus"*, *"Vahana"*, and *"Cora"*, but significantly increase in the *"Joby"* and *"Lilium"* concepts. An increase of the required hover time by 30s to a total of 2min has a distinct effect on the DGM of especially *"Lilium"*, *"Joby"*, and *"Cora"*. The three configuration's DGM similarly reacts to variations in PL and f_{Struct}, pointing toward a high sensitivity of fixed-wing configurations with a small effective rotor disk area toward high-power flight states. It is, in turn, observable how the DGM of multi-rotor configurations with a higher effective disk area, like of *"Volocopter"* and *"CityAirbus"*, is influenced little by changes in t_{hover}, PL, f_{Struct}. Transferring to the analysis of DGM in Figure 4.2, where those concepts converged at lower DGM than published by the companies, allows again to conclude that the projects have specified a substantially higher hover time to be met by their eVTOL aircraft.

The sensitivity of DGM on L/D decreases with higher baseline values of L/D, as is the case for fixed-wing configurations like *"Joby"* and *"Lilium"*. This is hardly surprising, as it indicates how fixed-wing configurations are quite robust toward the achieved L/D, given it is high enough. In their case, the aerodynamic performance is as influential as the available energy density. In contrast, Multi-Rotor configurations and Lift & Cruise concepts are much more sensitive toward aerodynamics than toward the battery cells' specific energy. In the case of *Wisk*, which displays the highest sensitivity toward L/D, this must be accounted to the low baseline value in combination with high deviations toward *min* and *max*. When comparing DGM variations due to changing different inputs,
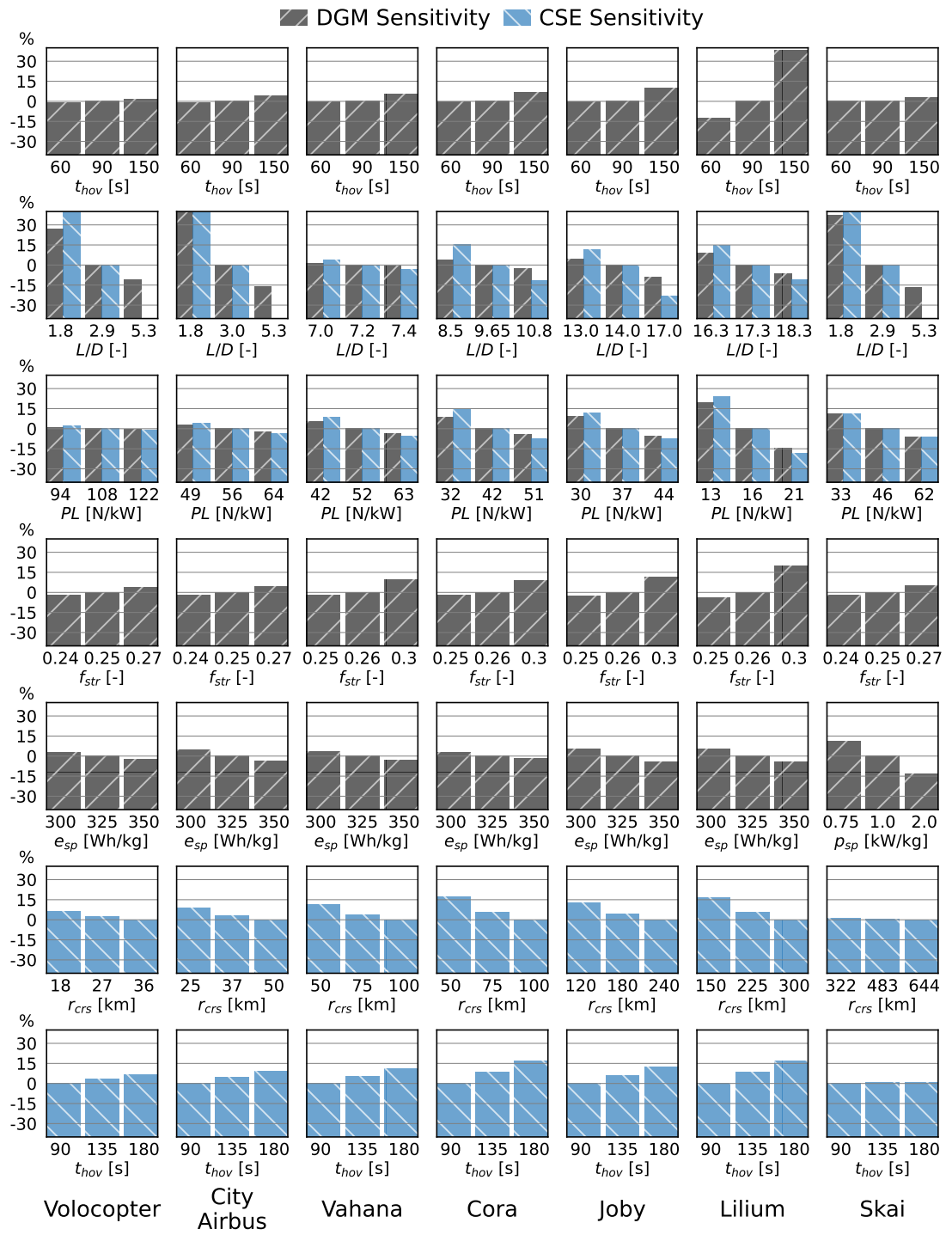
Figure 4.5: Sensitivities of Design Gross Mass on Parameters

one must furthermore note how the input parameters of a concept are interdependent. Aerodynamically efficient configurations like *"Joby"* and *"Lilium"* require higher baseline structural mass fractions, while multi-rotor configurations have a comparably lower f_{Struct}. This interdependency between the parameters L/D, PL, and f_{Struct} (among others, such as the cruise velocity) is used in Section 4.3 to decouple the design, analysis, and assessment from fixed configurations and provide a more general insight.

Discussion of CSE sensitivities: Observing the sensitivity of CSE regarding input variations, displayed by the blue bars in Figure 4.5, underlines two central findings. First, the SA of the design domain in terms of input L/D and PL shows how variations in the two parameters have a bigger influence on CSE than on DGM. The flight states' power calculation outlined in Equation 3.2 displays the increased order of relation toward L/D. As such, it marks how the DGM can be unfit if used as the sole parameter to judge the viability of a configuration. The CSE of all configurations except *"Joby"* and *"Lilium"* is more than 25% higher than its baseline value if L/D is estimated at its lower end in Table 4.2. As such, and in accordance with the assessment of Datta et al. [33] and the analysis performed in Section 3.1, the high importance of L/D to assess a configuration's viability and environmental impact is stressed. In contrast, although also increased versus the DGM bar height, the sensitivity of CSE toward PL is less critical. Note how the underlying data to PL relies on more detailed assumptions such as the Figure of Merit and rotor radius and is less prone to uncertainty.

The second finding concerns the results presented in rows six and seven of Figure 4.5. Recall how they provide the sensitivities toward off-design performance in the operational domain, i.e. shorter actual cruise ranges of 50%, 75%, and 100%, and longer hover times of 100%, 150%, and 200%, respectively. It is apparent how all configurations except the hydrogen-powered *"Skai"* aircraft show considerable sensitivity toward off-design performance. Moreover, variations in battery-powered configurations appear to grow from left to right and peak for *"Joby"* and *"Lilium"*. In that, the high sensitivity toward an increased hover time (row seven) appears straightforward, as the earlier analysis has shown how those concepts are optimized toward cruise flight but sensitive toward high-power flight states. Depending on potential operational constraints in application scenarios, such as a minimum cruise altitude over populated areas requiring an extended high-power vertical flight segment, the flight envelope in terms of range and endurance of battery-powered fixed-wing configurations could therefore be significantly confined. The high sensitivity on the reduced cruise range (row six) can be explained by a relatively longer hover mode. The earlier discussed Figure 4.3 showed how hover flight contributes to 20% of the *"Lilium"*'s CSE in design conditions, albeit the aircraft only spends 90s of its 1h mission, i.e. 2.5% in hover mode. A shorter cruise segment accordingly increases the hover share. At the bottom line, off-design mission requirements have as much influence on the performance as the designers' choices and the technology's readiness. Assuming that eVTOLs operations will divert from their design optimum, one must infer that the assessment of environmental impact, primarily based on the CSE, must be performed case-by-case.

4.2 Carbon Impact Assessment

4.2.1 Material sourcing and production

The carbon life cycle impact eVTOLs is determined by the amount of GHG emitted in the processes related to the vehicles' production, operation, and disposal. Modeling includes impacts from the sourcing of materials, the recurring sourcing of powertrain components, and from the production of the means of energy, i. e. electricity, or hydrogen. This section provides the required data for the first two of the three.

Materials	Unit	Impact	Refs.
Aluminum		8.3 - 27.7	
Steel		1.9 - 3.0	
Titanium		31.3 - 49.0	
Copper	$\frac{\text{kg CO}_2\text{eq}}{\text{kg material}}$	1.3 - 2.3	[216]–[219]
Carbon Fiber		28.5 - 35.2	
Glass Fiber		7.5 - 8.3	
Polymers		2.6 - 8.3	

Table 4.5: Greenhouse gas impact indices of used materials.

Table 4.5 presents the amount of GHG emitted in the sourcing of the eVTOLs materials. As displayed by the considerable difference of the data, i. e. concerning the sourcing of Aluminum, it is essential to understand the implications of regional differences and variations in companies' sourcing strategy. A common presumption is that parts and materials sourced in, for example, China, have a higher carbon footprint due to a high grid carbon intensity. However, the latter is not imperatively dependent on geography but might be affected by policy. Therefore, a thorough assessment requires either a case-by-case perspective or a valid quantification of uncertainties.

Materials	Material shares				
	Structural Mass	Electric Motors	Other Masses	Fuel Cell Stack	Fuel Tank
Aluminum	0.10	-	0.20	0.10	-
Steel	0.05	0.50	-	0.75	-
Titanium	0.05	-	-	-	-
Copper	-	0.50	-	0.10	-
Carbon Fiber	0.60	-	0.30	-	0.80
Glass Fiber	0.10	-	0.10	-	-
Polymers	0.10	-	0.40	0.05	0.20

Table 4.6: Assumptions of eVTOL component material compositions.

Subsequently, Table 4.6 introduces the materials' fractions in the seVTOL components, as provided by the design module of the methodology. As André and Hajek describe

in an earlier publication, the data may contain significant uncertainties [41]. Potential remedies include further breakdowns of sub-systems into elements as well as interviews of experts. However, such options do not solve the apparent knowledge gap compared to actual material shares due to the inherent a priori perspective of the assessment of a yet-to-emerge eVTOL aircraft. The following results indicate that precise knowledge of materials' fractions within the aircraft's subsystems is less influential on eVTOLs environmental performance than other incorporated parameters and domains. Hence, the qualitative approach to material fractions suffices the thesis scope. Nevertheless, the implemented thesis allows to assess uncertainties within the fractions of single or multiple materials and quantify their impact.

4.2.2 Electrochemical power source scenarios

Battery-powered eVTOLs are only as sustainable as the technology behind the production of electricity and batteries themselves [40], [41]. Likely the same applies to hydrogen fuel cell-powered systems. Therefore, upstream carbon emissions associated with both the battery-electric and the hydrogen-electric energy storage and conversion system are provided as input to the environmental domains of the implemented framework. As outlined, data describing such systems is prone to regional and temporal variations and changes. The grid carbon intensity invoked by electricity production is dependent on the energy mix, i. e. on the type of primary energy production. This mix varies from country to county, and is gradually changing toward an overall cleaner production mix, with ambitious but deemed necessary goals set for the coming decades. Figure 4.6 shows the grid carbon intensity of selected regions up until 2018, as well as the prediction of the International Energy Agency (IEA) on how the grid carbon intensity will develop in those regions until 2040.
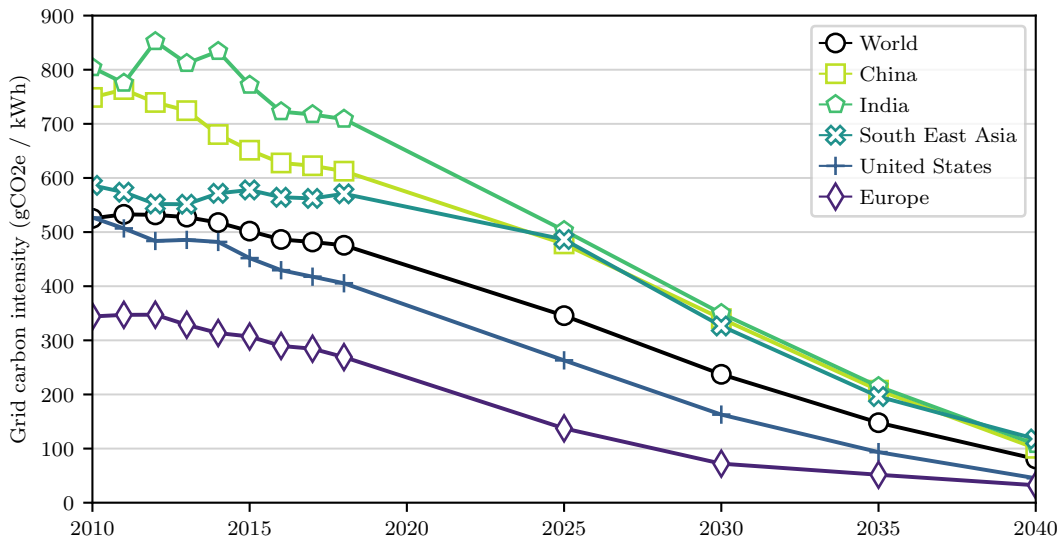

Figure 4.6: Recording and outlook of grid carbon intensity development

Top-down predictions of the impact of electricity production, like the one presented in Figure 4.6, are readily available from multiple sources due to the agreed-upon relevance of grid carbon intensity in light of the transformation toward a sustainable economy. The other impact sources relevant for the study, like the production of batteries, hydrogen, and fuel cells, are represented mainly by studies using a bottom-up approach and an ex-post perspective. Existing production processes are decomposed and reviewed in terms of their environmental impact, but predictions on future developments are harder to find. Therefore, this thesis pursues a scenario-based approach and determines sets of impact data to be fed into the assessment methodology. The three scenarios used in the following represent the reference state-of-the-art sourcing impacts, labeled *Today*, and two different future cases labeled *2030 Basic* and *2030 Green*. Values used in *2030 Green* do not predict the actual 2030 values but indicate a potential *what-if* scenario. As such, *2030 Green* represents an economy primarily supplied by renewable power, where carbon impact is a prioritized criterion in the choices of eVTOL companies and their partners and suppliers. Although *2030 Green* collects impact optima as published today and therefore pictures a challenging scenario, it is also possible that the actual 2030 scenario will be even more *sustainable*. The underlying assumptions are provided in Section 2.4. The impact of hydrogen is calculated according to the share of involved production methods. The *2030 Basic* assumes that production through gas reforming, solar, and wind energy each account for a third.

Parameter	Unit	Today	2030 Basic	2030 Green	Refs.
Electricity	$gCO_2e/\ kWh_e$	237.	72.	20.	[220]–[223]
Battery	$kgCO_2e/\ kWh_c$	212	112.	62.	[157]–[159]
Hydrogen	$kgCO_2e/\ kg$	10.9	5.0	0.97	[192]–[194]
Fuel stack	$kgCO_2e/\ kW_p$	43.	25.	17.	[224]–[226]
Tank & systems	$kgCO_2e/\ kW_p$	58.	23.	23.	[224]

Table 4.7: Scenarios for operational impact assessment.

4.2.3 Impact Assessment

Based on the sizing and analysis performed in Section 4.1 and the material- and energy carrier-related impacts outlined earlier in Section 4.2, it is now possible to perform an environmental assessment. Recall that a system's environmental impact is determined by combining the system's elementary flows with those flow's impact. Thus, the eVTOL's DGM determines the impact of its primary production, and the CSE determines the impact caused by the generation, storage, and conversion of energy. As such, Figures 4.7 and 4.8 are constructed similarly to Figures 4.2 and 4.3, respectively. For each of the studied eVTOL configurations, Figure 4.7 depicts

- the GHG emission of primary production by stacked grey bars on the left,

- and the life cycle impact per PKT by stacked green bars on the right.

As outlined in Section 3.3.3, the life cycle carbon impact comprises the vehicle's primary production, the production of energy, i. e. electricity or hydrogen, due to the vehicle's operation, and the recurring production of energy carrier system, i. e. the battery or fuel cell, due to the vehicle's operation. The vehicle's operating life is assumed at $8,000$ flight hours, based on statements made by the eVTOL company Lilium concerning their public offering and expected profits and losses [227]. While Brown and Harris assume a comparable eVTOL lifetime of $10,000$ flight hours, commercial aviation aircraft are usually operated for about $35,000$ pressurization cycles, which can result in over $100,000$ flight hours [37]. However, assuming a comparably low lifetime of eVTOL aircraft prevents the environmental assessment from underestimating the airframe' life cycle impact. The lifetime of the energy system is considerably shorter, and outlined by Table 4.4. The average seat utilization is $f_{util} = 0.75$. In non-comparative assessments, the flight route's circuity factor is assumed at $f_{circ} = 1.0$. In contrast, subsequent comparative analyses use a circuity factor of $f_{circ} = 1.2$ implying that a route is on average $20\,\%$ longer if one travels by road. According to Balou et al., the average road circuity in Europe is 1.46 [228]. As Balou et al. focus on inter-city routes and do not account for potential detrimental factors on the beeline, $f_{circ} = 1.2$ reflects a conservative assumption. As before, error bars display the 95% confidence interval of the statistical evaluation performed based on the outlined uncertainties. Two types of error bars resemble distinct sets of uncertainty samples and are discussed in the following.
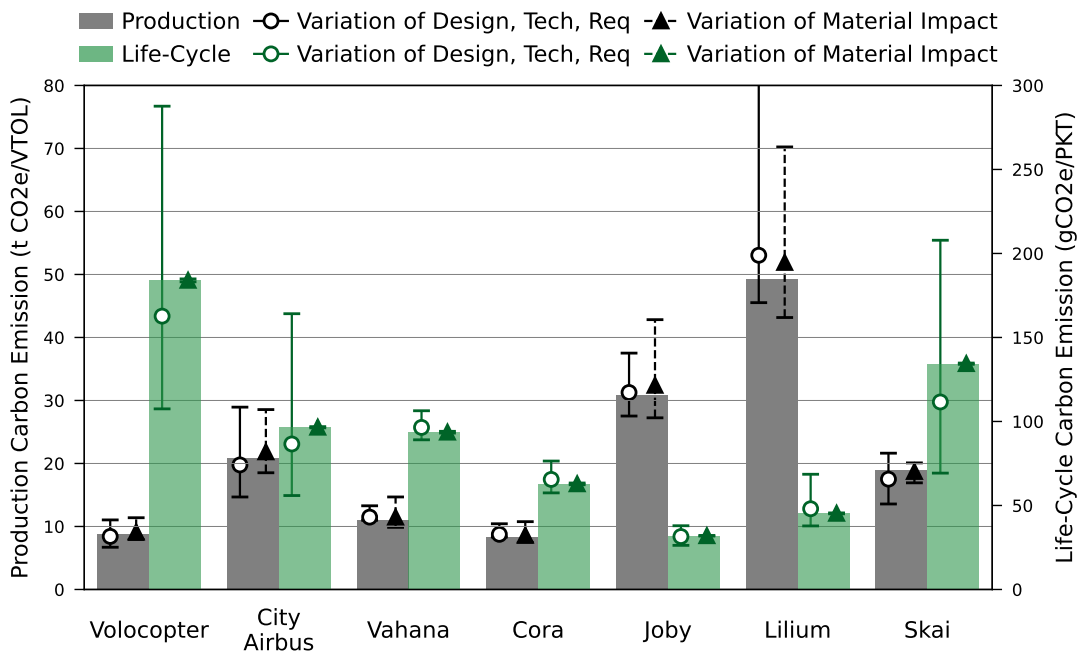

Figure 4.7: Production impact and Life Cycle Assessment of eVTOL configurations.

Discussion of greenhouse gas emissions: Observing both the emissions of the eV-TOL's primary production and the eVTOL's life cycle shows a distinct similarity regarding the DGM and CSE analyses of the configurations in the previous section. The lightweight configurations of *"Volocopter"*, *"Vahana"*, and *"Cora"* also show the lowest GHG impact of around $10\,t\text{CO}_2\text{e}$ due to vehicle production (grey bars). Similarly, the configurations that initially converged at a higher design gross mass, i. e. the designs reflecting *"Joby"* and *"Lilium"*, also exhibit the highest GHG emissions in their production. Concerning the six battery-powered eVTOLs, the order of production-related carbon impact resembles the order of DGM. This changes when comparing the battery-powered versions with the hydrogen-powered configuration. The previously reported DGM of *"Skai"* was around $300\,\text{kg}$ higher than that of the *"CityAirbus"* configuration. However, *"Skai's"* GHG production impact is a few tons lower than that of *"CityAirbus"*, depending on the exact impact of the sourcing of materials.

The life cycle GHG impact (green bars) per passenger-kilometer traveled (PKT), building on the future *2030 Basic* scenario as detailed in Table 4.7, behaves comparably to the priorly discussed analysis of the Consumed Specific Energy (CSE). Again, the configuration reflecting *"Volocopter"* scores the highest bar, displaying per passenger-kilometer GHG emissions of around 180g CO_2e/PKT. *"CityAirbus"*, *"Vahana"*, and *"Skai"* display the next lower class of GHG emissions at around 100g CO_2e/PKT. Operational carbon emissions of *"Cora"* are approximately 60g CO_2e/PKT, while *"Joby"* and *"Lilium"* again show the lowest value with a life-cycle carbon impact of below 50g CO_2e/PKT.

Discussion of uncertainties: Analyzing the two distinct error bars in Figure 4.7 indicates a weak dependency of the life cycle impact on the materials' sourcing impact. For each bar, the **left error bars**, depicted by circular markers, resemble uncertainties within the domains Design, Requirements, and Technology, based on the triangular input distributions used within the previous section's sizing. The **right error bars**, depicted by triangular markers, show how the carbon impact changes due to the uncertainties associated with the materials' sourcing presented in Table 4.6.

- On **grey bars**, i. e. concerning the carbon impact of the vehicles' primary production, the uncertainties within the domains Design, Requirements, and Technology (left error bars, circular markers) imply a sensitivity comparable to that seen in the DGM plot in Figure 4.2. The uncertainties of the materials' sourcing impact imply sensitivities onto the *"CityAirbus"*, *"Joby"*, and *"Lilium"* configurations. Notably, as found in the subsequent impact breakdown in Figure 4.8, those three show a larger battery production impact share compared to the other configurations.

- On **green bars**, i. e. concerning life cycle impacts, the left-side error bars again exhibit a behavior comparable to the CSE error bars in 4.2, while the right-side error bars essentially collapse to their median.

Therefore, one can conclude that uncertainties present in the materials' sourcing may leverage the GHG impact of eVTOLs in primary production according to the size of the

required battery, but have negligible influence on the overall life cycle perspective. Of all uncertainties associated with components and materials, battery parameters like the allowed depth of discharge and charging cycle life are most influential.
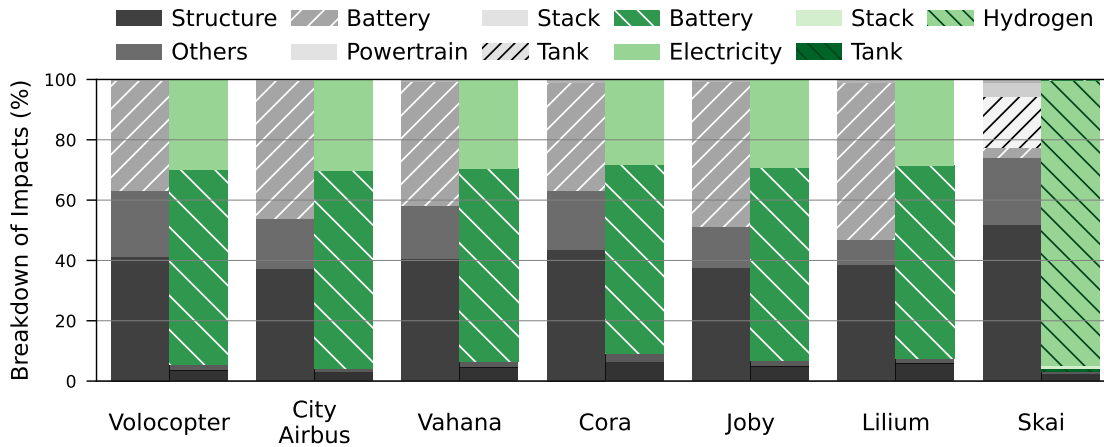

Figure 4.8: Component break down of eVTOL production and life cycle impact.

Discussion of impacts by components: Building on the last observation, Figure 4.8 analyzes the main contributions to GHG emissions regarding the eVTOLs primary production and the life cycle perspective. As outlined in Chapter 3.3, impacts associated with the production of components which are subject to wear out and replacement are accounted for as if they were a means of operation. For the battery-powered eVTOL configurations, the component breakdown (stacked grey bars in Figure 4.8) shows how the *battery's* primary production accounts for 40 to 55 % of the vehicle's carbon impact. Other significant contributors are the vehicle's *structure* with its high share of carbon fiber reinforced plastic and *other* components, containing aluminum, carbon fiber, and polymers. The impact due to the production of the *powertrain*, i. e. the electric motors, is barely perceptible at the bar's top ends.

In addition to the impact component-wise depiction, Figure 4.9 depicts the sensitivities of the primary production impact on uncertainties in the material's sourcing. The plot shows one-at-a-time sampling-based sensitivities of the four materials whose sourcing impact uncertainties lead to the highest variations in the total production impact. As is perceptible, the uncertainty in the batteries' sourcing is most influential within the battery-powered concepts. The batteries impact also indicates a considerable share within the hybrid hydrogen-powered ”Skai”, which requires a high-discharge LiPo battery for power-intense flight states. Furthermore, note the uncertainties in carbon fiber and aluminum. Carbon fiber accounts for 60 % of the vehicles' body and lifting surfaces, i. e. its *structure*, while aluminum makes for only 10 %. However, the primary production sensitivities concerning the two are of a comparable order of magnitude. This is substantiated by the much higher uncertainty related to aluminum's sourcing, as shown in Table 4.4, while carbon fiber's production emissions are always considered high.
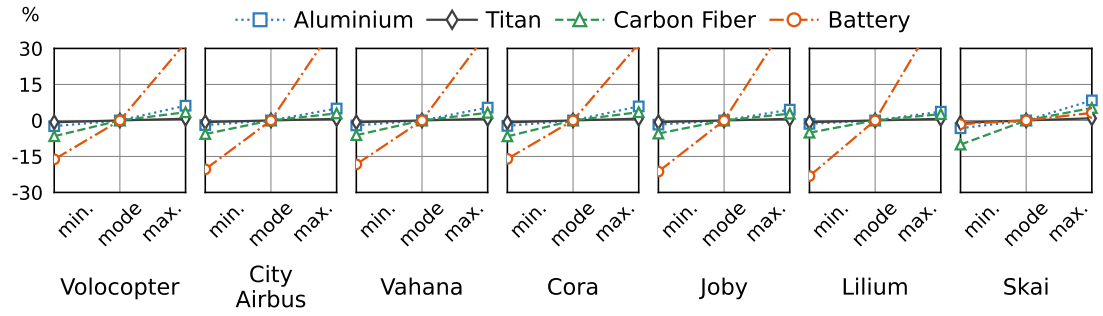
Figure 4.9: Sensitivities of material uncertainties on primary production impact.

Discussion of impacts due to life cycle phases: As for the life cycle perspective depicted in Figure 4.8, the green bars underline how the GHG emissions per PKT are almost exclusively determined by primary energy production and energy carrier production. One the one hand, the latter comprise the battery's recharging, i. e. the respective impacts of the underlying grid carbon intensity, and the production, transport, and compression of hydrogen. One the other, such impacts accounts for the (recurring) production of the battery, the fuel cell stack, and the hydrogen tank. The relative impacts of the production and end-of-life phases depend on the eVTOLs lifetime. However, as discussed herein and in accordance with a prior publication, the excessive energy consumption in flying applications lets respective emissions surpass even high production impacts by orders of magnitude [41]. In summary, the LCA of the eVTOL configurations yields the following conclusions:

1. The carbon impact of the primary production of eVTOL aircraft scales with the configurations DGM. The life cycle carbon impact of eVTOL aircraft scales with the vehicle operations CSE.

2. The primary production impact of non-recurring eVTOL components, i. e. structure and other materials, accounts for around 5 to 10% of the vehicle's life cycle carbon impact, at the lower end of 8, 000 flight hours life expectancy.

3. Uncertainties regarding the sourcing of materials in non-recurring eVTOL components, i. e. structure and other materials, have no substantial influence on the life cycle carbon impact of eVTOL aircraft.

With the high influence of CSE and the large share of energy carrier related carbon impact, it is required to perform distinct scenario-based assessments of eVTOL configurations. In line with the thesis' aims and in light of the present uncertainties in underlying domains, future analyses exclude the primary production impact of non-recurring eVTOL components and solely report the Specific Carbon Impact (SCI) per passenger-kilometer.

4.2.4 Comparative case study and discussion

The carbon impact assessment is completed by the scenario-based case study presented in Figure 4.10. It presents the Specific Carbon Impact (SCI) of eVTOLs, including the primary production of consumed energy and the recurring production of energy carrier systems, in light of the uncertainties concerning configurations, technological capabilities, design choices, and mission scenarios. As in the previous analyses, the seven eVTOL configurations in scope are "Volocopter", "CityAirbus", "Vahana", "Cora", "Joby", "Lilium", and "Skai". The configurations' results are again ordered by their maximum design range along the x-axis. For reference, the x-axis is complemented by the life cycle carbon impact of a Battery Electric Vehicle (BEV) in the rightmost column. Three distinct application scenarios are analyzed and displayed in the subplots of Figure 4.10:

- An **Urban Commute** of 25km (upper subplot).

- A medium-range flight of 60km denoted as **Airport Transport** (medium subplot).

- A long-range **Intercity Travel** of 150km (bottom subplot).

Not all configurations meet each scenario's range requirement. Configurations like "Volocopter" and "CityAirbus" only show results for the Urban Commute. The difference between the maximum design range and the operational range is displayed by grey bars in lighter and darker shades, respectively. The configurations' carbon impact is visualized by green-edged squares and green-filled circles for the *2030 Basic* and *2030 Green* scenarios. Uncertainties associated with the Design, Requirements, and Technology domains are marked by error bars displaying the 95% confidence intervals, based on $10,000$ samples evaluated in a Monte Carlo scheme.

The BEV assessment yields a life-cycle carbon impact range from 17 to 34gCO$_2$/PKT in the *2030 Basic* setting, and from 12 to 22gCO$_2$/PKT in *2030 Green*. As discussed in Section 3.3, the BEV's carbon impact is evaluated without accounting for construction and maintenance of road, which would add another 8gCO$_2$/PKT. Uncertainty within the BEV data is represented in triangular distributions of the possible battery pack mileage ($100k$, $300k$, and $400k$ km), the fuel economy (0.1, 0.13, and 0.15 kWh/km), the primary production impact (4.6, 5.7, 6.8 tCO$_2$), and learning factors to account for a decreased grid carbon intensity in the respective scenarios. There is certainly no shortage of BEV LCAs, thus interested readers may refer to Woo and Choi for a distinct well-to-wheel environmental assessment of various models [229].

The operational impact of eVTOL configurations qualitatively follows the trend of CSE of configurations shown in Figure 4.2, irrespective of the underlying energy scenario. Nevertheless, the distinction of scenarios brings about a notable finding. The sensitivity due to the combined uncertainties of the Design, Requirements, and Technology domains falls short of the uncertainty present in the energy scenario for every analyzed configuration. Moreover, the influence of those "domain uncertainties" on the operational impact is distinctly smaller in the *2030 Green* scenario compared to *2030 Basic*. The same applies to the influence of the operational scenario on the operational
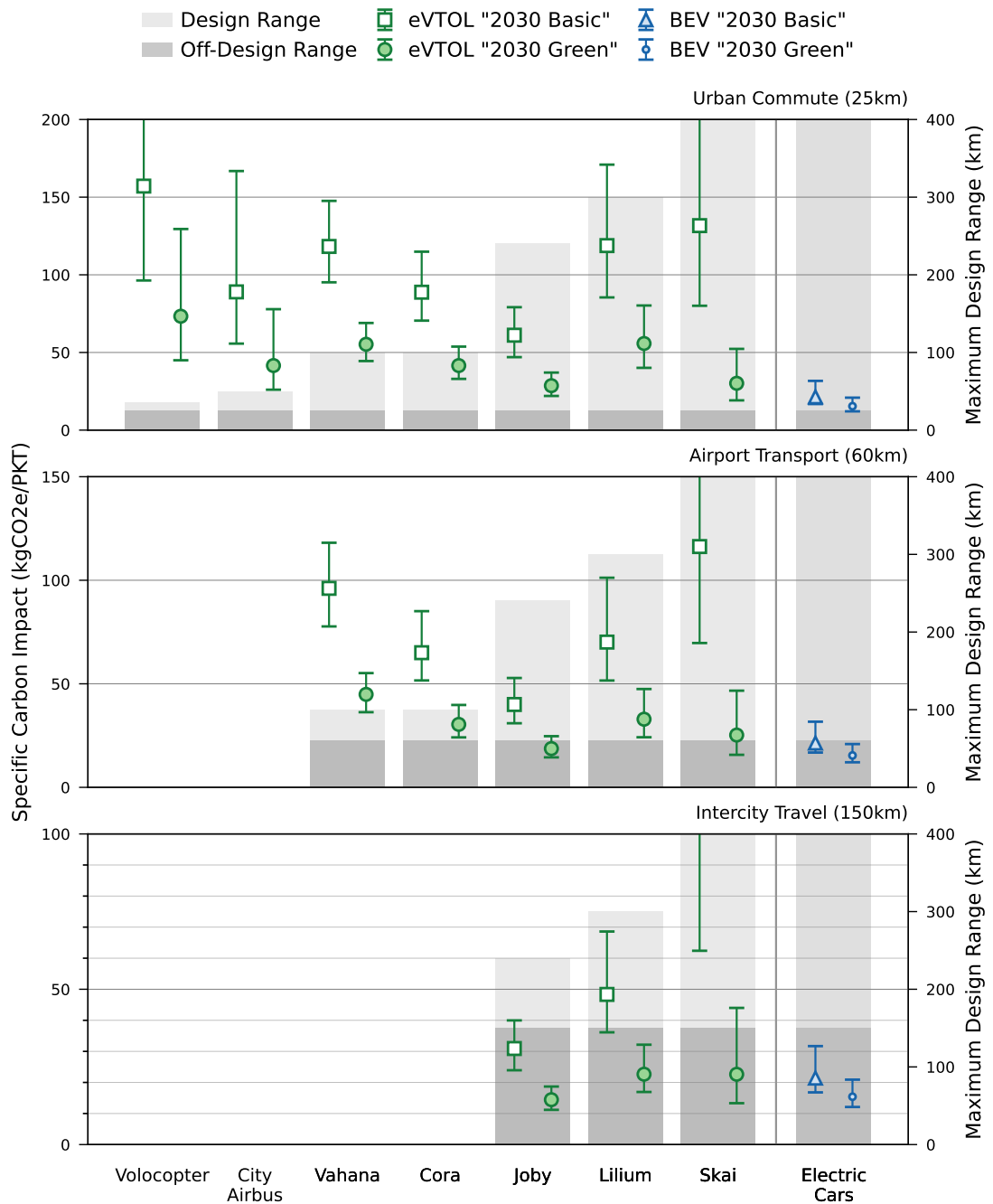
Figure 4.10: Comparative case-by-case impact assessment of eVTOL configurations.

impact. While the *"Lilium"* configuration emits around 40 to 75gCO$_2$/PKT if employed on a 150km mission in the *2030 Basic* scenario, an off-design *Urban Commute* of 25km increases its impact to around 100 to 220gCO$_2$/PKT. The observation stresses the high

importance of the operational domain and underlying background system regarding the assessment result. Therefore, the remainder of the discussion is oriented along the three operational scenarios.

- **Urban Commute**: While all analyzed configurations can serve the short 25 km route, none can "environmentally compete" with BEVs, given that the *2030 Basic* scenario is assumed. Of all configurations, the *"Joby"* concept yields the lowest median SCI at around $60gCO_2$/PKT. Employing the *2030 Green* scenario, the assessment finds four of the seven eVTOL configurations at an SCI of below $50gCO_2$/PKT and two configurations, namely *"Joby"* and *"Skai"* within the order of magnitude of, yet still above the median impact of BEVs. Therefore, the assessed eVTOL configurations are, in comparison to future electric cars, unlikely to provide a more sustainable form of transport on short commutes.

- **Airport Transport**: With increasing operational range, the remaining "capable" configurations yield a median SCI below $100gCO_2$/PKT in the *2030 Basic* scenario and below $50gCO_2$/PKT in the *2030 Green* scenario. In the latter scenario, the two least-emitting configurations, *"Joby"* and *"Skai"*, even achieve SCI levels below $25gCO_2$/PKT. Albeit not "beating" the $18gCO_2$/PKT of the *2030 green* BEV, the eVTOL SCI's error bars overlap with those of the electric vehicle. The error bars in eVTOLs mark uncertainties of different parameters than in the BEV. Therefore it can be concluded that a medium range of 60 km could "environmentally favor" the operation of eVTOLs over electric vehicles. However, carefully note the much lower utilization of BEVs (1.4 passengers on average) versus $f_{Util} = 0.75$ for eVTOLs.

- **Intercity Travel**: At the longes mission ranges the SCI of the remaining "capable" eVTOL configurations *"Joby"*, *"Lilium"*, and *"Skai"* all yield a median SCI below $30gCO_2$/PKT in the *2030 green* scenario. However, due to the underlying uncertainties, the upper SCI confidence intervals reach almost $40gCO_2$/PKT. In contrast, the SCI of *"Joby"* is between 10 and $20gCO_2$/PKT with high certainty and thus spreads over a similar interval as the BEV's carbon impact. Evidently, the longer operational range and consequently shorter relative hover share support the "environmental competitiveness" of eVTOL versus electric cars.

Three conclusions stand out at the bottom line of the comparative case study:

1. Of the diverse set of configurations, fixed-wing, high-payload concepts like *"Joby"* or *"Lilium"*, the hydrogen-powered *"Skai"* are most likely to provide comparably sustainable form of transportation in future "low-carbon" scenarios.

2. The share of renewably sourced energy in future economies is more influential on the life cycle carbon emissions of eVTOL aircraft than the uncertainties present in low-fidelity models of the Requirements, Design, and Technology domains.

3. The impact of eVTOL is driven by the operational mission length, i.e. the hover share, and other operational factors. Refer to the previous publication of André and Hajek for a discussion of the respective main drivers [41].

4.3 Generalized Design, Analysis, and Assessment

The utilization of distributed electric propulsion (DEP) in eVTOLs allows novel aircraft configurations, compared to the exhausted design spaces of turboshaft-powered rotorcraft and fixed-wing aircraft. However, eVTOL are confronted by the same multi-disciplinary design problem as conventional aircraft, as increases of distinct parameters are possible only at the expense of others. A simple representation of this conflict is whether a configuration should be reasonably fit for vertical flight, i. e. through a large effective rotor disk area, or for an efficient horizontal flight at comparably higher speed. The previous sections demonstrated the application of the integrated design and assessment methodology using a selection of eVTOL representatives as proxy configurations for real-world eVTOL designs. This section explores the characteristics and capabilities of eVTOL aircraft on a generalized conceptual design level. A central question in this analysis is how those characteristics and capabilities are affected by the availability and choice of the alternative electrochemical energy carriers.
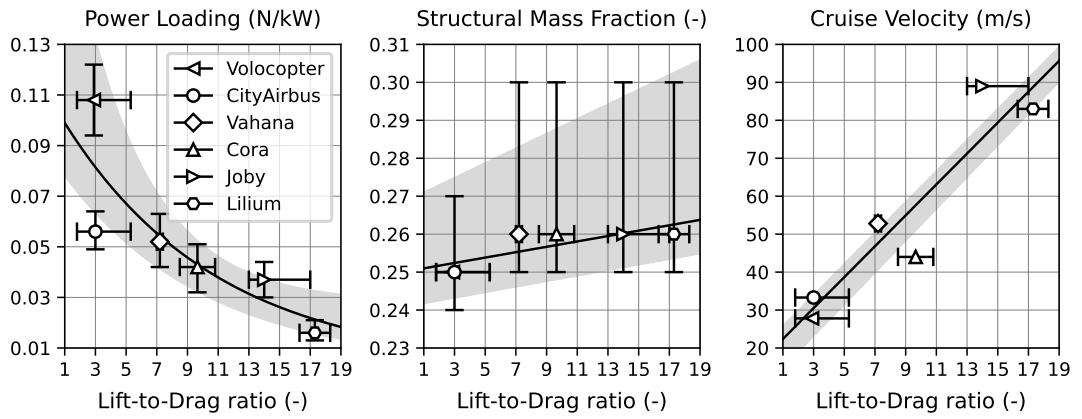
Figure 4.11: Regressions of eVTOL system-level metrics.

The design, analysis, and assessment performed in the previous sections built on selecting distinct values and distributions for parameters of the domains. Within the present framework, each eVTOL configuration was represented by a ***Parameter Tuple*** describing the mission requirement, design characteristics, and technological capabilities. This section's generalization approach uses the parameter tuples of the previously assessed configurations to derive regression-based relationships between parameters and reduce the number of required inputs to one central design parameter.

Figure 4.11 outlines this approach. The central design parameter is the configurations' lift-to-drag ratio (L/D), shown on the x-axis[9]. The y-axes of the subplots span the space for the power loading (PL), the structural mass fraction (f_{Struct}), and the respective cruise velocity (V_{crs}). The previously analyzed proxy configurations are depicted by var-

---

[9]Recall that L/D refers to the typical cruise speed of each configuration

ious markers. In each subplot, lines depict the regressional relationship for the input distributions *mode* values, i. e. the values with the highest probability according to the triangular input distributions[10]. Grey shades outline the area between regressions of *minimum* and *maximum* values, which are depicted by error bars in the three subplots. The relation between L/D and PL is modeled through a non-linear least-squares fit using the Levenberg-Marquardt algorithm and described by $PL = 0.103 \cdot \exp\left(-0.114\, L/D\right) + 0.009$. The tuple values of f_{Struct} and V_{crs} are found through linear least-squares regression and given by $f_{Struct} = 7.1 \cdot 10^{-4}\, L/D + 0.25$ and $V_{crs} = 4.72\, L/D + 18.3$. Figure 4.11 illustrates the interdependency of design parameters at the state-of-the-art in eVTOL engineering, as well as the associated uncertainties. Adding data on further configurations and revising the data toward the actual capabilities of eVTOL aircraft, either by testing or by higher-fidelity modeling and analyses, will improve the robustness of the depiction and provide insight into the boundaries of the eVTOL design space.

4.3.1 Boundaries of eVTOL configurations

Figure 4.12 illustrates the first application of the generalization approach and gives insight into the state-of-the-art eVTOL design space facilitated by today's LIB technology. The following sections will build on the same type of **Design Tuple Contour Plot** as shown in Figure 4.12. Therefore, the following introduces the Design Tuple Contour Plot:

- **Input on x-axes:** The x-axis at the subplots' bottom side represents the central design parameter, here chosen to be the lift-to-drag ratio (L/D). Based on the previously introduces regressional relations, the parameters PL, f_{Struct}, and V_{crs} are linked to L/D and shown on the top side of the subplots. Each point along the x-axis of the subplots in Figure 4.12 represents a **Parameter Tuple** and, therefore, a specific eVTOL configuration. Consequently, concepts on the x-axis' left-hand side are Multi-Rotor configurations, while the right-hand side shows Tilt-Rotor and Vectored Thrust configurations. Note that the relation between parameters within the tuples depends on the underlying data and its uncertainty. Therefore, the relationship between Parameter Tuples depicted can change if more data is added.

- **Input on y-axis:** The y-axis at the subplot's left side depicts the second contour variable besides L/D and the associated tuple. In all subsequent contour plots, the y-axis reflects the maximum design mission range and covers ranges from 10 to 400 km. It is possible to use the contour plot for configuration analyses over other parameters, such as the required hover time, the payload, or the capabilities of the underlying energy carrier.

- **Underlying inputs and assumptions (not depicted):** Besides R_{crs}, which is provided in the second contour variable, the requirements domain is described by

---

[10]See Tables 4.1 and 4.2

t_{hov} =90 s, n_{PAX} = 4, n_{Crew} = 1, f_{Util} = 0.75, and f_{Circ} = 1.0. The technology domain variables are set according to the *mode* values outlined in Table 4.4.

- **Output - Contour levels:** At the core of the approach is the design, analyses, and assessment methodology developed in this thesis. Therefore, each point within the area spanned by the x- and y-axes reflects an evaluation of the framework based on the input design tuple (x-axis) and the second contour variable (y-axis). The contours in the left and right subplots in Figure 4.12 show the eVTOL Design Gross Mass (DGM) and the Consumed Specific Energy (CSE), respectively. Contours are grey (DGM) and blue (CSE), with darker shades at increasing value. Distinct contour levels contain hatches to facilitate readability. In addition, the dash-dotted black line reflects the maximum weight of eVTOL aircraft (3.175 kg) according to EASA's specified limits for this aircraft class [196]. The framework generally yields convergence for heavier aircraft irrespective of certification requirements if the parameter set allows finding a solution.

- **Output - Dashed lines:** In addition to the contour levels, both subplots contain dashed lines providing additional information: In **DGM contour plots**, the gray dashed line depicts the mass-optimum eVTOL configuration at a given range. It is found by connecting the range maxima of all potential DGM levels, of which the contours are representatives. In **CSE contour plots**, the blue dashed line denotes the energy-optimum eVTOL configuration at a given range requirement. The blue line connects the range minima of all CSE levels, i. e. vice versa marks the configuration tuple leading to the lowest CSE for each range requirement.

As outlined, the contour levels reflect results at the distinct design point, specified by the tuples of $^L/_D$, PL, f_{Struct}, V_{Cruise}, and the required maximum design range R_{cruise}. Contour levels can be read in multiple ways, i. e. along the x-axis from left to right at a fixed y-value or maximum design range. Each point along the x-axis represents a distinct eVTOL configuration. Left areas on the x-axis resemble wingless, Multi-Rotor configurations at lower $^L/_D$ up to around 5.0, good hover efficiency through high PL above 100 N/kW, a low f_{Struct} around 24 % indicating lightweight airframes, and lower specified flight speeds up around 35 m/s. Design points in the middle area of the subplots' abscissas reflect Lift & Cruise and Tilt-Wing configurations, with $^L/_D$ between 7 and 11. Design points toward the right boundary of the x-axis reflect increasingly complex Tilt-Rotor and Vectored Thrust configurations, marked by a high $^L/_D$ of more than 13 but lower hover efficiencies of PL <0.05 N/W, heavy airframes, and high cruise velocities. Such analyses of the contour plot along the x-axis facilitate interpreting the resulting DGM of various configurations to cover a distinct range requirement. Vice versa, the contour plot can be read along the y-axis at a fixed point on the x-axis, and thus with a specific configuration type in scope. Such analyses allow concluding on the resulting DGM of a distinct configuration over an increasing range requirement. The following paragraphs provide a comprehensive discussion of the DGM and CSE subplots in Figure 4.12.
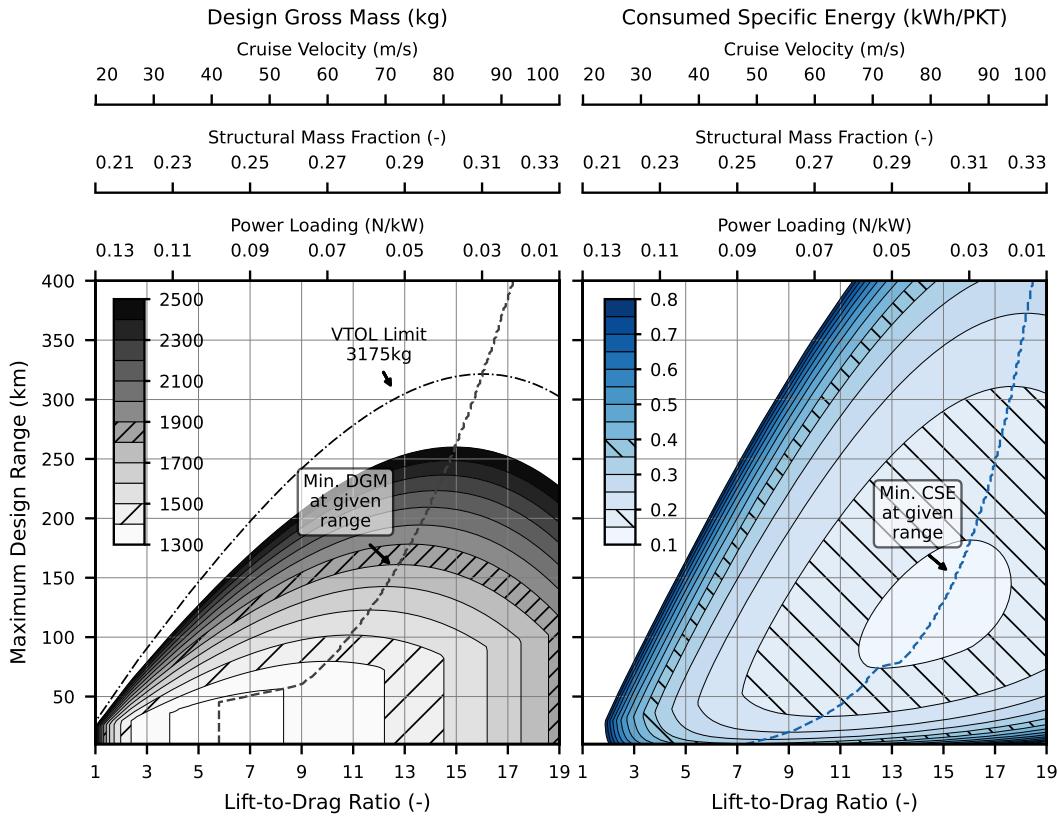
Figure 4.12: Contours of LIB-powered eVTOL mass and energy consumption.

Discussion of DGM (Figure 4.12 left): Unsurprisingly, the DGM contours generally show how the weight of eVTOL aircraft strongly increases if only reasonable ranges of 50 to 100 km are to be covered. As expected for battery-powered vertical lift aircraft, the lowest DGM levels are found at the shortest required range and relatively high hover efficiencies of $PL \geq 90 N/kW$. Further distinct observations regarding the shape and orientation of DGM contours follow in the next paragraphs.

- The **gradient orientation** of DGM contours is mainly along with increasing range for all configuration types (i. e. along the full abscissa). However, the gradient shows a steeper slope at $^L/_D$ coefficients below around 10, indicating a substantial influence of cruise efficiency on range capability. This shape and orientation of contours reflect the earlier sensitivity analysis results, which identified the insufficient specific energy of batteries combined with high range requirements to influence the DGM of battery-powered eVTOL significantly.

- Each DGM contour features a **range maximum**. Not only does it reflect the maximum range achievable by a configuration of a distinct DGM, it moreover marks the weight-optimum configuration tuple at a given range. As described, the collection of range maxima is shown by a grey dashed line. Range maxima

indicate that the beneficial effect of aerodynamic efficiency is limited if harnessed at the expense of structural weight and hover performance. With increasing DGM, the maximum moves from low L/D ratios to higher values and higher ranges. At values of L/D $\geq$ 15, the slope of maxima is oriented almost vertically, indicating that higher ranges are only achieved at the expense of heavier aircraft.

- Contours have a **vertical edge** to their left and right ends. Such vertical contour edges indicate how the resulting DGM solely depends on the type of configuration, as the gradient is oriented purely horizontally. On the right side, this vertical edge stretches over longer ranges with increasing L/D and DGM. It was shown in Equation 3.8 that the battery capacity is determined by both its energy and its power requirement. In all battery-powered cases, the latter is limited by the maximum discharge rate of high-energy batteries, which is assumed at $C - Rate = 2.5$. The range independence of DGM, as indicated by the vertical edge in Figure 4.12, implies that the battery capacity is determined by the maximum required power. Nonetheless, the contour behavior provides reason to critically refine and test the underlying models and the interdependency of the domain's parameters, especially focusing on the implications of hybridization[11].

Discussion of CSE (Figure 4.12 right): The CSE contours exhibit a different behavior. One may interpret them as a superposition of the DGM contours on the left side and operational considerations. In essence, the transfer from the left DGM plot to the right CSE plot is covered by Equations 3.2 and 3.3, as the design tuples provide the relevant inputs to those equations. For all subsequent analyses, note that the analysis assumes that operational conditions reflect the design requirements and that the off-design mission range equals the maximum design range. However, it was shown, notably by Shamiyeh et al., Brown and Harris, and in Section 4.1, that off-design operation of the vehicle can substantially decrease the overall energy performance [37], [45]. Therefore bear in mind that the real-world CSE performance of eVTOL configurations is potentially underestimated here.

- Most notably, the **contour level locations** differ from the DGM contours. The minimum CSE is around 100 to 200 km for configurations with an L/D $\geq$ 12 and therefore reflects Tilt-Rotor and Vectored Thrust configurations, as compared to the DGM minimum at distinctly lower ranges. In essence, this is due to the relatively lower share of hover flight at longer ranges, as inversely described in the second finding.

- Contours indicate a **minimum range** for each CSE level, which moves toward lower values of L/D, i. e. more hover-efficient configurations with decreasing range. As introduced, the range minima of all possible CSE values are denoted by a dashed blue line. For instance, in Figure 4.12, the configuration leading to the lowest possible CSE is found at the configuration tuple at L/D = 15. Note how,

---

[11]Recall the formulation of f_{DoH} in Section 3.2.3

based on the underlying LIB technology, the optimum configuration tuple exceeds $L/D = 19$ if the required range is 230 km or higher.

- At ranges below 50 km, one observes narrow horizontal contours, i. e. a strong vertical CSE **gradient orientation**. This effect occurs due to the relatively high hover share at short ranges. However, note that eVTOL concepts developed for such short ranges, like *Volocoper* and *CityAirbus*, have an $L/D \leq 5$. As such, Multi-Rotor configurations fall into an area of narrow, vertically oriented contours, indicating the sensitivity of their CSE performance to aerodynamic efficiency in horizontal flight. At higher design mission ranges, the CSE contours are shaped similarly to the DGM slopes on the left. The CSE contours are steeper than the DGM contours, indicating that CSE is more dependent on configuration choice. Although the slopes flatten out at the top right, the CSE contours do not show a range maximum.

As shown, a weight-optimized eVTOL configuration, resembled by the design tuple marking the range maximum of a DGM contour, does not coincide with a CSE optimum. Comparison of the dashed lines in Figure 4.12 yields the deduction that, per given range, CSE optima are found at higher L/D design tuples than DGM optima. This underscores the beneficial effect of increased aerodynamic efficiency in eVTOL design despite the detrimental effects of reduced hover efficiency and increased structural weight. However, note the interdependency of the design tuples' parameters, which may change with improved data quality or refined models. At the bottom line, the analysis of potential DGM and CSE yields four deductions:

1. It is possible, and a promising approach in the context of improving models and underlying data, to inherit regression-based interdependencies from classical rotorcraft design to the design space of eVTOL in a meaningful way.

2. Battery technology at the current state-of-the-art is sufficient to facilitate various eVTOL configurations with maximum design ranges from around 100 to around 300 km and at 90 sec hover time within the regulatory frame.

3. The main driver for system weight at the given battery maturity is the design range requirement.

4. Aiming for a good CSE performance, i. e. energy-efficient eVTOL aircraft, prefers aerodynamic efficiency of configurations at the expense of hover efficiency and aircraft weight.

4.3.2 Implications of future powertrains

The capability of batteries and alternative propulsion technologies, like hydrogen fuel cells, is expected to increase significantly in the coming years. This section reflects the implication of potential novel cell types and powertrain technologies on the design and capabilities of eVTOL aircraft.

Implications on DGM. Figure 4.13 shows a version of the ***Design Tuple Contour Plot*** with DGM contours of eVTOL configurations based on four different powertrain alternatives. The color bars in the four subplots are scaled equally and are, as before, partly hatched for enhanced clarity. The underlying values reflecting the technological domain parameters are, as described in Section 2.4, subject to uncertainty. Therefore, interpret the subsequent analyses as *what-if* scenarios displaying the technological potential of alternative powertrain technologies. The energy carrier types in scope of Figure 4.13 are:

- A Lithium-Metal Battery (LMB) on the upper left.

- A Lithium-Air Battery (LAB)[12] on the lower left.

- A H_2 fuel cell using high-pressure gaseous storage (GH$_2$) on the upper right.

- A H_2 fuel cell using liquid, cryogenic storage (LH$_2$) on the lower right.

The first finding from Figure 4.13 is the significant impact of the underlying energy carrier through the unequivocal difference in shape, orientation, and relative position of the DGM contours. For instance, Lift & Cruise aircraft powered by LMB packs, at a DGM of $1,200$ to $1.300\,\text{kg}$, are able to cover a range up to $60\,\text{km}$. Exchanging the battery with a GH$_2$ powertrain increases the range to over $250\,\text{km}$ at identical DGM. Like with the previous analysis on LIB configurations, the following provides a detailed discussion of the different powertrain alternatives, focusing on the **gradient orientation**, the contour's **range maxima**, and the apparent **vertical edge**.

- The **gradient orientation** of eVTOL configurations using LMB cells is similar to that of LIBs but shifted to higher ranges, especially in Tilt-Rotor and Vectored Thrust configurations. This trend continues for LAB-powered eVTOL configurations, with contour levels distinctly shifted to higher ranges than the LMB case and a stronger configuration-dependent component of DGM gradients. A further significant shift of DGM contours toward even higher ranges, along with a steepening of DGM gradients, follows in the GH$_2$ configurations. Ultimately, for the LH$_2$ configurations, the gradient in DGM is essentially oriented horizontally, i. e. along the configuration design tuple and relatively independent of the design range requirement. Increases of DGM at higher values of $^L/_D$ are mainly accountable to the heavier structural weight and a larger electric capacity of the high-power system (HPS), compensating for the reduced power loading.

- The DGM contour's **range maximum** shifts to design tuples marked by a decreasing $^L/_D$ in the order of the four powertrain alternatives. The dashed black line vividly depicts how eVTOL DGM is less dependent on $^L/_D$ with increasing specific energy of the energy carrier. For LH$_2$, only Multi-Rotor and Lift & Cruise configurations show a significant DGM gradient along the required cruise range.

---

[12]Li-O$_2$ Refer to Table 2.1
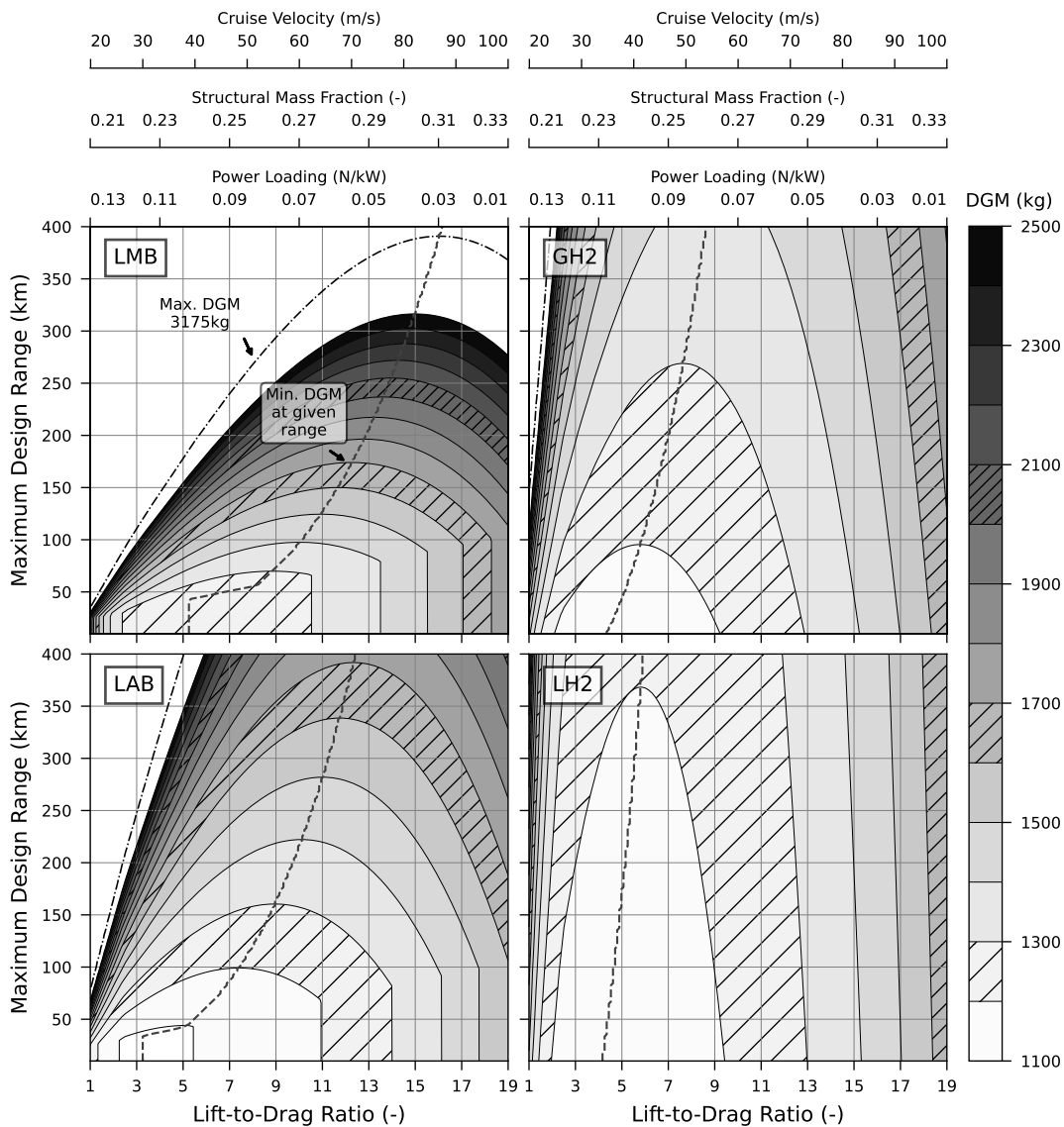
Figure 4.13: Contours of eVTOL mass using future energy carriers.

Arguably, this optimum reflects the conventional rotorcraft design paradigm of a high power loading, as the effective specific energy of hydrogen-powered architectures comparable to kerosene-powered turboshaft engines. At this point, remember that the requirement concerning hover flight is set to the relatively low value of 90sec and that the shifting effect could be increased if eVTOLs are sized for longer hover intervals.

- A **vertical edge** is only apparent in battery-powered eVTOL configuration. Recall that the vertical edge marks a decoupling of required battery capacity from required range. Instead, the determinator of high-energy system's capacity is the battery's

specific power. The vertical edge grows longer for heavier eVTOL configurations, which leads to an increase of both hover and cruise power according to Equation 3.2 and consequently to a higher capacity requirement toward the battery packs. On the contrary, the fuel cell-powered eVTOL versions GH_2 and LH_2 do not display the characteristic vertical edge of DGM contours at low ranges. This is due to the indifference of the fuel stack's weight regarding the requirement energy, as opposed to the need of batteries to yield both high energies as well as high discharge rates.

In essence, Figure 4.13 displays how battery-powered eVTOL are inherently limited in their potential range, while the DGM of configurations using hydrogen is only marginally affected by an increased required range. Nevertheless, it demonstrates that a shift toward future high-energy battery technology, like LAB, would allow eVTOL aircraft to cover well over 200 to 400km, depending on their configuration. High-energy battery systems would reduce the extraordinary demand regarding the aerodynamic efficiency of eVTOL concepts, which the current UAM sector reflects in highly complex yet unproven configurations. Simply put: The results suggest that the availability of significantly improved battery technology in the future will provide configurations like *Vahana* or *Cora* with a comparable range envelope than (using today's battery technology) what is projected for configurations like *Joby* or *Lilium*. However, bear in mind the respective cruise speed of configurations: Albeit technically possible, the higher ranges of both future LAB-powered and hydrogen-powered eVTOL aircraft only make sense if respectively increased cruise speeds facilitate reasonable trip times. For instance, a GH_2-powered Multi-Rotor configuration with a DGM of up to 2000kg could cover a range of over 400km, However, it would require about 2.8 hours for the segment, proving a significant barrier for potential customers. Herein, the previous section's deduction that DGM is an insufficient metric to assess an eVTOL configuration's viability is qualitatively confirmed. Thus, the following section extends the contour analysis to the CSE of the four respective eVTOL configurations.

Implications on CSE. The following presents the respective ***Design Tuple Contour Plot*** and analysis of the Consumed Specific Energy (CSE) for various configuration design tuples, similar to the previously discussed DGM of configurations. Figure 4.14 displays the results resembling the four powertrain alternatives LMB, LAB, GH_2, LH_2. Note that, like in the LIB-based analysis in Figure 4.12, the underlying *Operations* domain resembles the *Requirements* domain in that the CSE is calculated based on a design mission. Operation of configurations in off-design conditions may significantly alter the result. Continuing the analysis structure of the CSE contours in the previously analyzed Figure 4.12, the following paragraphs discuss the CSE plots in terms of the present **contour level locations**, **gradient orientation**, and **range minima**.

- Like with the DGM contours, a shift of CSE **contour levels** throughout increasing specific energy of batteries and hydrogen fuel cell systems is visible. With increasing specific energy of the underlying technology grows the area covered by low-CSE contour levels. For the majority of configuration types and powertrain alternatives,
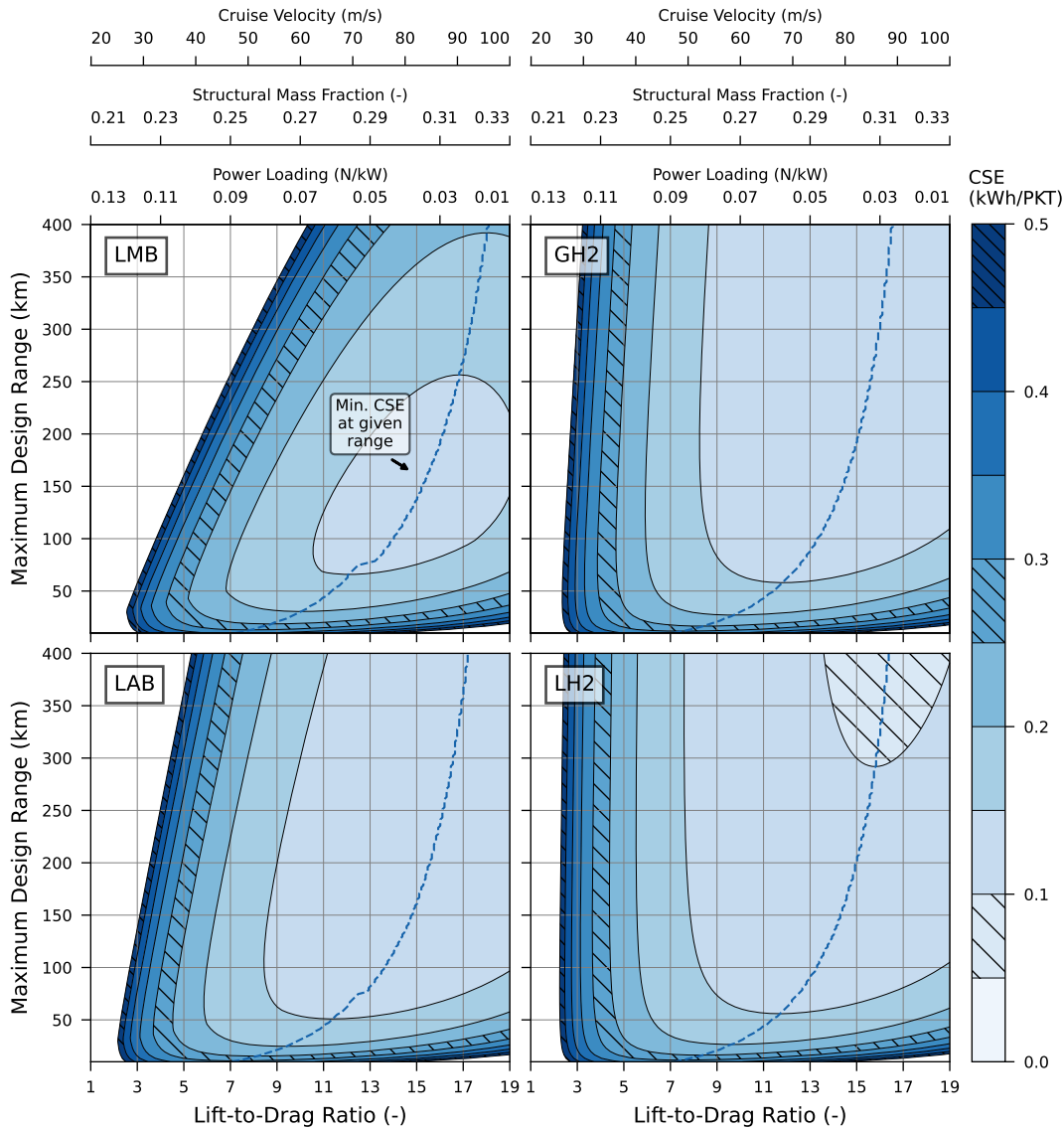
Figure 4.14: Contours of eVTOL energy consumption using future energy carriers.

Figure 4.14 reports CSE levels between 0.1 and 0.3 kWh/PKT. Such values are found at design ranges above 100 km and facilitated by moderate and high values of L/D, excluding Multi-Rotor configurations. CSE values below 0.1 kWh/PKT are only attained by GH_2-, and LH_2-powered eVTOL configurations at the highest L/D and ranges over 250 and 300 km, respectively.

- The following is found in terms of **gradient orientation and magnitude**: Beginning with the shape of the LMB contours, which appear much like the LIB depiction in Figure 4.12, i. e. slope of the contours at higher ranges gets steeper

for LAB-, GH$_2$-, and LH$_2$-powered eVTOLs. For ranges of 100 km or more, the trend marks how the increase of available specific energy of the high-energy system leads to a decrease, and ultimately the indifference, of CSE toward the required mission range. Here, CSE primarily depends on the type of configuration, which confirms the previous observation concerning the LIB contours in Figure 4.12. Again, gradient magnitude increases toward higher CSE contours, and as such, toward configuration tuples marked by a lower $^L/_D$ and higher PL.

- Most notably, throughout the four powertrain alternatives, the lower contour edges and their **range minima** shift only by a little. Similarly, the collection of range minima, and vice versa the representation of CSE minima per given range, depicted by the dashed blue line, shows little alteration throughout the subplots. Conversely, recall how the minimum DGM per given range (the grey dashed line in Figure 4.13) steepened for and shifted toward lower values of $^L/_D$. An increase in the specific energy of the underlying powertrain technology promotes a divergent behavior of DGM and CSE optima.

The outlined decrease of CSE and its reduced range dependency may be put into perspective by comparing results with CSE levels of other modes of transport. For electric cars, ADAC, Europe's largest motoring association, reports car-specific energy consumptions of between 0.16 and 0.28kWh/km based on a test of 27 models [230]. Assuming an average seat utilization of 1.5 passengers per car, this drops to values between 0.10 and 0.18 kWh/PKT. From Figure 4.14, such values seem attainable by Lift & Cruise, Tilt-Rotor, and Vectored Thrust configurations using next-generation LMB technology, if employed on ranges above 100 km and operated close to their design point. In comparison, modern aircraft[13] used on regional flights have an average fuel consumption of between 2.2 and 3.4 L/100km per seat, or 0.28 to 0.43 kWh/PKT if utilized at 75%. While eVTOL configuration can not compete with the CSE of modern aircraft using LMB technology, the commercial availability of LAB could change that: In combination, Figures 4.13 and 4.14 suggest that eVTOL aircraft using LAB could, at a DGM of around 2.000 kg, easily cover ranges of over 400 km, while consuming between 0.1 and 0.2 kWh/PKT. Such deductions may appear surprising, given the extraordinarily high utilization of large fixed-wing aircraft, but require a differentiated elaboration. For instance, fixed-wing aircraft are designed for distinctly higher ranges, fly much faster (recall the travel time argument outlined before), and are subject to compressibility effects and, consequently, a high energy consumption. At the bottom line, the following conclusions can be made:

1. The CSE of eVTOL configurations is directly related to the available net specific energy of the used energy carrier and, in theory, favors hydrogen-powered concepts over battery-powered systems.

2. The optima of eVTOL configurations for a given range differ, depending on whether the optimization objective is the DGM or the CSE.

---

[13]released since 2015

3. If powered by any of the studied future powertrain alternatives, eVTOL config-
   urations can be competitive to electric vehicles and regional aviation in terms of
   energy consumption. However, for battery-powered concepts, this is limited to
   aerodynamically efficient fixed-wing configurations and medium range. However,
   note that the observation does not account for life cycle effects, i. e. upstream
   effects like grid efficiencies. Therefore, assessing future powertrain systems in
   terms of their expected carbon footprint requires adding a third perspective on
   the regression-based contour analysis.

4.3.3 Impact assessment of generalized eVTOL configurations

This section concludes the generalized configuration study by a carbon impact assess-
ment and a complementary sensitivity analysis of essential impact drivers. Figure 4.15
shows a matrix of subplots, each depicting the SCI of eVTOL configurations, i. e. their
GHG emissions per passenger-kilometer traveled (PKT), for distinct input quantities
and their variations. It builds on the previously utilized regression approach to couple
the configuration parameters L/D, PL, f_{Struct}, and V_{Cruise} in tuples. The subplot's x-
axes reflect the x-axes of the previous Figures 4.12, 4.13, and 4.14, spanning the range of
potential eVTOL configurations. Note that albeit not explicitly depicted in Figure 4.15,
the parameters PL, f_{Struct}, and V_{Cruise} follow their regression-based relation with L/D
and thus vary along the x-axes. The three rows reflect distinct settings of the required
maximum design range at 50, 100, and 200 km. Compared to the previously discussed
contour plots, each subplot row thus refers to horizontal sections through the plot at
these respective ranges. The output data, which has been provided within the contour
levels so far, is now depicted on the y-axis. The four columns of subplots reflect sen-
sitivity analyses regarding the four uncertainty instances. They are comparable to one
another by the black line with dotted marks, which refers to the *baseline* data through-
out the scenarios. which are introduced in the following. The four uncertainty instances
depicted by those columns are:

1. **Regression Variation:** The first column provides insight on how the SCI changes
   for variations within the input tuple, i. e. if the regression relations between L/D
   and the three "dependent" design parameters PL, f_{Struct}, and V_{Cruise} vary. The
   three regression formulations are labeled "Lower Bound", "Baseline", and "Up-
   per Bound". They build on the regression depiction in Figure 4.11, reflecting the
   lower shaded boundary, the black middle line, and the upper shaded boundary,
   respectively. Those characteristic lines, i. e. the regressions, are found using the
   "minimum", "mode", and "maximum" values of the four parameters, which were
   outlined in Table 4.2. The coefficients of the "minimum" and "maximum" least-
   squares regressions are listed in the following. The "mode" regressions were pro-
   vided within the onset of Section 4.3. The coefficients of the non-linear regression
   for $PL = A \cdot \exp\left(-B \cdot L/D\right) + C$ are:

   - $A_{min} = 0.079$, $B_{min} = 0.122$, $C_{min} = 0.008$
   - $A_{max} = 0.213$, $B_{max} = 0.233$, $C_{max} = 0.030$

The coefficients of the inear regression for $f_{Struct}, V_{crs} = m \cdot L/D + c$ are:

- $m_{f_{Struct},min} = 7.3 \cdot 10^{-4}$, $c_{f_{Struct},min} = 0.241$
- $m_{f_{Struct},max} = 19.3 \cdot 10^{-4}$, $c_{f_{Struct},max} = 0.270$
- $m_{V_{crs},min} = 4.08$, $c_{V_{crs},min} = 22.0$
- $m_{V_{crs},max} = 4.18$, $c_{V_{crs},max} = 10.3$

2. **Operations Variation**: The case analysis in Section 4.2.4 demonstrates that the SCI can significantly change, depending on the operational scheme of the eVTOL aircraft. The generalized assessment is thus, in its second column, subjected to uncertainties regarding the operational scenario. The two distinct variations from the baseline scenario reflect an "Optimum" and "Pessimum" regarding their influence on the SCI. The "Optimum" scenario assumes:

   - A shortest-possible hover of $t_{hov} = 30\,\mathrm{sec}$ according to Brown and Harris [37].
   - An operational mission range that equals the required maximum design range ($n_{Leg} = 1$) and thus reflects the least-possible hover share.
   - A maximum seat utilization of $100\,\%$.
   - A beneficial road circuity factor of $f_{Circ} = 1.46$, implying that ground-based routes are $46\,\%$ longer than the direct air link. The factor reflects the average European road circuit published by Balou et al. [228].

   In contrast, the "Pessimum" scenario assumes to following deviation from the baseline scenario:

   - Vehicle operation on routes with a length of a quarter of the maximum design range (i. e. $n_{Leg} = 4$). Therefore, the effective operational ranges of the three vehicle classes (50, 100, and $200\,\mathrm{km}$) are 12.5, 25, and $50\,\mathrm{km}$. Note that even shorter missions legs will further impair the SCI.
   - A minimum seat utilization of $50\,\%$, which may appear relatively low, but can be assumed to account for dead-head missions, i. e. required empty vehicle transfers, according to Brown and Harris [37].

3. **2030 Basic Scenario**: The third column depicts different results of SCI for the five powertrain alternatives analyzed before. The alternatives comprise state-of-the-art LIB technology and the four prospective energy carriers LMB, LAB, GH_2, and LH_2. The latter were compared in the previous DGM and CSE contour plots.

4. **2030 Green Scenario**: The only perspective on SCI including the beneficial effects of the "2030 Green" scenario is depicted in the fourth column, again based on the five powertrain alternatives shown in column three. The shift of the black line with small markers, comparing the first three columns with column four, depicts the isolated influence of this future scenario on the "baseline" case.
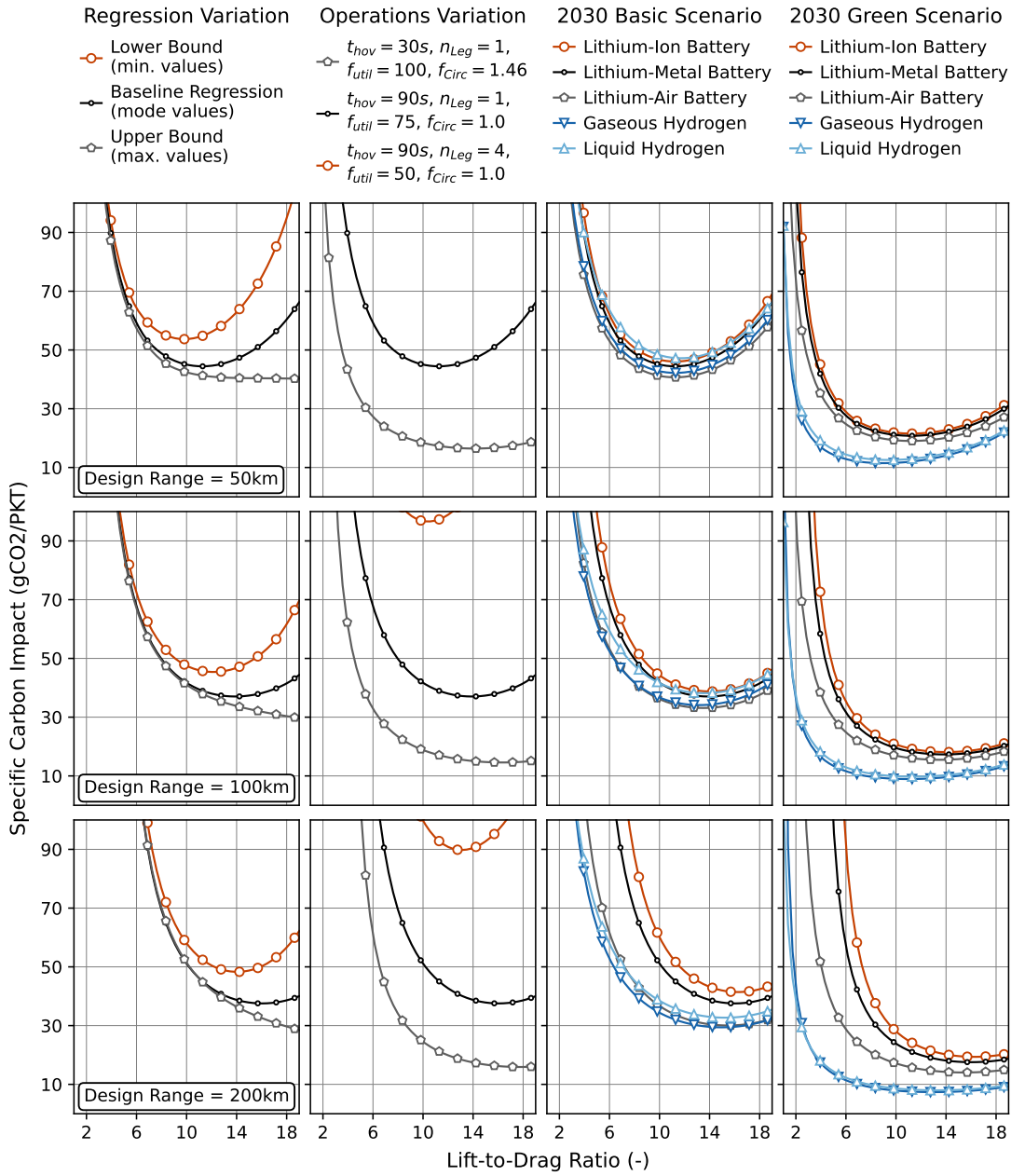
Figure 4.15: Carbon impact assessment and sensitivity analysis of generalized eVTOL.

The **first observation** from Figure 4.15 is the resulting SCI's order of magnitude in all of the subplots. Uniformly, the y-axes cover SCI values ranging from 0.0 to $100\,\mathrm{gCO_2}$/PKT. With these limits, the graphs cover the SCI of most eVTOL configurations, except Multi-Rotor configurations at the lower end of L/D tuples. The eVTOL carbon impact levels reported in Figure 4.15 are in the same order of magnitude as ground-based mass trans-

portation modes[14], including high-speed rail ($29\,gCO_2$/PKT at $70\,\%$ utilization), regional trains ($54\,gCO_2$/PKT at $28\,\%$ utilization), intercity buses ($29\,gCO_2$/PKT at $56\,\%$ utilization), and urban public transport ($54\,gCO_2$/PKT at $19\,\%$ utilization). Moreover, the SCI's order of magnitude is distinctly lower than the reported GHG emissions of short-haul aviation ($214\,gCO_2$/PKT at $70\,\%$ utilization and including effects from radiative forcing) and conventionally powered personal vehicles ($54\,gCO_2$/PKT at, on average, 1.4 passengers per car). Sensitivities persist toward the outlined scenarios and will be discussed in the following. However, note that concluding a "lowest-impact winner" from such a comparison is not valid due to the differences in underlying data and modeling approaches. As shown in Figure 4.6, the grid carbon intensity of electricity production is anticipated to fall. Consequently, the baseline scenario "2030 Basic" assumes a European grid carbon intensity of $72\,gCO_2$/kWh, which is significantly lower than the German grid carbon intensity of $441\,gCO_2$/kWh in 2016, reflecting the underlying economy to the transport mode data published by the German Federal Environmental Agency and referenced above. Arguably the same applies to the production impact of components with a limited cycle-life, like batteries and fuel cells, as it is coupled to grid carbon intensity and likely to benefit from economic effects of scale in the current decade [159].

The **second finding** of the data in Figure 4.15 is that the SCI, depending on the uncertainty instance and design range, either continuously decreases toward higher-L/D tuples or has a minimum at configuration tuples marked by medium to high values of L/D. Vice versa, the SCI of configurations marked by low-L/D tuples is consistently higher than $100\,gCO_2$/kWh. Moreover, the impact value is highly sensitive toward little variations of the configuration type. The findings continue the prior CSE contour analyses, which indicated CSE optima at configurations of higher L/D. Note that SCI minima move from the x-axes middle to its right side for increasing design ranges, coinciding with the blue dashed lines marking the optimum CSE over increasing ranges in Figures 4.12 and 4.14. It is furthermore perceptible how the SCI levels decrease with increasing design range, which is also in accordance with the previous observations of the CSE.

A **third finding** results from comparing the spread of SCI based on distinct variates, i. e. the sensitivity of SCI regarding the respective uncertainty instance: Notably, SCI reacts most sensitive to changes of the operational domain and, at the low and medium range, least sensitive to the different energy carriers. To extend the SA of SCI regarding distinct variates, the following paragraphs provide an analysis of each of the uncertainty instances:

1. **Regression Variation:** The uncertainty on SCI induced by the underlying parameter values and regression coefficients is relatively small at lower values of L/D but significantly grows to over $\pm 30\%$ for tuples at high L/D. The sensitivity is most significant within the shortest design mission ($50\,km$) and decreases for the medium ($100\,km$) and long ($200\,km$) design mission. The SCI of the "Lower Bound" uncertainty, which reflects "minimum" parameters, begins to diverge from the baseline at relatively small L/D values. It consequently leads to one of the leftmost minima

---

[14]Based on a 2019 report by the German Federal Environmental Agency[231]

of the SCI with respect to all subplots in Figure 4.15. In contrast, the "Upper Bound" uncertainty diverges a little later, indicates a smaller sensitivity, and does not imply a minimum SCI within the configuration design space. The increased sensitivity at higher values of L/D can be accounted to three factors:

- The data uncertainty in the underlying *"Joby"* and *"Lilium"* configurations.
- The high sensitivity to PL for those configurations, as seen in Figure 4.5.
- The increasing spread in f_{Struct} data, visible in Figure 4.11.

2. **Operations Variation**: Variations of hover time, effective operational *off-design* range, seat utilization, and the potential route circuity are most impactful regarding the SCI of eVTOL operation. For instance, a short hover time and high utilization can lead to operational carbon impacts as low as 15 to $20\,\mathrm{gCO_2/PKT}$ for a Tilt-Rotor eVTOL designed for and operated on a 100 km route. However, it is much more likely that such an aircraft will primarily serve shorter routes, according to the demand analysis by Ploetner et al. [39], which would impair this best-case result. Suppose the actual mission range is only 25 km, operational constraints require a longer hover interval of 45 sec for each take-off and landing, and an unbalanced demand direction during rush hours implies a lower utilization of 50 %. Now, the SCI of the same Tilt-Rotor aircraft exceeds $100\,\mathrm{gCO_2/PKT}$. In fact, such a scenario would favor a Lift & Cruise configuration over the mentioned Tilt-Rotor eVTOL, as the shifted SCI optima between the base-case and worst-case curves show.

3. **2030 Basic Scenario**: The five different powertrain alternatives show surprisingly little divergence of the SCI of their eVTOL configurations. For the short-range sizing mission, the highest carbon impacts are found for the LIB and LH_2 energy carriers, and the lowest carbon impact is shown by the (LAB) curve. These worst-case and best-case curves differ by only 5 to $10\,\mathrm{gCO_2/PKT}$. For Tilt-Wing configurations at L/D tuples around 6 to 7 and sized for the medium-ranged mission of 100 km, the spread grows to around $30\,\mathrm{gCO_2/PKT}$. Still, the deviation is small compared to the previously discussed sensitivity toward the operational aspects. It underpins how, for all eVTOL configurations except Multi-Rotor concepts, the availability of an advanced energy carrier is of subordinate importance if the aircraft's design range is 100 km at maximum. Nevertheless, the 100 km subplot shows how an increasing range requirement leads to relatively lower carbon impacts of the hydrogen powertrains. In the $R_{crs} = 200$ km scenario, a visible divergence of LAB, GH_2, and LH_2 curves from LIB and LMB curves appears. This divergence of the latter two technologies is due to the relatively low energy density and the respective exponential DGM increase at longer ranges. Still, the LH_2 curve indicates higher carbon emissions than the GH_2 version due to a high energy requirement in the liquefication process.

4. **2030 Green Scenario**: The SCI curves essentially follow their respective versions in the "2030 Basic" scenario, albeit reduced by 20 to $30\,\mathrm{gCO_2/PKT}$ if measured

at the optimum configuration. Hydrogen-powered versions show a distinct offset to lower carbon emissions compared to battery-powered vehicles, visualizing the beneficial effect of a purely renewable sourcing of hydrogen. Moreover, the curves' sections around their minimum SCI are relatively flat, pointing toward a decreased sensitivity of the carbon impact toward a *close-to-optimum* configuration choice. In the short-ranged design mission, the GH_2-, and LH_2-powered configuration types arguably show the leftmost impact minima, at $^L/_D$ values between 8 and 10. The same orientation of GH_2 and LH_2 minima to the left appears for the medium- and long-range design mission, albeit to a lesser extent. The reason for this lies in the distribution between hover and cruise power in the hydrogen-hybrid system and the respective relative impact of the LiPo battery and the fuel cell system. In case of a high hover share, such as in the 50 km mission, a relatively large portion of consumed energy is provided by the LiPo battery. Consequently, the share of the LiPo battery's production impact increases. Furthermore, as shown in Table 4.7 for the "2030 Green" scenario, the LiPo battery's carbon impact is relatively high compared to the impact of the sourcing of hydrogen. The required hover power, which serves as a multiple to the *production impact per kWh*, depends on PL and is lowest for Multi-Rotor configurations at the x-axes left end. Consequently, the SCI of configurations marked by lower $^L/_D$ but higher PL on the left side of x-axes benefits more from a decreased DGM than initially suggested by the right-leaning CSE optima.

Note that the outlined sensitivities may superimpose each other, potentially improving or impairing the eVTOL's Specific Carbon Impact. At the bottom line of the SCI assessment of generalized eVTOL configurations, the following is concluded:

- It will be possible to design and operate eVTOL configurations in urban and regional scenarios so that their associated carbon impact is in the order of magnitude from 10 to $100\,gCO_2/PKT$.

- A low carbon impact is achieved by cruise-efficient eVTOLs such as Lift & Cruise, Tilt-Rotor, and Vectored Thrust configurations, with design tuples marked by $^L/_D = 10$ or higher.

- Most decisive regarding the carbon impact of eVTOL are the operational scenario and the carbon intensity of the underlying economy, besides the configuration choice.

- Refining and further verifying the underlying regression database may influence the results and provide a more robust evaluation framework, especially regarding the mentioned cruise-efficient eVTOL configurations.

- Advanced energy carrier technologies will significantly improve the SCI of hover-efficient eVTOL configurations designed for ranges of 100 km or more. However, the evaluation of aircraft designed for longer ranges should always include a sensitivity analysis of the operational scheme due to the reported divergence in off-design performance.

5 Conclusion and Future Work

The overarching target of this thesis was to elaborate on the environmental sustainability of electrically powered Vertical Take-Off and Landing (eVTOL) aircraft for Urban Air Mobility (UAM). Environmental sustainability was defined to be valued by greenhouse gas (GHG) emissions and therefore measured by the amount of carbon equivalents emitted over the life cycle of eVTOL aircraft. The specific aims of the work were:

1. An assessment of the impact of design choices regarding configuration and powertrain technology on the environmental impact.
2. A comparative analysis of eVTOL configurations and future electric cars in light of uncertainties regarding the underlying scenarios.
3. A discussion of the interdependency of domains to provide readers with an understanding of confidence and validity of such predictive analyses.

To this end, the thesis developed and implemented a methodology to perform an integrated conceptual design, performance analysis, and environmental assessment.

5.1 Conclusion to Research Questions

I. eVTOL aircraft can be designed to provide a sustainable transport mode.

The configuration of eVTOL aircraft and the type of electrochemical energy carrier and respective powertrain system have a crucial impact on eVTOL's sustainability. Combining "environmentally advantageous" design choices concerning the **configuration** and **energy carrier** enables to design eVTOL aircraft that can be operated "sustainably", i. e. causing a carbon impact equivalent to other transport modes. The thesis' conclusions regarding those choices are outlined in the following:

The **choice of configuration** is the single most influential determinant of eVTOL sustainability 4.3.3). It is usually a choice between wingless Multi-Rotor, Lift & Cruise, Tilt-Wing, Tilt-Rotor, and Vectored Thrust concepts. The thesis finds evidence for the "environmental superiority" of cruise-efficient aircraft over hover-efficient aircraft (4.2.3). Highly cruise-efficient Tilt-Rotor and Vectored Thrust aircraft cause the smallest environmental impact, irrespective of uncertainties within the requirements, design parameters, and technological capabilities of systems (4.2.4). Notably, this holds despite the higher design masses and carbon impact of primary production of Tilt-Rotor and Vectored Thrust aircraft, compared to Multi-Rotor configurations (4.1.4). Carbon emissions associated with the life cycle of supposedly "emission-free" eVTOL correlate with the energy requirement in operation (4.2.3). The choice of configuration is strongly affected by the unique requirements of eVTOL aircraft and their essential purpose, which

is to enable transportation over a particular range in a desirably short time. Although mimicking helicopters in their ability to hover, eVTOL aircraft perform vertical flight only to the extent of enabling their business model, which requires accessibility via a decentral infrastructure. Consequently, designers and operators aim to minimize the share of energy-consuming hover flight to prevent detrimental effects on the performance (4.1.5 and 4.3.3). Hover efficiency, marked by a low disk loading and high power loading, is a central theorem of helicopter design. However, in eVTOL design, the optimum hover efficiency depends on the required hover time, dictated by regulative and operational constraints.

The **choice of energy carrier** is, unsurprisingly, strongly correlated to the three examined eVTOL performance metrics: design gross mass, consumed specific energy, and specific carbon impact (4.3.2). The study shows how the high specific energy of potential future battery types and the high energy density of both gaseous and liquid hydrogen will decrease eVTOL weights and increase potential mission envelopes. An increase of specific energy of energy storage systems will reduce the life-cycle carbon impact of eVTOL, regardless of the configuration type. However, the study demonstrates that, on urban and regional routes, the influence of advanced energy carriers on the sustainability of eVTOL is relatively moderate compared to the impact of operational conditions and the carbon intensity of the underlying economy (4.3.3). Concerning longer mission ranges, the study's results indicate that potential intercity-eVTOLs will depend on advanced energy carriers, such as Lithium-Air batteries and hydrogen fuel cells (4.3.2). Moreover, the availability of capable hydrogen fuel cell systems will likely shift the environmental design choice optimum, which aims for highly cruise-efficient aircraft, toward more hover-efficient configurations, depending on the carbon intensity of the respective hydrogen economy (4.3.3).

II. eVTOL sustainability is scenario-dependent.

Design choices can enable eVTOL configurations like *"Joby"*, *"Lilium"*, and *"Skai"* to "environmentally compete" with ground-based electric cars in specific scenarios (4.2.4). Following the eVTOL configuration choice, those scenarios have the second-largest influence on eVTOLs' life cycle impact (4.3.3). The thesis distinguishes scenario-related conclusions into two dimensions:

The **environmental background scenario** determines the amount of GHG emissions due to production and operation by a significant extent (4.2.4). Albeit grid carbon intensity directly affects the carbon impact of every electrically powered transport mode, its influence on eVTOL impact is leveraged by the high energy requirement in vertical flight, especially if the hover share is relatively high (4.2.4). One may consider the influence of grid carbon intensity academic, as eVTOL operators are free to choose their underlying energy mix, and eVTOL manufacturers may provide for a sustainable procurement strategy and offset the impact of their vehicle production. However, such consideration includes out-of-scope factors like policy and the environmental consciousness of eVTOL customers and companies.

The **operations scenario** can potentially alter the results of an eVTOL's carbon impact by a factor of 10 (4.3.3). Therefore, it must, in any case, be considered and discussed when assessing the environmental impact of UAM. The most determining factors within the operations scenario are the off-design range and actual hover time, crucially impacting the effective hover share. Further factors are the vehicle utilization and the circuity factor, which depends on the relative distance saving compared to the alternative transport mode (4.3.3). It is shown how eVTOL aircraft employed on short missions below $25km$, i. e. in "Urban Mobility", do not provide an environmentally sustainable alternative to road-bound transport (4.2.4). In contrast, commuting by eVTOL can be the sustainable option versus, say, using electric ride-hailing services in areas of high demand, medium distances, and confined road infrastructure due to geography, like the San Francisco bay area.

III. Environmental assessment should elaborate on associated uncertainties.

An early conceptual design stage, with uncertainties present in the design parameters, the technological capability, and even in the actual requirements, is sufficient to distinguish configurations based on their environmental impact (4.2.4). In contrast, operational and background uncertainties present at this stage can potentially distort the findings on the environmental impact of configurations. Readers may recognize this pattern from the recent emergence of electric vehicles, which evoked a great number of publications on their sustainability with varying degrees of simplification and, sometimes, tilted assumptions. Arguably the same will happen concerning eVTOL if and as soon as UAM becomes a reality. The methodology and results of the present thesis may serve readers as a guide to cautiously studying such sustainability assessments. Uncertainties can significantly alter and potentially superimpose results of environmental assessments, for instance, if an eVTOL is employed on significantly shorter ranges than designed for (4.2.4 and 4.3.3). To produce reliable results, sustainability assessments of eVTOL aircraft should:

1. Perform a distinct assessment for every potential scenario of interest.

2. Conduct sensitivity analyses regarding uncertain domains and parameters.

3. Refine the underlying vehicle, technology, and scenario databases according to identified areas of uncertainty and sensitivity.

At the bottom line, the superior environmental performance of UAM claimed by eVTOL companies remains a promise. In specific application scenarios, eVTOL operation can become the less carbon-intense choice of transportation compared to electric vehicles. From a sustainability perspective, the author suggests employing eVTOL as a complementary transport mode on suburban and regional routes with a high mobility demand, confined ground-based infrastructure, and available renewable power. Judging the envisioned broad application of eVTOL in UAM requires additional interdisciplinary assessment efforts and more knowledge on technological capabilities.

5.2 Recommended Future Works

- **Implementation of additional sustainability metrics.** The Life Cycle Assessment methodology allows many different impact metrics. The developed framework can be enhanced twofold:

  1. It is possible to include additional categories measuring the environmental impact and sustainability, such as acidification, ozone layer depletion, and freshwater use. The latter is of interest when comparing various battery cell production and hydrogen sourcing scenarios, as both processes require large quantities of water, albeit at different geographic locations.

  2. Sustainability metrics could be altered concerning their impact point, i. e. mid-point vs. end-point. However, as the *climate change* metric is comparably far down the cause-effect-chain of LCA, such expansions are only of interest when studying additional metrics depicting the impact on, for instance, human health. The implementation of additional metrics requires improving the modeling and data fidelity, depending on the area of interest.

- **Assessment of life cycle cost.** The developed framework is extendable toward the assessment of life cycle cost of eVTOL aircraft. Expanding the thesis' scope and analyzing the cost incurred during the production and operation of vehicles would add an interesting perspective. Customer prices of the transport mode UAM may, in early scenarios, not affect the adoption, as eVTOLs are believed to primarily address wealthy individuals. However, a potential further market penetration could pose a substantial question: Will the economic optimum of eVTOL configurations and their operational profile coincide with the minimum environmental impact? The author suggests further studies of the operational domain as a good starting point and recommends the study of Brown and Harris for further reading [37]. Life cycle costs presumably depend on pilot cost, overhaul and maintenance expenses including component replacements, fees for landing, parking, and recharging at vertiports, and insurance expenses.

- **Macroscopic, transport mode-independent mobility assessments.** The implemented low fidelity approach can be employed within broader frameworks to assess multi-modal mobility systems. The author suggests utilizing the developed framework in interdisciplinary analyses, which include domains like UAM demand modeling (see Ploetner et al. [39]), operational constraints (see Vascik et al. [11]), and the bottom-up assessment of multiple alternative transport modes using identical underlying scenarios.

- **Increase in modeling and data fidelity.** While the low fidelity approach employed in this thesis is sufficient to determine the carbon impact and identify its particular sensitivities, a fidelity increase can help assess the identified areas in more detail. It improves the understanding of the interdependence of uncertainties between higher fidelity parameters and facilitates identifying and studying

technological challenges of future configurations and powertrains. Increasing the modeling fidelity can be done *by hand*, which the author considers time-consuming given the rapid growth in complexity at higher fidelity. Alternatively, one can expand the implemented framework by existing computational tools to support the design and analysis of eVTOL, like NDARC or SUAVE, and commercial tools to perform life cycle assessments.

- **Regression data improvement and design optimization.** The dependencies between design and requirements parameters formulated in Section 4.3 base on a limited number of eVTOL configurations. They reflect assumptions for the assessed configurations and are thus neither validated nor reflecting physical measurements of technical realizations. Section 4.3.3 found significant sensitivity regarding the regressions uncertainty, especially within the carbon impact of cruise-efficient eVTOLs. Therefore, the author suggests improving the database quality and quantity to strengthen future eVTOL assessments of any kind. Future works can build on the formulated regression database as a constraint used in eVTOL configuration optimization. Such an approach could yield eVTOL designs optimized toward their life cycle carbon impact, operational carbon impact, energy consumption, or, if implemented, life cycle cost.

Bibliography

[1] D. S. Lee, D. Fahey, A. Skowron, M. Allen, U. Burkhardt, Q. Chen, S. Doherty, S. Freeman, P. Forster, J. Fuglestvedt, *et al.*, "The contribution of global aviation to anthropogenic climate forcing for 2000 to 2018," *Atmospheric Environment*, vol. 244, p. 117 834, 2021. DOI: `10.1016/j.atmosenv.2020.117834`.

[2] IPCC, "Summary for policymakers," in *Global warming of 1.5°C*, V. Masson-Delmotte, P. Zhaiand, H.-O. Pörtner, D. Roberts, J. Skea, P. Shukla, A. Pirani, W. Moufouma-Okia, C. Péan, R. Pidcock, S. Connors, J. Matthews, Y. Chen, X. Zhou, M. Gomis, E. Lonnoy, T. Maycock, M. Tignor, and T. Waterfield, Eds. Geneva, Switzerland: World Meteorological Organization, 2018, 32 pp.

[3] UNDP. (2020). "The united nations sustainable development goals," [Online]. Available: `https://www.undp.org/content/undp/en/home/sustainable-development-goals.html` (visited on 03/12/2021).

[4] UNFCCC, "Paris agreement," in *Report of the Conference of the Parties to the United Nations Framework Convention on Climate Change (21st Session, 2015: Paris). Retrieved December*, HeinOnline, vol. 4, 2015, p. 2017.

[5] IATA. (2021). "Working towards ambitious goals," [Online]. Available: `https://www.iata.org/en/programs/environment/climate-change/`.

[6] IEA, *Energy technology perspectives 2020*, 2020. [Online]. Available: `https://www.iea.org/reports/energy-technology-perspectives-2020`.

[7] W. Johnson and C. Silva, "Observations from exploration of vtol urban air mobility designs," Report No. ARC-E-DAA-TN61332, Jeju Island, South Korea, 2018.

[8] F. Valente, "Analysis of urban air mobility and the evolving air taxi landscape," Frost & Sullivan, Tech. Rep., 2019.

[9] IEA. (2019). "Atlas of energy," [Online]. Available: `http://energyatlas.iea.org/#!/tellmap/1378539487`.

[10] D. Wirth, "A hierarchical probabilistic approach to rotorcraft preliminary design," Ph.D. dissertation, Technische Universität München, 2018.

[11] P. D. Vascik, R. J. Hansman, and N. S. Dunn, "Analysis of urban air mobility operational constraints," *Journal of Air Transportation*, vol. 26, no. 4, pp. 133–146, 2018. DOI: `10.2514/1.D0120`.

[12] J. Sinsay, J. Alonso, D. Kontinos, J. Melton, and S. Grabbe, "Air vehicle design and technology considerations for an electric vtol metro-regional public transportation system," in *12th AIAA Aviation Technology, Integration, and Operations (ATIO) Conference and 14th AIAA/ISSMO Multidisciplinary Analysis and Optimization Conference*, 2012, p. 5404. DOI: `10.2514/6.2012-5404`.

[13] M. Moore, "Aviation frontiers-on demand aircraft," in *10th AIAA Aviation Technology, Integration, and Operations (ATIO) Conference*, 2010. DOI: `10.2514/6.2010-9343`.

[14] J. Holden and N. Goel, *Uber elevate: Fast-forwarding to a future of on-demand urban air transportation*, Uber Technologies, Inc., San Francisco, CA, USA, 2016.

[15] D. P. Thipphavong, R. Apaza, B. Barmore, V. Battiste, B. Burian, Q. Dao, M. Feary, S. Go, K. H. Goodrich, J. Homola, *et al.*, "Urban air mobility airspace integration concepts and considerations," in *2018 Aviation Technology, Integration, and Operations Conference*, 2018, p. 3676. DOI: `10.2514/6.2018-3676`.

[16] A. Straubinger, R. Rothfeld, M. Shamiyeh, K.-D. Büchter, J. Kaiser, and K. O. Plötner, "An overview of current research and developments in urban air mobility–setting the scene for uam introduction," *Journal of Air Transport Management*, vol. 87, p. 101 852, 2020. DOI: `10.1016/j.jairtraman.2020.101852`.

[17] VFS. (2020). "eVTOL aircraft directory," [Online]. Available: `https://www.evtol.news/aircraft`.

[18] D. Etherington. (2019). "Volocopter extends series C funding to 94M with backing from logistics giant DB Schenker," [Online]. Available: `https://tcrn.ch/2HL9tHH` (visited on 11/22/2020).

[19] A. Technologies. (2019). "Skai," [Online]. Available: `https://www.skai.co/vehicle` (visited on 12/19/2020).

[20] L. Blain. (2019). "Skai revises targets for its liquid-hydrogen, long-range eVTOL," [Online]. Available: `https://newatlas.com/aircraft/alakai-skai-liquid-hydrogen-evtol-update/` (visited on 12/22/2020).

[21] ——, (2020). "ZeroAvia's Val Miftakhov makes a compelling case for hydrogen aviation," [Online]. Available: `https://newatlas.com/aircraft/interview-zeroavia-val-miftakhov-hydrogen-aviation/` (visited on 02/24/2021).

[22] Airbus. (2020). "CityAirbus - Our four-seat eVTOL demonstrator," [Online]. Available: `https://www.airbus.com/innovation/zero-emission/urban-air-mobility/cityairbus.html#specifications` (visited on 11/22/2020).

[23] ——, (2020). "Vahana - Our single-seat eVTOL demonstrator," [Online]. Available: `https://www.airbus.com/innovation/zero-emission/urban-air-mobility/vahana.html#specifications` (visited on 11/22/2020).

[24] Acubed. (2019). "A celebratory, bittersweet moment: Vahana's final flight," [Online]. Available: `https://acubed.airbus.com/blog/vahana/a-celebratory-bittersweet-moment-vahanas-final-flight/` (visited on 11/22/2020).

[25] Wisk. (2020). "Cora," [Online]. Available: `https://wisk.aero/` (visited on 11/22/2020).

[26] The Robot Report. (2020). "Wisk partners with NASA to accelerate autonomous passenger aircraft nationwide," [Online]. Available: `https://www.therobotreport.com/wisk-partners-nasa-accelerate-autonomous-passenger-aircraft-nationwide/` (visited on 11/22/2020).

[27] I. Lunden. (2020). "Lilium adds 35M from Baillie Gifford at a 1B+ valuation for its electric aircraft taxi service," [Online]. Available: `https://techcrunch.com/2020/06/08/lilium-adds-35m-from-baillie-gifford-at-a-1b-valuation-for-its-electric-aircraft-taxi-service/` (visited on 11/22/2020).

[28] J. Flottau. (2020). "Stoff für Flugtaxis," [Online]. Available: `https://www.sz.de/wirtschaft/lilium-jet-kohlenstofffaser-1.4965687` (visited on 11/23/2020).

[29] P. Nathen, *Architectural performance assessment of an evtol aircraft based on a ducted vectored thrust concept*, Lilium GmbH, Wessling, Germany, 2021.

[30] D. Etherington. (2020). "Joby Aviation raises 590M led by toyota to launch an electric air taxi service," [Online]. Available: `https://tcrn.ch/2tkbW8o`.

[31] K. Korosec. (2021). "Joby Aviation takes flight into the public markets via a SPAC merger," [Online]. Available: `https://tcrn.ch/2ZM90yg`.

[32] C. Silva, W. R. Johnson, E. Solis, M. D. Patterson, and K. R. Antcliff, "VTOL urban air mobility concept vehicles for technology development," in *2018 Aviation Technology, Integration, and Operations Conference*, 2018, p. 3847. DOI: `10.2514/6.2018-3847`.

[33] A. Datta, S. Elbers, S. Wakayama, J. Alonso, E. Botero, C. Carter, and F. Martins, "Commercial intra-city on-demand electric-VTOL status of technology," Tech. Rep., 2018.

[34] M. Clarke, J. Smart, E. M. Botero, W. Maier, and J. J. Alonso, "Strategies for posing a well-defined problem for urban air mobility vehicles," in *AIAA Scitech 2019 Forum*, 2019, p. 0818. DOI: `10.2514/6.2019-0818`.

[35] W. J. Fredericks, M. D. Moore, and R. C. Busan, "Benefits of hybrid-electric propulsion to achieve 4x cruise efficiency for a VTOL UAV," in *2013 International Powered Lift Conference*, Los Angeles, CA, USA, 2013. DOI: `10.2514/6.2013-4324`.

[36] M. J. Duffy, S. R. Wakayama, and R. Hupp, "A study in reducing the cost of vertical flight with electric propulsion," in *17th AIAA Aviation Technology, Integration, and Operations Conference*, 2017, p. 3442. DOI: `10.2514/6.2017-3442`.

[37] A. Brown and W. L. Harris, "Vehicle design and optimization model for urban air mobility," *Journal of Aircraft*, pp. 1–11, 2020. DOI: `10.2514/1.C035756`.

[38] M. N. Postorino and G. M. Sarné, "Reinventing mobility paradigms: Flying car scenarios and challenges for urban mobility," *MDPI Sustainability*, vol. 12, no. 9, p. 3581, 2020. DOI: `10.3390/su12093581`.

[39] K. Ploetner, C. Al Haddad, C. Antoniou, F. Frank, M. Fu, S. Kabel, C. Llorca, R. Moeckel, A. Moreno, A. Pukhova, *et al.*, "Long-term application potential of urban air mobility complementing public transport: An upper bavaria example," *CEAS Aeronautical Journal*, vol. 11, no. 4, pp. 991–1007, 2020. DOI: `10.1007/s13272-020-00468-5`.

[40] A. Kasliwal, N. J. Furbush, J. H. Gawron, J. R. McBride, T. J. Wallington, R. D. De Kleine, H. C. Kim, and G. A. Keoleian, "Role of flying cars in sustainable mobility," *Nature Communications*, 2019. DOI: `10.1038/s41467-019-09426-0`.

[41] N. André and M. Hajek, "Robust environmental life cycle assessment of electric VTOL concepts for urban air mobility," in *AIAA Aviation 2019 Forum*, 2019. DOI: `10.2514/6.2019-3473`.

[42] S. P. Melo, F. Cerdas, A. Barke, C. Thies, T. S. Spengler, and C. Herrmann, "Life cycle engineering of future aircraft systems: The case of eVTOL vehicles," *Procedia CIRP*, vol. 90, pp. 297–302, 2020. DOI: `10.1016/j.procir.2020.01.060`.

[43] S. V. Mudumba, H. Chao, A. Maheshwari, D. A. DeLaurentis, and W. A. Crossley, "Modeling CO2 emissions from trips using urban air mobility and emerging automobile technologies," *Transportation Research Record*, 2021. DOI: `10.1177/03611981211006439`.

[44] A. Pukhova, "Environmental evaluation of urban air mobility operation," M.S. thesis, Technichal University of Munich, 2019.

[45] M. Shamiyeh, R. Rothfeld, and M. Hornung, "A performance benchmark of recent personal air vehicle concepts for urban air mobility," in *Proceedings of the 31st Congress of the International Council of the Aeronautical Sciences, Belo Horizonte, Brazil*, 2018, pp. 9–14.

[46] E. M. Murman, M. Walton, and E. Rebentisch, "Challenges in the better, faster, cheaper era of aeronautical design, engineering and manufacturing," vol. 104, 1040 2000. DOI: `10.1017/S0001924000091983`.

[47] A. K. Kundu, M. A. Price, and D. Riordan, *Conceptual Aircraft Design: An Industrial Approach*. John Wiley & Sons, 2019, ISBN: 978-1-119-50028-5.

[48] Airbus, *ZEROe: Towards the world's first zero-emission commercial aircraft*, 2020. [Online]. Available: `https://www.airbus.com/innovation/zero-emission/hydrogen/zeroe.html` (visited on 02/23/2021).

[49] M. Price, S. Raghunathan, and R. Curran, "An integrated systems engineering approach to aircraft design," *Progress in Aerospace Sciences*, vol. 42, no. 4, pp. 331–376, 2006. DOI: `10.1016/j.paerosci.2006.11.002`.

[50] E. Torenbeek, *Synthesis of subsonic airplane design: an introduction to the preliminary design of subsonic general aviation and transport aircraft, with emphasis on layout, aerodynamic design, propulsion and performance.* Springer Science & Business Media, 2013. DOI: `10.1007/978-94-017-3202-4`.

[51] J. D. Sinsay, "Re-imagining rotorcraft advanced design," *The Aeronautical Journal*, vol. 122, no. 1256, pp. 1497–1521, 2018. DOI: `10.1017/aer.2018.107`.

[52] R. W. Prouty, *Helicopter performance, stability, and control.* R.E. Krieger Publishing Company, 1995.

[53] D. Layton, "Introduction to helicopter conceptual design," *American Institute of Aeronautics and Astronautics (AIAA)*, 1992.

[54] M. N. Tishchenko, V. T. Nagaraj, and I. Chopra, "Preliminary design of transport helicopters," *Journal of the American Helicopter Society*, vol. 48, no. 2, pp. 71–79, 2003. DOI: `10.4050/JAHS.48.71`.

[55] O. Rand and V. Khromov, "Helicopter sizing by statistics," *Journal of the American Helicopter Society*, vol. 49, no. 3, pp. 300–317, 2004. DOI: `10.4050/JAHS.49.300`.

[56] M. Lier, "Statistical methods for helicopter preliminary design and sizing," 2011.

[57] D. Raymer, *Aircraft design: a conceptual approach.* American Institute of Aeronautics and Astronautics, Inc., 2012. DOI: `10.2514/4.869112`.

[58] W. Johnson, "NDARC - NASA Design and Analysis of Rotorcraft," Tech. Rep., 2015, NASA Ames Research Center Moffett Field, CA United States. [Online]. Available: `https://ntrs.nasa.gov/citations/20150021267`.

[59] D. N. Mavris, A. P. Baker, and D. P. Schrage, "Development of a methodology for the determination of technical feasibility and viability of affordable rotorcraft systems," Presented at the American Helicopter Society 54th Annual Forum, Washington D.C., American Helicopter Society, Inc., 1998. [Online]. Available: `https://smartech.gatech.edu/handle/1853/6261`.

[60] D. P. Schrage, "Technology for rotorcraft affordability through integrated product/process development (IPPD)," 1999, Presented at the American Helicopter Society 55th Annual Forum, Montreal, Canada. [Online]. Available: `https://smartech.gatech.edu/handle/1853/6391`.

[61] C. Pornet, C. Gologan, P. C. Vratny, A. Seitz, O. Schmitz, A. T. Isikveren, and M. Hornung, "Methodology for sizing and performance assessment of hybrid energy aircraft," *Journal of Aircraft*, vol. 52, no. 1, pp. 341–352, 2015. DOI: `10.2514/1.C032716`.

[62] M. D. Moore, "Misconceptions of electric aircraft and their emerging aviation markets," in *52nd Aerospace Sciences Meeting*, National Harbor, Maryland, USA, 2014. DOI: `10.2514/6.2014-0535`.

[63] J. McMasters and R. Cummings, "Rethinking the airplane design process-an early 21st century perspective," in *42nd AIAA Aerospace Sciences Meeting and Exhibit*, Reno, Nevada, USA, 2004. DOI: `10.2514/6.2004-693`.

[64] F. Olsson, "Systematisk konstruktion (systematic engineering design)," Ph.D. dissertation, Department of Machine Design, Lund Institute of Technology, 1976.

[65] S. Vajna, *Integrated Design Engineering: Interdisciplinary and Holistic Product Development*. Springer Nature, 2019. DOI: `10.1007/978-3-030-19357-7`.

[66] K. Ehrlenspiel and H. Meerkamm, *Integrierte Produktentwicklung*. Hanser München, 2007. DOI: `10.3139/9783446421578`.

[67] C. Haskins, K. Forsberg, and M. Krueger, "INCOSE systems engineering handbook," *Seattle, Washington, USA, INCOSE*, 2006.

[68] N. Aeronautics and S. Administration, "NASA systems engineering handbook," *NASA/SP-2007-6105 Rev1*, 2007.

[69] ISO 15288:2015, "Systems and software engineering – System life cycle processes," International Organization for Standardization, Geneva, CH, Standard, 2015.

[70] T. Brown, "Design thinking," *Harvard business review*, vol. 86, no. 6, p. 84, 2008.

[71] D. N. Mavris and D. A. DeLaurentis, "A stochastic design approach for aircraft affordability," 1998, Presented at the 21st Congress of the International Council on the Aeronautical Sciences (ICAS), Melbourne, Australia. [Online]. Available: `http://hdl.handle.net/1853/6278`.

[72] M. Krosche and W. Heinze, "Robustness analysis of an aircraft design for short takeoff and landing," *Journal of aircraft*, vol. 52, no. 4, pp. 1235–1246, 2015. DOI: `10.2514/1.C032876`.

[73] W. E. Walker, P. Harremoës, J. Rotmans, J. P. Van Der Sluijs, M. B. Van Asselt, P. Janssen, and M. P. Krayer von Krauss, "Defining uncertainty: A conceptual basis for uncertainty management in model-based decision support," *Integrated assessment*, vol. 4, no. 1, pp. 5–17, 2003. DOI: `10.1076/iaij.4.1.5.16466`.

[74] M. B. Van Asselt and J. Rotmans, "Uncertainty in integrated assessment modelling," *Climatic change*, vol. 54, no. 1-2, pp. 75–105, 2002. DOI: `10.1023/A:1015783803445`.

[75] W. Johnson, "NDARC - NASA Design and Analysis of Rotorcraft: Theoretical basis and architecture," 2010, Presented at the American Helicopter Society Aeromechanics Specialists' Conference, San Francisco, CA, USA.

[76] ——, "NDARC - NASA Design and Analysis of Rotorcraft: Validation and demonstration," Presented at the American Helicopter Society Aeromechanics Specialists' Conference, San Francisco, CA, USA, 2010.

[77] W. Johnson and J. D. Sinsay, "Rotorcraft conceptual design environment," U. S. Army Research, Development & Engineering Command, Aeroflightdynamics Directorate (AMRDEC), Tech. Rep., 2009.

[78] L. A. Meyn, "Rotorcraft optimization tools: Incorporating rotorcraft design codes into multi-disciplinary design, analysis, and optimization," Presented at the International Technical Meeting on Aeromechanics Design for Transformative Vertical Flight, San Francisco, CA, USA, 2018. [Online]. Available: `https://ntrs.nasa.gov/search.jsp?R=20180000894`.

[79] J. Hirsh, J. Wilkerson, and R. Narducci, "An integrated approach to rotorcraft conceptual design," in *45th AIAA Aerospace Sciences Meeting and Exhibit*, Reno, Nevada, USA, 2007, p. 1252. DOI: `10.2514/6.2007-1252`.

[80] M. Lier, A. Krenik, P. Kunze, D. Kohlgrüber, D. Schwinn, and M. Lützenberger, "A toolbox for rotorcraft preliminary design," 2015, Presented at the AHS 71st Annual Forum, Virginia Beach, USA.

[81] P. Weiand, D. Schwinn, M. Schmid, and M. Buchwald, "A multidisciplinary process for integrated rotorcraft design," *CEAS Aeronautical Journal*, vol. 11, no. 1, pp. 145–160, 2020. DOI: `10.1007/s13272-019-00408-y`.

[82] P. Basset, A. Tremolet, F. Cuzieux, C. Schulte, D. Tristrant, T. Lefebvre, G. Reboul, M. Costes, F. Richez, S. Burguburu, *et al.*, "The creation project for rotorcraft concepts evaluation: The first steps," 2011.

[83] C. Russell and P.-M. Basset, "Conceptual design of environmentally friendly rotorcraft-a comparison of nasa and onera approaches," 2015, Presented at the AHS Annual Forum and Technology Display, Virginia Beach, VA, USA. [Online]. Available: `https://ntrs.nasa.gov/citations/20150011434`.

[84] P.-M. Basset, G. Reboul, B. DangVu, and S. Mercier, "Rotorcraft performance and environmental impact evaluation by multidisciplinary modelling," *World Academy of Science, Engineering and Technology, International Journal of Mechanical, Aerospace, Industrial, Mechatronic and Manufacturing Engineering*, vol. 11, no. 2, pp. 284–298, 2017.

[85] P.-M. Basset, B. D. Vu, P. Beaumier, G. Reboul, and B. Ortun, "Models and methods at ONERA for the presizing of eVTOL hybrid aircraft including analysis of failure scenarios," Presented at the AHS Forum, Phoenix, USA, 2018.

[86] T. W. Lukaczyk, A. D. Wendorff, M. Colonno, T. D. Economon, J. J. Alonso, T. H. Orra, and C. Ilario, "SUAVE: An open-source environment for multi-fidelity conceptual vehicle design," in *16th AIAA/ISSMO Multidisciplinary Analysis and Optimization Conference*, Dallas, TX, USA, 2015. DOI: `10.2514/6.2015-3087`.

[87] T. MacDonald, E. Botero, J. M. Vegh, A. Variyar, J. J. Alonso, T. H. Orra, and C. R. Ilario da Silva, "SUAVE: An open-source environment enabling unconventional vehicle designs through higher fidelity," in *55th AIAA Aerospace sciences meeting*, Grapevine, TX, USA, 2017. DOI: `10.2514/6.2017-0234`.

[88] T. MacDonald, M. Clarke, E. M. Botero, J. M. Vegh, and J. J. Alonso, "SUAVE: An open-source environment enabling multi-fidelity vehicle optimization," in *18th AIAA/ISSMO Multidisciplinary Analysis and Optimization Conference*, Denver, CO, USA, 2017. DOI: `10.2514/6.2017-4437`.

[89]   J. M. Vegh, E. Botero, M. Clarke, J. Smart, and J. Alonso, "Current capabilities and challenges of NDARC and SUAVE for eVTOL aircraft design and analysis," in *AIAA Propulsion and Energy Forum*, Indianapolis, IN, USA, 2019. DOI: `10.2514/6.2019-4505`.

[90]   A. Brown and W. Harris, "A vehicle design and optimization model for on-demand aviation," in *2018 AIAA/ASCE/AHS/ASC Structures, Structural Dynamics, and Materials Conference*, Kissimee, FL, USA, 2018. DOI: `10.2514/6.2018-0105`.

[91]   A. Gnadt, S. Isaacs, R. Price, M. Dethy, and C. Chappelle, "Hybrid turbo-electric STOL aircraft for urban air mobility," in *AIAA Scitech 2019 Forum*, San Diego, CA, USA, 2019. DOI: `10.2514/6.2019-0531`.

[92]   P. G. Kirschen, E. Burnell, and W. Hoburg, "Signomial programming models for aircraft design," in *54th AIAA Aerospace Sciences Meeting*, San Diego, CA USA, 2016. DOI: `10.2514/6.2016-2003`.

[93]   M. A. York, B. Öztürk, E. Burnell, and W. W. Hoburg, "Efficient aircraft multi-disciplinary design optimization and sensitivity analysis via signomial programming," *AIAA Journal*, vol. 56, no. 11, pp. 4546–4561, 2018. DOI: `10.2514/1.J057020`.

[94]   E. Burnell and W. Hoburg, "GPkit software for geometric programming," *Software Package, Ver. 0.5*, vol. 3, 2017.

[95]   E. Burnell, N. B. Damen, and W. Hoburg, "GPkit: A human-centered approach to convex optimization in engineering design," in *Proceedings of the 2020 CHI Conference on Human Factors in Computing Systems*, 2020, pp. 1–13. DOI: `10.1145/3313831.3376412`.

[96]   A. Bacchini and E. Cestino, "Electric VTOL configurations comparison," *MDPI Aerospace*, vol. 6, no. 3, p. 26, 2019. DOI: `10.3390/aerospace6030026`.

[97]   ——, "Key aspects of electric vertical take-off and landing conceptual design," *Proceedings of the Institution of Mechanical Engineers, Part G: Journal of Aerospace Engineering*, vol. 234, no. 3, pp. 774–787, 2020. DOI: `10.1177/0954410019884174`.

[98]   A. Bacchini, "Electric VTOL preliminary design and wind tunnel tests," Ph.D. dissertation, Politecnico di Torino, 2020.

[99]   M. Kraenzler, M. Schmitt, and E. Stumpf, "Conceptual design study on electrical vertical take off and landing aircraft for urban air mobility applications," in *AIAA Aviation 2019 Forum*, 2019. DOI: `10.2514/6.2019-3124`.

[100]   D. F. Finger, C. Braun, and C. Bil, "An initial sizing methodology for hybrid-electric light aircraft," in *2018 Aviation Technology, Integration, and Operations Conference*, 2018. DOI: `10.2514/6.2018-4229`.

[101] D. F. Finger, F. Götten, C. Braun, and C. Bil, "Mass, primary energy, and cost: The impact of optimization objectives on the initial sizing of hybrid-electric general aviation aircraft," *CEAS Aeronautical Journal*, pp. 1–18, 2019. DOI: `10.1007/s13272-020-00449-8`.

[102] Brundtland Commission, "Report of the world commission on environment and development: Our common future," World Commission on Environment and Development, Tech. Rep., 1987.

[103] United Nations, "Resolution adopted by the general assembly on 16 september 2005," UN General Assembly, A/RES/60/1, 16 September 2005, Tech. Rep., 2005.

[104] E. Holden, K. Linnerud, and D. Banister, "Sustainable passenger transport: Back to brundtland," *Transportation Research Part A: Policy and Practice*, vol. 54, pp. 67–77, 2013. DOI: `10.1016/j.tra.2013.07.012`.

[105] E. Holden, D. Banister, S. Gössling, G. Gilpin, and K. Linnerud, "Grand narratives for sustainable mobility: A conceptual review," *Energy Research & Social Science*, vol. 65, p. 101 454, 2020. DOI: `10.1016/j.erss.2020.101454`.

[106] ISO 14040:2006, "Environmental management – life cycle assessment – principles and framework," International Organization for Standardization, Geneva, CH, Tech. Rep., 2006.

[107] ISO 14044:2006, "Environmental management – life cycle assessment – requirements and guidelines," International Organization for Standardization, Geneva, CH, Tech. Rep., 2006.

[108] R. Heijungs and S. Suh, *The computational structure of life cycle assessment.* Springer, Dordrecht, 2002. DOI: `10.1007/978-94-015-9900-9`.

[109] M. Finkbeiner, *Special types of life cycle assessment.* Springer, Dordrecht, 2016. DOI: `10.1007/978-94-017-7610-3`.

[110] M. Z. Hauschild, R. K. Rosenbaum, and S. Olsen, *Life cycle assessment.* Springer, Cham, 2018. DOI: `10.1007/978-3-319-56475-3`.

[111] J. B. Guinee, R. Heijungs, G. Huppes, A. Zamagni, P. Masoni, R. Buonamici, T. Ekvall, and T. Rydberg, *Life cycle assessment: Past, present, and future*, 2011. DOI: `10.1021/es101316v`.

[112] G. Finnveden, M. Z. Hauschild, T. Ekvall, J. Guinée, R. Heijungs, S. Hellweg, A. Koehler, D. Pennington, and S. Suh, "Recent developments in life cycle assessment," *Journal of environmental management*, vol. 91, no. 1, pp. 1–21, 2009. DOI: `10.1016/j.jenvman.2009.06.018`.

[113] M. Finkbeiner, E. M. Schau, A. Lehmann, and M. Traverso, "Towards life cycle sustainability assessment," *MDPI Sustainability*, vol. 2, no. 10, pp. 3309–3322, 2010. DOI: `10.3390/su2103309`.

[114] M. A. Curran, M. Mann, and G. Norris, "The international workshop on electricity data for life cycle inventories," *Journal of Cleaner Production*, vol. 13, no. 8, pp. 853–862, 2005. DOI: `10.1016/j.jclepro.2002.03.001`.

[115] T. P. Wright, "Factors affecting the cost of airplanes," *Journal of the aeronautical sciences*, vol. 3, no. 4, pp. 122–128, 1936. DOI: 10.2514/8.155.

[116] T. Ekvall, A.-M. Tillman, and S. Molander, "Normative ethics and methodology for life cycle assessment," *Journal of Cleaner Production*, vol. 13, no. 13-14, pp. 1225–1234, 2005. DOI: 10.1016/j.jclepro.2005.05.010.

[117] B. A. Sandén and M. Karlström, "Positive and negative feedback in consequential life-cycle assessment," *Journal of Cleaner Production*, vol. 15, no. 15, pp. 1469–1481, 2007. DOI: 10.1016/j.jclepro.2006.03.005.

[118] L. Börjeson, M. Höjer, K.-H. Dreborg, T. Ekvall, and G. Finnveden, "Scenario types and techniques: Towards a user's guide," *Futures*, vol. 38, no. 7, pp. 723–739, 2006. DOI: 10.1016/j.futures.2005.12.002.

[119] J. B. Guinée and E. Lindeijer, *Handbook on life cycle assessment: operational guide to the ISO standards*. Springer Science & Business Media, 2002, vol. 7.

[120] B. Weidema, "Avoiding co-product allocation in life-cycle assessment," *Journal of industrial ecology*, vol. 4, pp. 11–33, 2000. DOI: 10.1162/108819800300106366.

[121] T. Ekvall and G. Finnveden, "Allocation in ISO 14041—a critical review," *Journal of cleaner production*, vol. 9, no. 3, pp. 197–208, 2001.

[122] M. A. Curran, "Co-product and input allocation approaches for creating life cycle inventory data: A literature review," *International Journal of Life Cycle Assessment*, vol. 12, pp. 65–78, 2007. DOI: 10.1065/lca2006.08.268.

[123] A. Ciroth, G. Huppes, and S. Lundie, *Inventory methods in LCA: towards consistency and improvement*. VDM Verlag Dr. Müller, 2008.

[124] J. B. Guinée, R. Heijungs, and G. Huppes, "Economic allocation: Examples and derived decision tree," *The international journal of life cycle assessment*, vol. 9, no. 1, p. 23, 2004. DOI: 10.1007/BF02978533.

[125] S. Suh and G. Huppes, "Methods for life cycle inventory of a product," *Journal of cleaner production*, vol. 13, no. 7, pp. 687–697, 2005. DOI: 10.1016/j.jclepro.2003.04.001.

[126] R. H. Crawford, P.-A. Bontinck, A. Stephan, T. Wiedmann, and M. Yu, "Hybrid life cycle inventory methods–a review," *Journal of Cleaner Production*, vol. 172, pp. 1273–1288, 2018. DOI: 10.1016/j.jclepro.2017.10.176.

[127] M. Lenzen, "Errors in conventional and input-output based life cycle inventories," *Journal of industrial ecology*, vol. 4, no. 4, pp. 127–148, 2000. DOI: 10.1162/10881980052541981.

[128] S. Suh, M. Lenzen, G. J. Treloar, H. Hondo, A. Horvath, G. Huppes, O. Jolliet, U. Klann, W. Krewitt, Y. Moriguchi, *et al.*, "System boundary selection in life-cycle inventories using hybrid approaches," *Environmental science & technology*, vol. 38, no. 3, pp. 657–664, 2004. DOI: 10.1021/es0263745.

[129] M. Hauschild, J. Potting, *et al.*, "Spatial differentiation in life cycle impact assessment-the EDIP2003 methodology," *Environmental news*, vol. 80, pp. 1–195, 2005.

[130] M. Z. Hauschild and M. A. Huijbregts, *Introducing life cycle impact assessment.* Springer, Dordrecht, 2015. DOI: 10.1007/978-94-017-9744-3_1.

[131] G. Wernet, C. Bauer, B. Steubing, J. Reinhard, E. Moreno-Ruiz, and B. Weidema, "The ecoinvent database version 3 (part i): Overview and methodology," *The International Journal of Life Cycle Assessment*, vol. 21, no. 9, pp. 1218–1230, 2016. DOI: 10.1007/s11367-016-1087-8.

[132] S. Hellweg and L. M. i Canals, "Emerging approaches, challenges and opportunities in life cycle assessment," *Science*, vol. 344, no. 6188, pp. 1109–1113, 2014. DOI: 10.1126/science.1248361.

[133] S.-C. Lo, H.-w. Ma, and S.-L. Lo, "Quantifying and reducing uncertainty in life cycle assessment using the bayesian monte carlo method," *Science of the total environment*, vol. 340, no. 1-3, pp. 23–33, 2005. DOI: 10.1016/j.scitotenv.2004.08.020.

[134] M.-L. Hung and H.-w. Ma, "Quantifying system uncertainty of life cycle assessment based on monte carlo simulation," *The International Journal of Life Cycle Assessment*, vol. 14, no. 1, p. 19, 2009. DOI: 10.1007/s11367-008-0034-8.

[135] A. Misra, "Energy storage for electrified aircraft: The need for better batteries, fuel cells, and supercapacitors," *IEEE Electrification Magazine*, vol. 6, no. 3, pp. 54–61, 2018. DOI: 10.1109/MELE.2018.2849922.

[136] M. Winter and R. J. Brodd, "What are batteries, fuel cells, and supercapacitors?" *Chemical Reviews*, vol. 104, no. 10, pp. 4245–4270, 2004. DOI: 10.1021/cr020730k.

[137] Z. P. Cano, D. Banham, S. Ye, A. Hintennach, J. Lu, M. Fowler, and Z. Chen, "Batteries and fuel cells for emerging electric vehicle markets," *Nature Energy*, vol. 3, no. 4, pp. 279–289, 2018. DOI: 10.1038/s41560-018-0108-1.

[138] E. Budsberg, J. T. Crawford, H. Morgan, W. S. Chin, R. Bura, and R. Gustafson, "Hydrocarbon bio-jet fuel from bioconversion of poplar biomass: Life cycle assessment," *Biotechnology for biofuels*, vol. 9, no. 1, pp. 1–13, 2016. DOI: 10.1186/s13068-016-0582-2.

[139] R.-U. Dietrich, F. G. Albrecht, and S. Estelmann, "Synthetic jet fuel from renewable energy sources for sustainable aviation," 6th International Conference on Petroleum Engineering, Madrid, Spain, 2017.

[140] F. G. Albrecht, D. H. König, N. Baucks, and R.-U. Dietrich, "A standardized methodology for the techno-economic evaluation of alternative fuels–a case study," *Fuel*, vol. 194, pp. 511–526, 2017. DOI: 10.1016/j.fuel.2016.12.003.

[141] T. Placke, R. Kloepsch, S. Dühnen, and M. Winter, "Lithium ion, lithium metal, and alternative rechargeable battery technologies: The odyssey for high energy density," *Journal of Solid State Electrochemistry*, vol. 21, no. 7, pp. 1939–1964, 2017. DOI: `10.1007/s10008-017-3610-7`.

[142] R. Van Noorden, "The rechargeable revolution: A better battery," *Nature News*, vol. 507, no. 7490, p. 26, 2014. DOI: `10.1038/507026a`.

[143] O. Schmidt, A. Hawkes, A. Gambhir, and I. Staffell, "The future cost of electrical energy storage based on experience rates," *Nature Energy*, vol. 2, no. 8, pp. 1–8, 2017. DOI: `10.1038/nenergy.2017.110`.

[144] M. Azevedo, N. Campagnol, T. Hagenbruch, K. Hoffman, A. Lala, and O. Ramsbottom, "Lithium and cobalt: A tale of two commodities," *McKinsey & Co*, 2018.

[145] E. J. Berg, C. Villevieille, D. Streich, S. Trabesinger, and P. Novák, "Rechargeable batteries: Grasping for the limits of chemistry," *Journal of The Electrochemical Society*, vol. 162, no. 14, A2468, 2015. DOI: `10.1149/2.0081514jes`.

[146] G. Zubi, R. Dufo-López, M. Carvalho, and G. Pasaoglu, "The lithium-ion battery: State of the art and future perspectives," *Renewable and Sustainable Energy Reviews*, vol. 89, pp. 292–308, 2018. DOI: `10.1016/j.rser.2018.03.002`.

[147] Q. Abbas, M. Mirzaeian, A.-G. Olabi, and D. Gibson, "Solid state electrolytes," in *Reference Module in Materials Science and Materials Engineering*, Elsevier B.V., 2020. DOI: `10.1016/B978-0-12-803581-8.11740-0`.

[148] X.-B. Cheng, R. Zhang, C.-Z. Zhao, and Q. Zhang, "Toward safe lithium metal anode in rechargeable batteries: A review," *Chemical reviews*, vol. 117, no. 15, pp. 10 403–10 473, 2017. DOI: `10.1021/acs.chemrev.7b00115`.

[149] X. Shen, H. Liu, X.-B. Cheng, C. Yan, and J.-Q. Huang, "Beyond lithium ion batteries: Higher energy density battery systems based on lithium metal anodes," *Energy Storage Materials*, vol. 12, pp. 161–175, 2018. DOI: `10.1016/j.ensm.2017.12.002`.

[150] Oxis Energy. (2020). "How lithium-sulfur is meeting the challenges of eVTOL," [Online]. Available: `https://evtol.com/opinions/oxis-energy-lithium-sulfur-batteries-evtol/` (visited on 02/19/2021).

[151] Cuberg. (2021). "The future of batteries is here," [Online]. Available: `https://www.cuberg.net/` (visited on 02/19/2021).

[152] S. Randau, D. A. Weber, O. Kötz, R. Koerver, P. Braun, A. Weber, E. Ivers-Tiffée, T. Adermann, J. Kulisch, W. G. Zeier, *et al.*, "Benchmarking the performance of all-solid-state lithium batteries," *Nature Energy*, vol. 5, no. 3, pp. 259–270, 2020. DOI: `10.1038/s41560-020-0565-1`.

[153] QuantumScape. (2021). "Introducing quantumscape. solid-state batteries that work," [Online]. Available: `https://www.quantumscape.com/#technology` (visited on 02/19/2021).

[154] Global Battery Alliance. (2019). "A vision for a sustainable battery value chain in 2030." World Economic Forum, [Online]. Available: `http://www3.weforum.org/docs/WEF_A_Vision_for_a_Sustainable_Battery_Value_Chain_in_2030_Report.pdf` (visited on 08/14/2020).

[155] M. Philippot, G. Alvarez, E. Ayerbe, J. Van Mierlo, and M. Messagie, "Eco-efficiency of a lithium-ion battery for electric vehicles: Influence of manufacturing country and commodity prices on GHG emissions and costs," *MDPI Batteries*, vol. 5, no. 1, p. 23, 2019. DOI: `10.3390/batteries5010023`.

[156] G. Majeau-Bettez, T. R. Hawkins, and A. H. Strømman, "Life cycle environmental assessment of lithium-ion and nickel metal hydride batteries for plug-in hybrid and battery electric vehicles," *Environmental science & technology*, vol. 45, no. 10, pp. 4548–4554, 2011. DOI: `10.1021/es103607c`.

[157] T. Le Varlet, O. Schmidt, A. Gambhir, S. Few, and I. Staffell, "Comparative life cycle assessment of lithium-ion battery chemistries for residential storage," *Journal of Energy Storage*, vol. 28, p. 101 230, 2020. DOI: `10.1016/j.est.2020.101230`.

[158] E. Emilsson and L. Dahllöf, "Lithium-ion vehicle battery production," Tech. Rep., 2019, VL Swedish Environmental Research Institute 2019, Stockholm, Sweden.

[159] A. Regett, W. Mauch, and U. Wagner, "Carbon footprint of electric vehicles-a plea for more objectivity," Tech. Rep., 2019, Forschungsstelle für Energiewirtschaft e.V.

[160] J. C. Kelly, Q. Dai, and M. Wang, "Globally regional life cycle analysis of automotive lithium-ion nickel manganese cobalt batteries," *Mitigation and Adaptation Strategies for Global Change*, vol. 25, no. 3, pp. 371–396, 2020. DOI: `10.1007/s11027-019-09869-2`.

[161] S. Bobba, A. Podias, F. Di Persio, M. Messagie, P. Tecchio, M. A. Cusenza, U. Eynard, F. Mathieux, and A. Pfrang, "Sustainability assessment of second life application of automotive batteries (saslab)," *JRC Exploratory Research (2016-2017), Final report*, 2018, RC112543. DOI: `10.2760/53624`.

[162] IEA, "The future of hydrogen," *Report prepared by the IEA for the G20*, 2019. [Online]. Available: `https://www.iea.org/reports/the-future-of-hydrogen`.

[163] R. Moradi and K. M. Groth, "Hydrogen storage and delivery: Review of the state of the art technologies and risk and reliability analysis," *International Journal of Hydrogen Energy*, vol. 44, no. 23, pp. 12 254–12 269, 2019. DOI: `10.1016/j.ijhydene.2019.03.041`.

[164] A. Dicks and D. A. J. Rand, *Fuel cell systems explained*. John Wiley & Sons, 2018.

[165] A. Olabi, T. Wilberforce, and M. A. Abdelkareem, "Fuel cell application in the automotive industry and future perspective," *Energy*, vol. 214, p. 118 955, 2020. DOI: `10.1016/j.energy.2020.118955`.

[166] B. C. Hacker and J. M. Grimwood, *On the Shoulders of Titans: A History of Project Gemini.* NASA, 1977, vol. 4203.

[167] B. A. Moffitt, "A methodology for the validated design space exploration of fuel cell powered unmanned aerial vehicles," Ph.D. dissertation, Georgia Institute of Technology, 2010.

[168] R. Scholz, N. Gläser, D. Paluch, and T. Schmidt, "Auf dem Weg zur Emissionsfreiheit im Zugverkehr," Ernst & Young GmbH, Tech. Rep., 2016.

[169] Alstom. (2020). "Coradia iLint – der weltweit erste Wasserstoffzug," [Online]. Available: `https://www.alstom.com/de/our-solutions/rolling-stock/coradia-ilint-der-weltweit-erste-wasserstoffzug` (visited on 07/20/2020).

[170] PV Magazine. (2020). "Eineinhalb Jahre erfolgreicher Probebetrieb der weltweit ersten beiden wasserstoffzüge," [Online]. Available: `https://www.pv-magazine.de/unternehmensmeldungen/eineinhalb-jahre-erfolgreicher-probebetrieb-der-weltweit-ersten-beiden-wasserstoffzuege/` (visited on 07/20/2020).

[171] A. Baroutaji, T. Wilberforce, M. Ramadan, and A. G. Olabi, "Comprehensive investigation on hydrogen and fuel cell technology in the aviation and aerospace sectors," *Renewable and Sustainable Energy Reviews*, vol. 106, pp. 31–40, 2019. DOI: `10.1016/j.rser.2019.02.022`.

[172] DLR. (2020). "Klimafreundlich abheben: Elektrisches Fliegen mit Batterie, Wasserstoff und Hybridkonzepten," [Online]. Available: `https://www.dlr.de/content/de/artikel/news/2020/01/20200220_klimafreundlich-abheben-elektrisches-fliegen-2.html` (visited on 02/23/2021).

[173] A. M. Abdalla, S. Hossain, O. B. Nisfindy, A. T. Azad, M. Dawood, and A. K. Azad, "Hydrogen production, storage, transportation and key challenges with applications: A review," *Energy conversion and management*, vol. 165, pp. 602–627, 2018. DOI: `10.1016/j.enconman.2018.03.088`.

[174] A. Wilson, G. Kleen, and D. Papageorgopoulos, "DOE hydrogen and fuel cells program record," US Department of Energy, Tech. Rep., 2017. [Online]. Available: `https://www.hydrogen.energy.gov/pdfs/17007_fuel_cell_system_cost_2017.pdf`.

[175] M. M. Whiston, I. L. Azevedo, S. Litster, K. S. Whitefoot, C. Samaras, and J. F. Whitacre, "Expert assessments of the cost and expected future performance of proton exchange membrane fuel cells for vehicles," *Proceedings of the National Academy of Sciences*, vol. 116, no. 11, pp. 4899–4904, 2019. DOI: `10.1073/pnas.1804221116`.

[176] O. Gröger, H. A. Gasteiger, and J.-P. Suchsland, "Electromobility: Batteries or fuel cells?" *Journal of The Electrochemical Society*, vol. 162, no. 14, 2015. DOI: `10.1149/2.0211514jes`.

[177] W. Ng, M. Patil, and A. Datta, "Hydrogen fuel cell and battery hybrid architecture for range extension of electric VTOL aircraft," *Journal of the American Helicopter Society*, vol. 66, no. 1, pp. 1–13, 2021. DOI: `10.4050/JAHS.66.012009`.

[178] B. G. Pollet, S. S. Kocha, and I. Staffell, "Current status of automotive fuel cells for sustainable transport," *Current opinion in Electrochemistry*, vol. 16, pp. 90–95, 2019. DOI: `10.1016/j.coelec.2019.04.021`.

[179] P. Scott, R. Calay, and Y. Chen, "Experimental evaluation into novel, low cost, modular pemfc stack," *Energy Procedia*, vol. 29, pp. 567–575, 2012. DOI: `10.1016/j.egypro.2012.09.066`.

[180] F. Ning, X. He, Y. Shen, H. Jin, Q. Li, D. Li, S. Li, Y. Zhan, Y. Du, J. Jiang, *et al.*, "Flexible and lightweight fuel cell with high specific power density," *ACS nano*, vol. 11, no. 6, pp. 5982–5991, 2017. DOI: `10.1021/acsnano.7b01880`.

[181] J. J. Minnehan and J. W. Pratt, "Practical application limits of fuel cells and batteries for zero emission vessels," Tech. Rep., 2017, Sandia National Laboratories, Albuquerque, NM, USA.

[182] HyPoint. (2020). "Technical white paper," [Online]. Available: `https://docsend.com/view/t9aw2mk`.

[183] E. Rivard, M. Trudeau, and K. Zaghib, "Hydrogen storage for mobility: A review," *MDPI Materials*, vol. 12, no. 12, p. 1973, 2019. DOI: `10.3390/ma12121973`.

[184] H. Barthélémy, M. Weber, and F. Barbier, "Hydrogen storage: Recent improvements and industrial perspectives," *International Journal of Hydrogen Energy*, vol. 42, no. 11, pp. 7254–7262, 2017. DOI: `10.1016/j.ijhydene.2016.03.178`.

[185] M. Prewitz, A. Bardenhagen, and R. Beck, "Hydrogen as the fuel of the future in aircrafts–challenges and opportunities," *International Journal of Hydrogen Energy*, vol. 45, no. 46, pp. 25 378–25 385, 2020. DOI: `10.1016/j.ijhydene.2020.06.238`.

[186] H. T. Hwang and A. Varma, "Hydrogen storage for fuel cell vehicles," *Current Opinion in Chemical Engineering*, vol. 5, pp. 42–48, 2014. DOI: `10.1016/j.coche.2014.04.004`.

[187] D. Verstraete, P. Hendrick, P. Pilidis, and K. Ramsden, "Hydrogen fuel tanks for subsonic transport aircraft," *International journal of hydrogen energy*, vol. 35, no. 20, pp. 11 085–11 098, 2010. DOI: `10.1016/j.ijhydene.2010.06.060`.

[188] A. Züttel, "Materials for hydrogen storage," *Materials today*, vol. 6, no. 9, pp. 24–33, 2003. DOI: `10.1016/S1369-7021(03)00922-2`.

[189] N. Sirosh, "Hydrogen composite tank program," in *Proceedings of the 2002 US DOE Hydrogen Program Review*, 2002, pp. 1–7.

[190] Y. Bicer and I. Dincer, "Life cycle evaluation of hydrogen and other potential fuels for aircrafts," *International Journal of Hydrogen Energy*, vol. 42, no. 16, pp. 10 722–10 738, 2017. DOI: `10.1016/j.ijhydene.2016.12.119`.

[191] K. Bareiß, C. de la Rua, M. Möckl, and T. Hamacher, "Life cycle assessment of hydrogen from proton exchange membrane water electrolysis in future energy systems," *Applied Energy*, vol. 237, pp. 862–872, 2019. DOI: `10.1016/j.apenergy.2019.01.001`.

[192] J. Burkhardt, A. Patyk, P. Tanguy, and C. Retzke, "Hydrogen mobility from wind energy–a life cycle assessment focusing on the fuel supply," *Applied energy*, vol. 181, pp. 54–64, 2016. DOI: `10.1016/j.apenergy.2016.07.104`.

[193] M. Mann and P. Spath, "Life cycle assessment of renewable hydrogen production via wind/electrolysis: Milestone completion report," National Renewable Energy Lab., Golden, CO.(US), Tech. Rep., 2004.

[194] E. Cetinkaya, I. Dincer, and G. Naterer, "Life cycle assessment of various hydrogen production methods," *International journal of hydrogen energy*, vol. 37, no. 3, pp. 2071–2080, 2012. DOI: `10.1016/j.ijhydene.2011.10.064`.

[195] Z. Berdowski, J. van den Broek-Serie, Y. K. Jetten, and Y. Kawabata, "Survey on standard weights of passengers and baggage," *European Aviation Safety Agency, Cologne, Germany*, 2009.

[196] EASA, *Special condition for small-category VTOL aircraft*, 2019. [Online]. Available: `https://www.easa.europa.eu/sites/default/files/dfu/SC-VTOL-01.pdf` (visited on 11/24/2020).

[197] M. Price, J. M. Early, R. Curran, E. Bénard, and S. Raghunathan, "Identifying interfaces in engineering systems," *AIAA journal*, vol. 44, no. 3, pp. 529–540, 2006. DOI: `10.2514/1.16200`.

[198] W. Ng and A. Datta, "An examination of hydrogen fuel cells and lithium-ion batteries for electric vertical take-off and landing aircraft," in *44th European Rotorcraft Forum*, Delft,TheNetherlands.

[199] W. Ng and A. Datta, "Hydrogen fuel cells and batteries for electric-vertical takeoff and landing aircraft," *Journal of Aircraft*, vol. 56, no. 5, pp. 1765–1782, 2019. DOI: `10.2514/1.C035218`.

[200] F. D. Harris and C. Dow, "Volume iii: Other v/stol aircraft," in *Introduction to Autogyros, Helicopters, and Other V/STOL Aircraft*, 2015.

[201] M. D. Moore. (2018). "Uber elevate, vehicle collaboration strategy and common reference models," [Online]. Available: `https://vtol.org/files/dmfile/3-TVF5-2018-Moore-Uber-Jan181.pdf` (visited on 07/29/2020).

[202] C. Vetter, "Conceptual modelling and performance analysis of an electric coaxial multicopter for uam applications," M.S. thesis, Technical University of Munich, 2019.

[203] G. J. Leishman, *Principles of helicopter aerodynamics*. Cambridge university press, 2006.

[204] L. W. Traub, "Range and endurance estimates for battery-powered aircraft," *Journal of Aircraft*, vol. 48, no. 2, pp. 703–707, 2011. DOI: `10.2514/1.C031027`.

[205] Y.-H. Sun, H.-L. Jou, and J.-C. Wu, "Multilevel peukert equations based residual capacity estimation method for lead-acid battery," in *2008 IEEE International Conference on Sustainable Energy Technologies*, IEEE, 2008, pp. 101–105. DOI: `10.1109/ICSET.2008.4746980`.

[206] L. A.-W. Ellingsen, G. Majeau-Bettez, B. Singh, A. K. Srivastava, L. O. Valøen, and A. H. Strømman, "Life cycle assessment of a lithium-ion battery vehicle pack," *Journal of Industrial Ecology*, vol. 18, no. 1, pp. 113–124, 2014. DOI: `10.1111/jiec.12072`.

[207] J. Rudzki, "Analysis of possible energy carriers and technical constraints in the conceptual design of vertical take-off and landing aircraft," M.S. thesis, Technical University of Munich, 2020.

[208] P. Stahl, C. Roessler, and M. Hornung, "Modelling and performance impact of high power/high energy battery hybrids on fixed-wing evtol uav," in *AIAA Scitech 2020 Forum*, 2020, p. 0260. DOI: `10.2514/6.2020-0260`.

[209] A. Lord Turner, *E-Mail correspondence*, 2020.

[210] European Commission. (2020). "Proposal for a regulation of the european parliament and of the council concerning batteries and waste batteries," [Online]. Available: `https://ec.europa.eu/environment/pdf/waste/batteries/Proposal_for_a_Regulation_on_batteries_and_waste_batteries.pdf` (visited on 05/17/2021).

[211] Federal Aviation Administration. (2020). "Fuel requirements for flight in vfr conditions," [Online]. Available: `https://www.govinfo.gov/content/pkg/CFR-2012-title14-vol2/pdf/CFR-2012-title14-vol2-sec91-151.pdf`.

[212] *Hybrid & electric propulsion performance measurement*, 2017. [Online]. Available: `https://gama.aero/wp-content/uploads/GAMA-Publication-No-16-Hybrid-and-Electric-Propulsion-Performance-Measurement-1.pdf`.

[213] M. Ballo, "eVTOL aircraft conceptual design and optimization," M.S. thesis, Politechnico di Milano, 2020.

[214] K. A. Severson, P. M. Attia, N. Jin, N. Perkins, B. Jiang, Z. Yang, M. H. Chen, M. Aykol, P. K. Herring, D. Fraggedakis, *et al.*, "Data-driven prediction of battery cycle life before capacity degradation," *Nature Energy*, vol. 4, no. 5, pp. 383–391, 2019. DOI: `10.1038/s41560-019-0356-8`.

[215] J. Bogaisky. (2021). "Lilium's new course: On verge of going public, it's working on a bigger air taxi. can it deliver?" [Online]. Available: `https://www.forbes.com/sites/jeremybogaisky/2021/02/10/lilium-evtol-spac-air-taxi/?sh=7c6bf092627c`.

[216] G. Wernet, C. Bauer, B. Steubing, J. Reinhard, E. Moreno-Ruiz, and B. Weidema, *The ecoinvent database version 3 (part i): Overview and methodology*, Sep. 2016.

[217] S. Das, "Life cycle assessment of carbon fiber-reinforced polymer composites," *The International Journal of Life Cycle Assessment*, vol. 16, no. 3, pp. 268–282, 2011. DOI: `10.1007/s11367-011-0264-z`.

[218] M. F. Ashby, *Materials and the environment: eco-informed material choice*. Elsevier, 2012.

[219] M. Zackrisson, L. Avellán, and J. Orlenius, "Life cycle assessment of lithium-ion batteries for plug-in hybrid electric vehicles–critical issues," *Journal of Cleaner Production*, vol. 18, no. 15, pp. 1519–1529, 2010. DOI: `10.1016/j.jclepro.2010.06.004`.

[220] IEA, *Carbon intensity of electricity generation in selected regions in the sustainable development scenario, 2000-2040*, 2019. [Online]. Available: `https://www.iea.org/data-and-statistics/charts/carbon-intensity-of-electricity-generation-in-selected-regions-in-the-sustainable-development-scenario-2000-2040`.

[221] A. Bonou, A. Laurent, and S. I. Olsen, "Life cycle assessment of onshore and offshore wind energy-from theory to application," *Applied Energy*, vol. 180, pp. 327–337, 2016. DOI: `10.1016/j.apenergy.2016.07.058`.

[222] B. Guezuraga, R. Zauner, and W. Pölz, "Life cycle assessment of two different 2 MW class wind turbines," *Renewable Energy*, vol. 37, no. 1, pp. 37–44, 2012. DOI: `10.1016/j.renene.2011.05.008`.

[223] F. Ardente, M. Beccali, M. Cellura, and V. L. Brano, "Energy performances and life cycle assessment of an italian wind farm," *Renewable and Sustainable Energy Reviews*, vol. 12, no. 1, pp. 200–217, 2008. DOI: `10.1016/j.rser.2006.05.013`.

[224] S. Evangelisti, C. Tagliaferri, D. J. Brett, and P. Lettieri, "Life cycle assessment of a polymer electrolyte membrane fuel cell system for passenger vehicles," *Journal of cleaner production*, vol. 142, pp. 4339–4355, 2017. DOI: `10.1016/j.jclepro.2016.11.159`.

[225] D. A. Notter, K. Kouravelou, T. Karachalios, M. K. Daletou, and N. T. Haberland, "Life cycle assessment of PEM FC applications: Electric mobility and μ-chp," *Energy & Environmental Science*, vol. 8, no. 7, pp. 1969–1985, 2015. DOI: `10.1039/C5EE01082A`.

[226] A. Simons and C. Bauer, "A life-cycle perspective on automotive fuel cells," *Applied energy*, vol. 157, pp. 884–896, 2015. DOI: `10.1016/j.apenergy.2015.02.049`.

[227] D. Perry. (2021). "Lilium puts $2.5 million price tag on initial jets," [Online]. Available: `https://www.flightglobal.com/aerospace/lilium-puts-25-million-price-tag-on-initial-jets/143724.article`.

[228] R. H. Ballou, H. Rahardja, and N. Sakai, "Selected country circuity factors for road travel distance estimation," *Transportation Research Part A: Policy and Practice*, vol. 36, pp. 843–848, 2002. DOI: `10.1016/S0965-8564(01)00044-1`.

[229] J. Woo, H. Choi, and J. Ahn, "Well-to-wheel analysis of greenhouse gas emissions for electric vehicles based on electricity generation mix: A global perspective," *Transportation Research Part D: Transport and Environment*, vol. 51, pp. 340–350, 2017. DOI: `10.1016/j.trd.2017.01.005`.

[230] ADAC, *Stromverbrauch Elektroautos: Aktuelle Modelle im ADAC Test*, 2021. [Online]. Available: `https : / / www . adac . de / rund - ums - fahrzeug / tests / elektromobilitaet/stromverbrauch-elektroautos-adac-test/` (visited on 03/20/2021).

[231] Umweltbundesamt, *Treibhausgasemissionen im Personenverkehr*, 2019. [Online]. Available: `https : / / www . umweltbundesamt . de / themen / verkehr - laerm / emissionsdaten#grafik` (visited on 07/01/2021).

[232] MIT. (2021). "The mit license," [Online]. Available: `https://opensource.org/ licenses/mit-license.php` (visited on 07/30/2020).

Computational Framework Access

The implemented computational framework is published under MIT Licence [232] and can be accessed via GitLab (Link).